



CENTRO DE CIÊNCIAS EXATAS
DEPARTAMENTO DE FÍSICA
UNIVERSIDADE FEDERAL DE SÃO CARLOS

GABRIELA AUGUSTA PRANDO

**Propriedades óticas e elétricas de
dicalcogenetos de metais de transição
sobre talco**

São Carlos, SP

2022

GABRIELA AUGUSTA PRANDO

Propriedades óticas e elétricas de dicalcogenetos de metais de transição sobre talco

Tese apresentada ao Programa de Pós-Graduação em Física aplicada, ao Departamento de Física da Universidade Federal de São Carlos, para obtenção do título de doutor(a) em ciências.

Orientador(a) (UFSCar): Prof.^a Dr^a Yara Galvão Gobato.

Coorientador(a) (sanduíche): Prof.^a Dr^a Monica Craciun

São Carlos, SP

2022




UNIVERSIDADE FEDERAL DE SÃO CARLOS

Centro de Ciências Exatas e de Tecnologia
Programa de Pós-Graduação em Física

Folha de Aprovação

Defesa de Tese de Doutorado da candidata Gabriela Augusta Prando, realizada em 24/02/2022.

Comissão Julgadora:


Prof. Dra. Yara Galvão Gobato (UFSCar)

Prof. Dr. José Pedro Donoso Gonzalez (USP)

Prof. Dr. Guilherme Matos Sipahi (USP)

Prof. Dr. Luís Alberto Mijam Barêa (UFSCar)

Prof. Dr. Alisson Ronieri Cadore (Mackenzie)

Agradecimentos

Agradeço primeiramente a professora Yara Galvão Gobato pela orientação, incentivo, paciência e ensinamentos.

A professora Monica Craciun por me receber na Universidade de Exeter, aos professores e pesquisadores Russo Saviero, Adolfo D'Sanctis e Fred Withers pelos ensinamentos e orientação.

A pesquisadora Ingrid D. Barcelos, do Laboratório Nacional de Luz Sincrotron, pelos ensinamentos e produção das amostras Iniciais.

Aos professores Fernando Ikawa e Odilon D. D. Couto, do IFGW-UNICAMP, por disponibilizar o laboratório do Grupo de Propriedades Ópticas para medidas e pela ajuda e instruções.

Aos amigos e família que me acompanharam nessa jornada.

E principalmente ao meu fiel companheiro, meu Sancho, sempre ao meu lado, meu gato Fluffy.

À CAPES, CNPq e FAPESP, pelos financiamentos do projeto de pesquisa e à banca examinadora.

*We are not to tell nature what she's gotta be...
She's always got better imagination than we have*

Richard P. Feynman

Resumo

Sistemas bidimensionais (2D) têm atraído um grande interesse nos últimos anos, tanto para estudos de física fundamental, como para possível aplicação em uma nova geração de dispositivos optoeletrônicos. Em particular, existe um grande interesse em materiais 2D baseados em dicalcogenetos de metais de transição (TMDs), devido ao forte acoplamento de spin-vale e a diversas propriedades excitônicas. Exploramos a possibilidade de usar o talco como um dielétrico alternativo para proteção de monocamadas de TMDs. Foram preparadas diversas amostras de WS_2 /talco que apresentaram alta qualidade ótica comparável a amostras de WS_2 /hBN. Com isso, observamos diversos picos de fotoluminescência que foram atribuídos à formação de diversos complexos excitônicos, incluindo trions “dark” (DT) e réplicas de fônons de trions “dark”. Realizamos um estudo sistemático de magneto-fotoluminescência em baixa temperatura e em altos campos magnéticos (até 30T) em amostras de monocamada WS_2 /Talco. Extraímos os fatores g e o grau de polarização circular dos diversos picos de emissão ótica. As naturezas desses picos foram discutidas e comparadas com resultados de amostras de monocamada de WS_2 encapsuladas com hBN. Além disso, foram fabricados dispositivos transistores de efeito de campo (FET), baseados em $MoSe_2$ /Talco e MoS_2 /Talco. Os dispositivos obtidos apresentaram uma pequena histerese quando comparados com dispositivos que utilizam SiO_2 . Observamos que as propriedades de transporte desses dispositivos são comparáveis a dispositivos que utilizam hBN como dielétrico. De forma geral, os resultados obtidos nessa tese sugerem que o talco é um material promissor para uso em heteroestruturas de van der Waals tanto para estudos de física fundamental e para o uso em dispositivos optoeletrônicos.

Palavras-Chave: dicalcogenetos de metais de transição 2D, heteroestrutura de van der Waals, talco, magneto-ótica, spin-vale, efeitos excitônicos, FET.

Abstract

Two-dimensional (2D) systems have attracted great attention in the last years, for fundamental physics and in potential applications as optoelectronic devices. There is a great interest in transition metal dichalcogenides (TMDs) due to their direct gap for monolayer, which makes them optically active, with strong spin-valley and excitonic effects. In this work, we explore the use of talc dielectrics as a potentially clean alternative substrate to hexagonal boron nitride (hBN). We have prepared monolayer WS_2 /talc samples that exhibit high optical quality. As a result, we have observed several emission peaks associated with excitonic complexes, including "dark" trions (DT) and phonon replicas of DT. We have performed magneto-photoluminescence studies on high-quality monolayer WS_2 /talc at low temperature, under high magnetic fields (up to 30T) applied perpendicular to the monolayer plane. The g-factors of the emission peaks were extracted, and the nature of the observed peaks was discussed in detail. In addition, we fabricated field-effect devices (FET) based on $MoSe_2$ /talc and MoS_2 /talc. Our devices have shown small hysteresis, which does not depend strongly on the sweep rate, and negligible leakage current. In general, our experimental results suggest that talc is a promising material for protecting van der Waals (VdW) heterostructures to explore fundamental physics and for use in optoelectronics.

keywords: Transition metal dichalcogenide, van der Waals heterostructure, talc, magneto-optics, spin-valley, excitonic effects, FET.

Publications

- 1) Prando, G.A.; Severijnen, M.E.; Barcelos, I.D.; Zeitler, U.; Christianen, P.C.M.; Withers, F.; Gobato, Y.G. Revealing Excitonic Complexes in Monolayer WS₂ on Talc Dielectric. *Phys. Rev. Applied* **16**, 064055 – Published 23 December 2021. DOI: 10.1103/PhysRevApplied.16.064055.
- 2) Nutting, D; Prando, G.A.; Severijnen, M.E.; Barcelos, I. D.; Guo, S.; Christianen, P.C.M.; Zeitler, U.; Gobato, Y. G.; Withers, F. Electrical and optical properties of transition metal dichalcogenides on talc dielectrics. *Nanoscale*, 2021, 13, 15853-15858.DOI:10.1039/D1NR04723J.
- 3) Peimyoo, N.; Wu H-Y.; Escolar, J.; De Sanctis, A.; Prando, G. A.; Vollmer, F.; Withers, F.; Riis-Jensen, A.C.; Craciun, M.F.; Thygesen, K.S. Engineering Dielectric Screening for Potential-well Arrays of Excitons in 2D Materials. *ACS Appl. Mater. Interfaces* 2020, 12, 49, 55134–55140. DOI:10.1021/acsami.0c14696.
- 4) Teixeira, M.M.; Gobato, Y.G.; Gracia, L.; Silva, L.F.; Avansi, W.; Assis, M.; Oliveira, R.C.; Prando, G.A.; Andrés, J.; Longo, E. Towards a white-emitting phosphor Ca₁₀V₆O₂₅ based material. *Journal of Luminescence*, 220, 116990, 2020. DOI:10.1016/j.jlumin.2019.116990.
- 5) Alghamdi, H.; Gordo, V. O.; Schmidbauer, M.; Felix, J. F. ; Alhassan, S.; Alhassni, A.; Prando, G. A.; Coelho-Júnior, H.; Gunes, M.; Galete, H.; Gobato, Y. G.; Henini, M. Effect of thermal annealing on the optical and structural properties of (311)B and (001)GaAsBi/GaAs single quantum wells grown by MBE. *Journal of applied physics*, v. 127, p.125704-1-125704-1-10, 2020.DOI: 10.1063/1.5140447.

- 6) Franco, D. F.; Manzani, D.; Carvajal, E.E.; Prando, G.A.; Donoso, J.P.; Magon, C.J.; Antonio, S.G.; Gobato, Y. G.; Nalin, M.O. Optical and EPR studies of zinc phosphate glasses containing Mn^{2+} ions. *Journal of materials science*, v. 55, p. 9948, 2020. DOI: 10.1007/s10853-020-04725-0.

- 7) Prando, G. A.; Gordo, V.O.; Puustinen, J.; Joonas Hilska, J.;Alghamdi, H.; SÖM,G.; Güneş, M.; Akyol, M.; Souto,S.; Rodrigues, A. D. G.; Henini, M; Gobato, G. Y.; Guina, M. Exciton localization and structural disorder of GaAsBi/GaAs quantum wells grown by Molecular Beam Epitaxy on (311)B GaAs substrates. *Semiconductor science and technology*, v. 33, p.084002, 2018. DOI: 10.1088/1361-6641/aad02e.

Sumário

Agradecimentos.....	4
Resumo.....	6
Abstract.....	7
Publications	8
1. Introduction.....	11
References.....	19
2. Published articles.....	29
2.1.Revealing Excitonic Complexes in Monolayer WS ₂ on Talc Dielectric.....	30
I. Introduction.....	32
II. Sample preparation and experimental methods.....	34
III. Results and discussion.....	35
IV. Conclusion.....	45
Acknowledgments.....	46
References.....	47
Supplementary Information.....	55
2.2. Electrical and optical properties of transition metal dichalcogenides on talc dielectrics.. ..	63
I. Introduction.....	65
II. Results.....	68
III. Conclusion.....	74
Methods.....	75
Acknowledgments.....	76
References.....	77
Supplementary Information.....	83
3. Conclusions.....	97
References.....	98
Annex A.....	100

1. Introduction

Two-dimensional (2D) systems have attracted considerable attention in recent years [1]. Once it was shown that dimensionality reduction has surprising effects. Scientists have begun to search for other 2D crystals, like graphene, which exhibits properties that are different from their bulk counterparts. A new field of research emerged and today more than 1000 2D materials are known, including semiconductors, superconductors, metals, semimetals, and insulators [2–7].

Suitable materials for a 2D system are denominated van der Waals (vdW) crystals, with in-plane covalent bonds and weak vdW interactions between planes. Therefore, it is easy to exfoliate them and stack different layers to create vdW heterostructures with unique physical properties, making 2D materials promising systems for the next generation of electronic and optoelectronic devices such as transistors, light sensors, solar cells, biological sensors, etc. However, there are still many unanswered questions about the fundamental physics of these materials and many challenges for the actual production of high-quality samples and large-scale fabrication for commercial use[1,5,7–14].

An interesting group of 2D materials is group VI of transition metal dichalcogenides (TMDs), with formula MX_2 , where M is a transition metal, Tungsten (W) or Molybdenum (Mo), and X is a chalcogen, Sulphur (S), Selenium (Se), and Tellurium (Te). In general, TMD materials have different crystal structures. The most common polymorphs are the trigonal 1T, hexagonal 2H, and rhombohedral 3R phases, as shown in Figure 1, where the digits correspond to the number of covalent bonds X-M-X in the unit cell. Depending on the crystalline phase and density of states (DOS), the material can be a metal or a semiconductor. TMD semiconductors in monolayers (ML) have a hexagonal structure (2H) (Figures 1.1(f) and 1.1(e)), corresponding to the most stable phase. Unlike graphene, they have a non-zero band gap, desirable for optoelectronic applications [9,14–17].

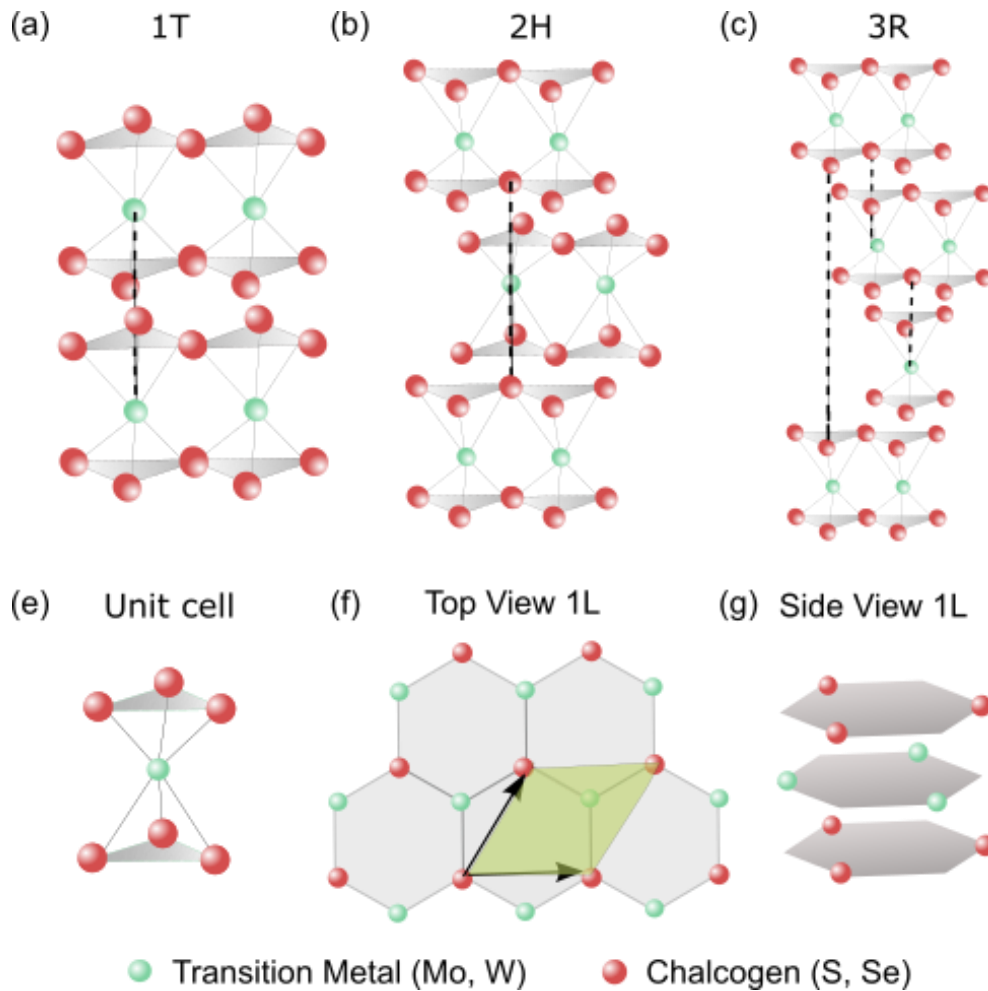


Figure 1.1 - Structural representation of (a) 1T, (b) 2H and (c) 3R TMD polytypes. The digits indicate the number of layers in the unit cell and the letters stand for trigonal, hexagonal, and rhombohedral, respectively. (e) the unit cell, (f) top view of 2H, and (g) side view of 1 layer.

The band structure for the TMD group VI in the 2H phase is shown in Figure 1.2. For the bulk and few layers (Figure 1.2(a)), the conduction band minimum (CBM) is located midway between the high symmetry points K, K', and Γ in the first Brillouin zone (BZ), while the valence band maximum (VBM) is located at the Γ -point. By reducing their dimensionality, the maximum of CBM and VBM shifts to points K and K' (Figure 1.2(b)). Consequently, they show a transition from the indirect to direct band gap for ML TMDs, accompanied by an increase in photoconductivity, absorption, and photoluminescence intensity [3,18,19]. The band gap for the group IV ML varies from 1 to 2.2 eV, which makes them

promising materials for optoelectronic devices such as light-emitting diodes, detectors in the visible range, light sensors, etc.[2,3,5,20–24].

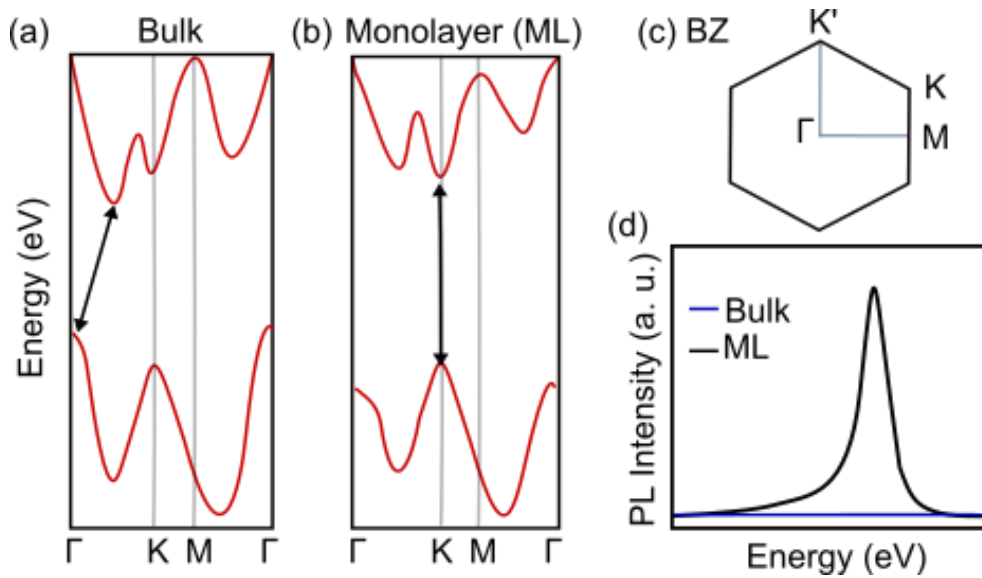


Figure 1.2 – Sketch of Band structure sketch for TMD group in (a) bulk and (b) Monolayer. (c) Brillouin zone with the high symmetry points and (d) Illustrated photoluminescence for bulk and monolayer.

Figure 1.2 is a simplified sketch of the band structure. In general, due to the heavy transition metal atoms, these systems have a strong spin-orbit interaction at the two non-equivalent points K and K' valleys, which play an important role in the band properties of ML TMDs and have a large SO splitting from 150 meV for MoS₂ to ~450 meV for WSe₂ in the VBM ($\Delta_{so,vb}$), as shown in Figure 1.3. Therefore, the valleys K and K' can be selected by optical selection rules with right and left circularly polarized light [25], a unique property that opens the possibility of developing devices based on valleytronics [5,26–35].

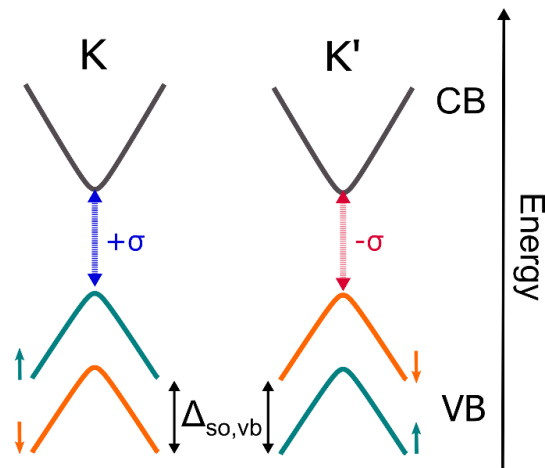


Figure 1.3 Band structure for 2D TMD at points K and K'.

They also have a smaller SO splitting at the conduction band ($\Delta_{so,cb}$) due to second-order effects of d-orbitals of the metal atoms and admixture of p-states of chalcogen (X) atoms. In particular, the SO splitting leads to a classification on bright ($\Delta_{so,cb} < 0$) and dark ($\Delta_{so,cb} > 0$) materials, where due to selection rules the bright materials (MoSe_2) have an optically active ground state transition with the aligned spins in the upper VB and lowest CB sub-bands, whereas the dark ones (MoS_2 , WS_2 , and WSe_2) have an optically inactive ground state transition [30,36]

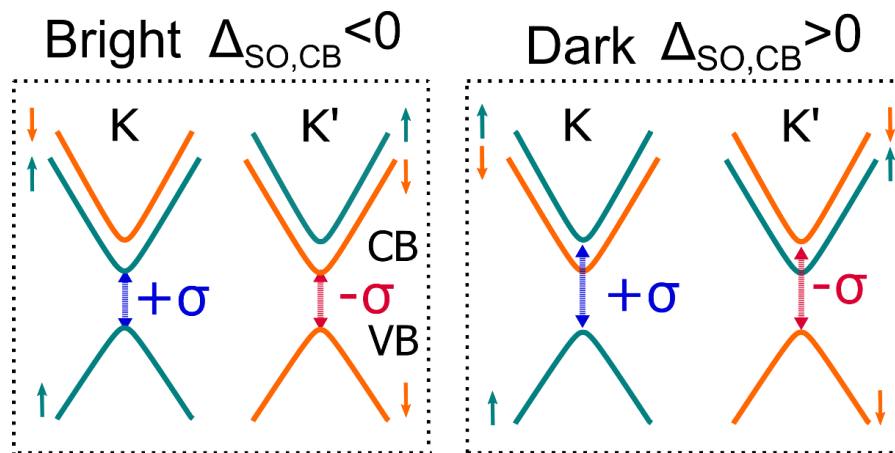


Figure 1.4 Band structure for 2D TMD, comparative materials (a) Bright and (b) dark at points K and K'

Optical transitions in direct-gap semiconductors occur when a photon is absorbed by an electron (e). It is excited from VB to CB leaving a quasiparticle, the hole (h), which forms an e-h pair, bound by Coulomb interaction, known as an

exciton. In the TMDs ML, the 2D confinement effects together with the reduction of electrostatic screening rise the Coulomb interaction, increasing the binding energy of the excitons to the order of 150-500 meV, which is very high compared to other quasi-2D systems such as GaAs quantum wells. Therefore, the light-matter interaction in 2D systems is dominated by excitons[16,37–42].

The high values of binding energy combined with the valley and spin degrees of freedom of ML TMDs promote the formation of multiple exciton complexes (see Figure 2.1). These rich many-body phenomena can be observed in photoluminescence (PL) experiments at low temperature on samples with high optical quality, i.e., small linewidth due to reduced disorders effects. In Figure 1.5 we compare typical normalized PL spectra at room and low temperatures of WS_2/talc [28,30,43,44].

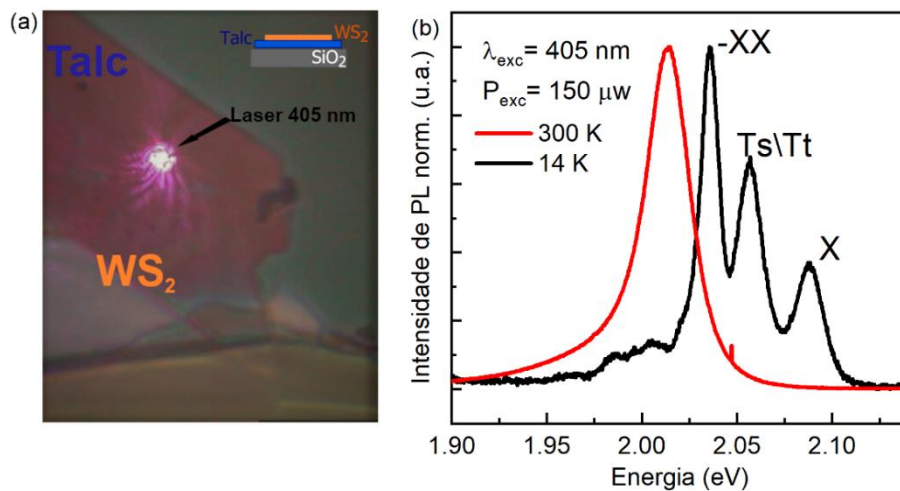


Figure 1.5 (a) WS_2/talc Sample and (b) Typical Photoluminescence spectra at room and low temperatures.

However, high-quality samples that allow observation and study of excitonic complexes, including dark trions, have only recently been achieved by improving the optical quality of ML TMDs encapsulated with hexagonal boron nitride (hBN) [45–48]. Prior to that 2D samples deposited on SiO_2 as a substrate showed poor quality due to disorder caused by impurities from trapped charges on SiO_2 and significant inhomogeneities in the band gap due to strain effects from surface

roughness[49–55]. The hBN is a vdW crystal with a hexagonal lattice and, for this reason, it is easily detached into a few layers. As a dielectric insulator (band gap of ~ 6 eV), it acts as a protection for the ML, insulates from trapped charges and impurities, also provides a smooth surface, and minimizes disorders effects, resulting in improved optical and electrical quality, i. e. reduces the width of luminescence line spectra and increases mobility. The 2D TMDs encapsulated with hBN have enabled the exploration of several new physical properties of many-body systems [56–59]. Therefore, high quality crystalline hBN is difficult to obtain and expensive. In this work, we explore the possibility of using natural talc as a potential alternative substrate for hBN[57,60].

Talc is a natural and abundant soft magnesium silicate mineral that is already widely used in industry and has similar properties to hBN. Its crystalline structure contains three octahedral Mg positions per four tetrahedral Si positions with chemical formula $\text{Mg}_3\text{Si}_4\text{O}_{10}(\text{OH})_2$, and it is a high gap dielectric layer material (band gap of 5.3 eV). Previous studies have shown that natural talc can also induce p-type doping in graphene, preserving its large electron mobility and enabling the observation of the quantum Hall effect at low magnetic fields [57,61–63].

We prepared the samples of ML WS_2 /talc using a standard dry transfer procedure (see Figure 1.6), which allows the preparation of samples with high optical quality [19,64]. The procedure consists of transferring the ML, which was first exfoliated with a scotch tape, onto a viscoelastic polydimethylsiloxane (PDMS) membrane. The PDMS is then placed on a microscope slide for inspection with an optical microscope and the ML is stacked in the talc layers previously exfoliated with scotch tape and finally on a SiO_2/Si substrate.

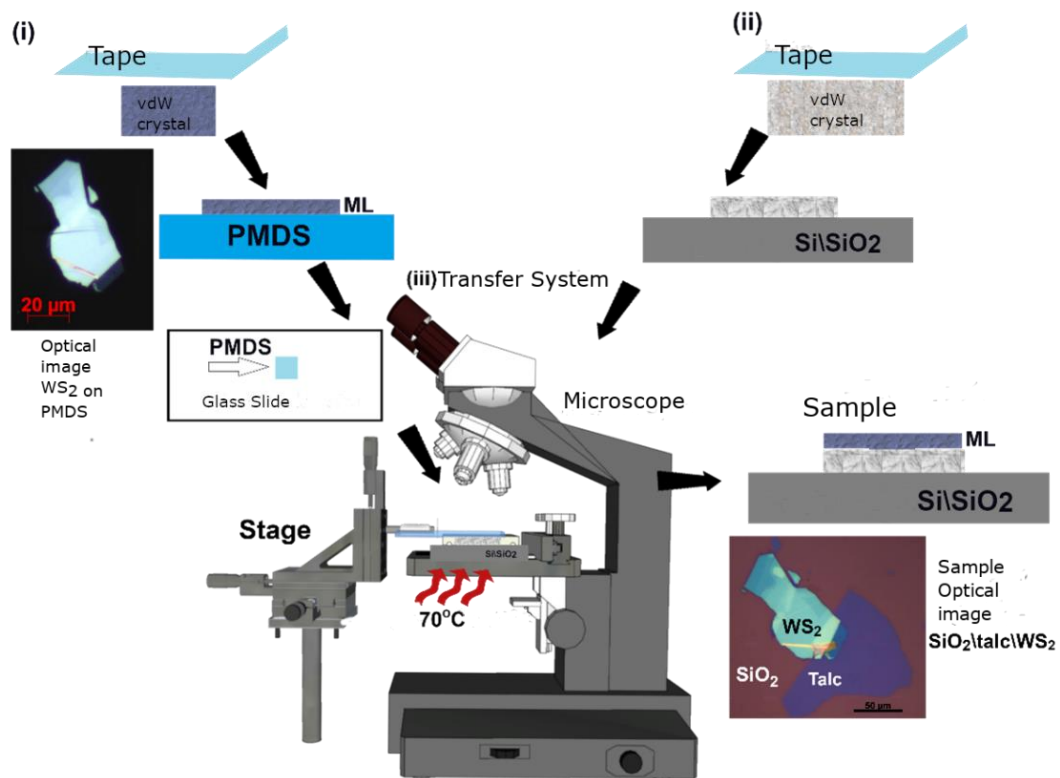


Figure 1.6 Illustration of standard Dry transfer method.

In the ML WS₂/talc sample, we performed a detailed study of magnetophotoluminescence at low temperatures under high magnetic fields (up to 30T) perpendicularly applied to the ML plane. In this study, we observed several emission peaks at low temperatures associated with excitonic complexes, including "dark" trions (DT) and phonon replicas of DT [30,45,65–70].

The magneto-PL measurements presented in Section 2.1 were performed with the setup shown in Figure 1.7 at the High Field Magnet Laboratory (HFML), an international research facility in Nijmegen, the Netherlands, using a 30-Tesla Bitter magnet. The technical specifications are described in the supporting information of the published article in Section 2.1. These measurements allowed us to study the valley properties of the exciton complexes and measure their g-factors (summarised in Annex A).

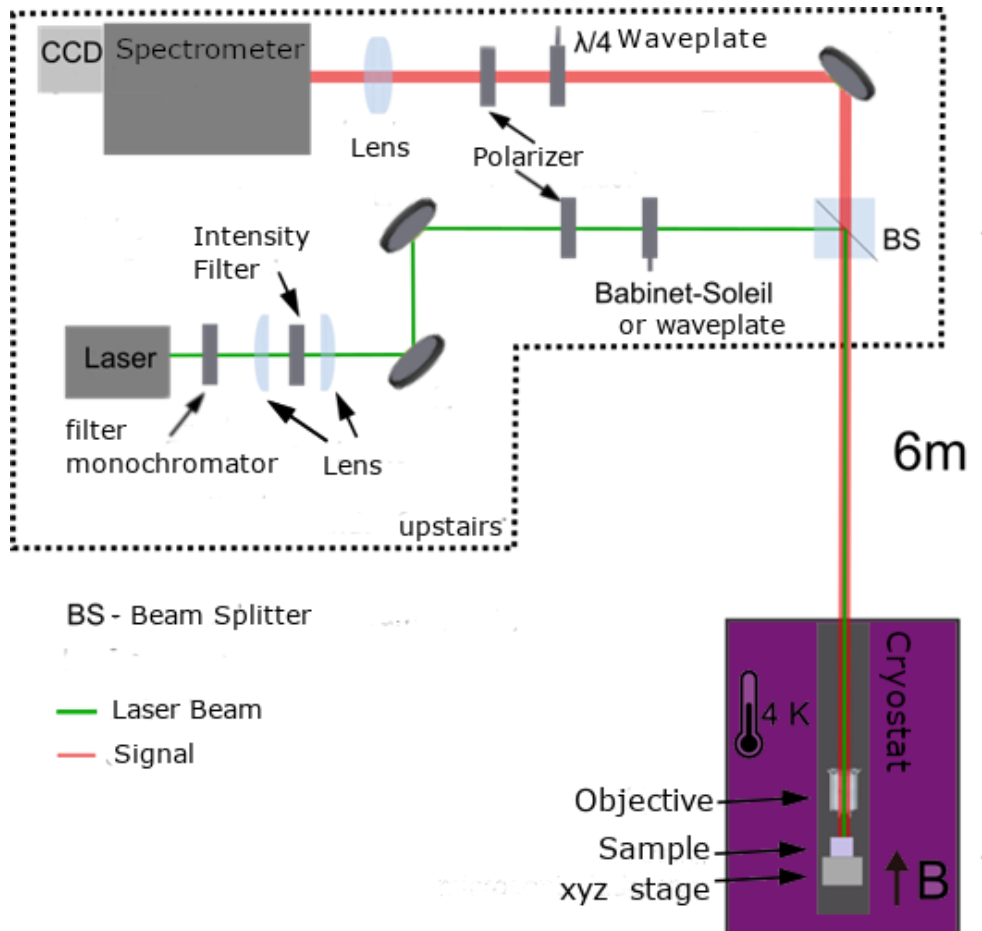


Figure 1.7 Sketch of the setups used for the measurements showing the main components. The dashed squares are the upper floor, the green line and red line illustrated laser and PL signal, respectively.

In addition, we have fabricated field-effect transistors (FET) based on MoSe₂/talc and MoS₂/talc in collaboration with the College of Exeter (Exeter, UK). The field-effect transistor (FET) is the fundamental building block of modern integrated circuits; new technologies that enable miniaturization on flexible and transparent devices are highly desirable for commercial use. The results are presented in the published article in Section 2.2. In general, the results of this work have shown that talc is a promising 2D oxide for the fabrication of van der Waals heterostructures/devices.

References

- [1] K.S. Novoselov, A.K. Geim, S. v. Morozov, D. Jiang, Y. Zhang, S. v. Dubonos, I. v. Grigorieva, A.A. Firsov, Electric Field Effect in Atomically Thin Carbon Films, *Science* (1979). 306 (2004) 666–669.DOI:10.1126/science.1102896.
- [2] W. Choi, N. Choudhary, G.H. Han, J. Park, D. Akinwande, Y.H. Lee, Recent development of two-dimensional transition metal dichalcogenides and their applications, *Materials Today*. 20 (2017) 116–130.DOI:10.1016/j.mattod.2016.10.002.
- [3] H.R. Gutiérrez, N. Perea-López, A.L. Elías, A. Berkdemir, B. Wang, R. Lv, F. López-Urías, V.H. Crespi, H. Terrones, M. Terrones, Extraordinary Room-Temperature Photoluminescence in Triangular WS₂ Monolayers, *Nano Letters*. 13 (2013) 3447–3454.DOI:10.1021/nl3026357.
- [4] K.S. Novoselov, A.H. Castro Neto, Two-dimensional crystals-based heterostructures: Materials with tailored properties, *Physica Scripta*. (2012).DOI:10.1088/0031-8949/2012/T146/014006.
- [5] D. Jariwala, V.K. Sangwan, L.J. Lauhon, T.J. Marks, M.C. Hersam, Emerging device applications for semiconducting two-dimensional transition metal dichalcogenides, *ACS Nano*. 8 (2014) 1102–1120.DOI:10.1021/nn500064s.
- [6] X. Wang, F. Xia, Stacked 2D materials shed light, *Nature Materials*. 14 (2015) 264–265.DOI:10.1038/nmat4218.
- [7] S. Manzeli, D. Ovchinnikov, D. Pasquier, O. V. Yazyev, A. Kis, 2D transition metal dichalcogenides, *Nature Reviews Materials*. 2 (2017).DOI:10.1038/natrevmats.2017.33.

- [8] A. V. Kolobov, J. Tominaga, Two-Dimensional Transition-Metal Dichalcogenides, Springer International Publishing, Cham, 2016.DOI:10.1007/978-3-319-31450-1.
- [9] H.Y. Hoh, Q. Bao, Introduction, in: 2D Materials for Photonic and Optoelectronic Applications, Elsevier, 2020: pp. 1–35.DOI:10.1016/B978-0-08-102637-3.00001-2.
- [10] K.S. Novoselov, A. Mishchenko, A. Carvalho, A.H. Castro Neto, 2D materials and van der Waals heterostructures, *Science (1979)*. 353 (2016).DOI:10.1126/science.aac9439.
- [11] A.K. Geim, I. V. Grigorieva, Van der Waals heterostructures, *Nature*. 499 (2013) 419–425.DOI:10.1038/nature12385.
- [12] H. Zeng, J. Dai, W. Yao, D. Xiao, X. Cui, Valley polarization in MoS 2 monolayers by optical pumping, *Nature Nanotechnology*. 7 (2012) 490–493.DOI:10.1038/nnano.2012.95.
- [13] A. Arora, Magneto-optics of layered two-dimensional semiconductors and heterostructures: Progress and prospects, *Journal of Applied Physics*. 129 (2021).DOI:10.1063/5.0042683.
- [14] M. Koperski, M.R. Molas, A. Arora, K. Nogajewski, A.O. Slobodeniuk, C. Faugeras, Optical properties of atomically thin transition metal dichalcogenides : Observations and puzzles, (n.d.).
- [15] M. Chhowalla, H.S. Shin, G. Eda, L.J. Li, K.P. Loh, H. Zhang, The chemistry of two-dimensional layered transition metal dichalcogenide nanosheets, *Nature Chemistry*. 5 (2013) 263–275.DOI:10.1038/nchem.1589.
- [16] C. Cong, J. Shang, Y. Wang, T. Yu, Optical Properties of 2D Semiconductor WS₂, *Advanced Optical Materials*. 6 (2018) 1–15.DOI:10.1002/adom.201700767.

- [17] A. Kuc, Low-dimensional transition-metal dichalcogenides, *Chemical Modelling*. 11 (2015) 1–29.DOI:10.1039/9781782620112-00001.
- [18] H. Zeng, X. Cui, An optical spectroscopic study on two-dimensional group-VI transition metal dichalcogenides, *Chemical Society Reviews*. 44 (2015) 2629–2642.DOI:10.1039/c4cs00265b.
- [19] A. McCreary, A. Berkdemir, J. Wang, M.A. Nguyen, A.L. Elías, N. Perea-López, K. Fujisawa, B. Kabius, V. Carozo, D.A. Cullen, T.E. Mallouk, J. Zhu, M. Terrones, Distinct photoluminescence and Raman spectroscopy signatures for identifying highly crystalline WS₂ monolayers produced by different growth methods, *Journal of Materials Research*. 31 (2016) 931–944.DOI:10.1557/jmr.2016.47.
- [20] P. Properties, Graphene-Based Light Sensing: Fabrication, Characterisation, Physical Properties and Performance, (2018).DOI:10.3390/ma11091762.
- [21] S. Two-dimensional, D. Jariwala, V.K. Sangwan, L.J. Lauhon, T.J. Marks, M.C. Hersam, Emerging Device Applications for, (2014) 1102–1120.DOI:10.1021/nn500064s.
- [22] T. Review, W. Xin-ran, S. Yi, Z. Rong, H. Doi, Field-effect transistors based on two-dimensional materials, 22 (2013) 1–15.DOI:10.1088/1674-1056/22/9/098505.
- [23] S. Mansouri, A. Salimi, F. Ghasemi, Biosensors and Bioelectronics An ultrasensitive detection of miRNA-155 in breast cancer via direct hybridization assay using two-dimensional molybdenum disulfide field-effect transistor biosensor, *Biosensors and Bioelectronic*. 105 (2018) 6–13.DOI:10.1016/j.bios.2018.01.009.
- [24] W. Zheng, Y. Jiang, X. Hu, H. Li, Z. Zeng, X. Wang, A. Pan, Light Emission Properties of 2D Transition Metal Dichalcogenides: Fundamentals and

- Applications, *Advanced Optical Materials*. 6 (2018).DOI:10.1002/adom.201800420.
- [25] T. Cao, G. Wang, W. Han, H. Ye, C. Zhu, J. Shi, Q. Niu, P. Tan, E. Wang, B. Liu, J. Feng, Valley-selective circular dichroism of monolayer molybdenum disulphide, *Nature Communications*. 3 (2012) 885–887.DOI:10.1038/ncomms1882.
- [26] M. He, P. Rivera, D. Van Tuan, N.P. Wilson, M. Yang, T. Taniguchi, K. Watanabe, J. Yan, D.G. Mandrus, H. Yu, H. Dery, W. Yao, X. Xu, Valley phonons and exciton complexes in a monolayer semiconductor, *Nature Communications*. 11 (2020) 1–7.DOI:10.1038/s41467-020-14472-0.
- [27] H. Yu, X. Cui, X. Xu, W. Yao, Valley excitons in two-dimensional semiconductors, *National Science Review*. 2 (2015) 57–70.DOI:10.1093/nsr/nwu078.
- [28] G. Bin Liu, W.Y. Shan, Y. Yao, W. Yao, D. Xiao, Three-band tight-binding model for monolayers of group-VIB transition metal dichalcogenides, *Physical Review B - Condensed Matter and Materials Physics*. 88 (2013) 1–10.DOI:10.1103/PhysRevB.88.085433.
- [29] X. Zheng, X. Zhang, Excitons in Two-Dimensional Materials, in: *Advances in Condensed-Matter and Materials Physics - Rudimentary Research to Topical Technology*, IntechOpen, 2020: p. 13.DOI:10.5772/intechopen.90042.
- [30] Z. Li, T. Wang, S. Miao, Z. Lian, S.F. Shi, Fine structures of valley-polarized excitonic states in monolayer transitional metal dichalcogenides, *Nanophotonics*. 9 (2020) 1811–1829.DOI:10.1515/nanoph-2020-0054.
- [31] G. Plechinger, P. Nagler, J. Kraus, N. Paradiso, C. Strunk, C. Schüller, T. Korn, Identification of excitons, trions and biexcitons in single-layer WS₂, *Physica Status Solidi - Rapid Research Letters*. 9 (2015) 457–461.DOI:10.1002/pssr.201510224.

- [32] S. Malte, B. Gunnar, R. Marten, B. Rudolf, K. Andreas, M. Ermin, Dark and bright exciton formation, thermalization, and photoluminescence in monolayer transition metal dichalcogenides, *2D Materials*. 5 (2018) 35017.
- [33] W. Zhao, Z. Ghorannevis, L. Chu, M. Toh, C. Kloc, P.H. Tan, G. Eda, Evolution of electronic structure in atomically thin sheets of WS₂ and WSe₂, *ACS Nano*. 7 (2013) 791–797. DOI:10.1021/nn305275h.
- [34] H. Zeng, X. Cui, An optical spectroscopic study on two-dimensional group-VI transition metal dichalcogenides, *Chemical Society Reviews*. 44 (2015) 2629–2642. DOI:10.1039/c4cs00265b.
- [35] H. Yuan, X. Wang, B. Lian, H. Zhang, X. Fang, B. Shen, G. Xu, Y. Xu, S.C. Zhang, H.Y. Hwang, Y. Cui, Generation and electric control of spin-valley-coupled circular photogalvanic current in WSe₂, *Nature Nanotechnology*. 9 (2014) 851–857. DOI:10.1038/nnano.2014.183.
- [36] M. Zinkiewicz, A.O. Slobodeniuk, T. Kazimierczuk, P. Kapuściński, K. Oreszczuk, M. Grzeszczyk, M. Bartos, K. Nogajewski, K. Watanabe, T. Taniguchi, C. Faugeras, P. Kossacki, M. Potemski, A. Babiński, M.R. Molas, Neutral and charged dark excitons in monolayer WS₂, *Nanoscale*. 12 (2020) 18153–18159. DOI:10.1039/d0nr04243a.
- [37] N. Peimyoo, H.Y. Wu, J. Escolar, A. De Sanctis, G. Prando, F. Vollmer, F. Withers, A.C. Riis-Jensen, M.F. Craciun, K.S. Thygesen, S. Russo, Engineering Dielectric Screening for Potential-well Arrays of Excitons in 2D Materials, *ACS Applied Materials and Interfaces*. 12 (2020) 55134–55140. DOI:10.1021/acsami.0c14696.
- [38] N. Peimyoo, J. Shang, C. Cong, X. Shen, X. Wu, E.K.L. Yeow, T. Yu, Nonblinking, intense two-dimensional light emitter: Monolayer WS₂ Triangles, *ACS Nano*. 7 (2013) 10985–10994. DOI:10.1021/nn4046002.

- [39] A. Raja, A. Chaves, J. Yu, G. Arefe, H.M. Hill, A.F. Rigosi, T.C. Berkelbach, P. Nagler, C. Schüller, T. Korn, C. Nuckolls, J. Hone, L.E. Brus, T.F. Heinz, D.R. Reichman, A. Chernikov, Coulomb engineering of the bandgap and excitons in two-dimensional materials, *Nature Communications*. 8 (2017) 1–7. DOI:10.1038/ncomms15251.
- [40] J. Wang, G. Li, L. Li, Synthesis Strategies about 2D Materials, in: *Two-Dimensional Materials - Synthesis, Characterization and Potential Applications*, InTech, 2016. DOI:10.5772/63918.
- [41] G. Bastard, E.E. Mendez, L.L. Chang, L. Esaki, Exciton binding energy in quantum wells, *Physical Review B*. 26 (1982) 1974–1979. DOI:10.1103/PhysRevB.26.1974.
- [42] B. Zhu, X. Chen, X. Cui, Exciton binding energy of monolayer WS₂, *Scientific Reports*. 5 (2015). DOI:10.1038/srep09218.
- [43] Z. He, W. Xu, Y. Zhou, X. Wang, Y. Sheng, Y. Rong, S. Guo, J. Zhang, J.M. Smith, J.H. Warner, Biexciton Formation in Bilayer Tungsten Disulfide, *ACS Nano*. 10 (2016) 2176–2183. DOI:10.1021/acsnano.5b06678.
- [44] A. Arora, Magneto-optics of layered two-dimensional semiconductors and heterostructures: Progress and prospects, *Journal of Applied Physics*. 129 (2021). DOI:10.1063/5.0042683.
- [45] M. Grzeszczyk, M. Bartos, K. Nogajewski, K. Watanabe, T. Taniguchi, M.R. Molas, C. Faugeras, P. Kossacki, M. Potemski, A. Babin, Excitonic Complexes in n-Doped WS₂ Monolayer, (2021). DOI:10.1021/acs.nanolett.0c05021.
- [46] G. Plechinger, P. Nagler, A. Arora, A. Granados Del Águila, M. v. Ballottin, T. Frank, P. Steinleitner, M. Gmitra, J. Fabian, P.C.M. Christianen, R. Bratschitsch, C. Schüller, T. Korn, Excitonic Valley Effects in Monolayer

- WS2 under High Magnetic Fields, *Nano Letters*. 16 (2016) 7899–7904. DOI:10.1021/acs.nanolett.6b04171.
- [47] Z. Ye, T. Cao, K. O'Brien, H. Zhu, X. Yin, Y. Wang, S.G. Louie, X. Zhang, Probing excitonic dark states in single-layer tungsten disulphide, *Nature*. 513 (2014) 214–218. DOI:10.1038/nature13734.
- [48] Z. Ye, T. Cao, K. O'Brien, H. Zhu, X. Yin, Y. Wang, S.G. Louie, X. Zhang, Probing excitonic dark states in single-layer tungsten disulphide, *Nature*. 513 (2014) 214–218. DOI:10.1038/nature13734.
- [49] Z.W. Wang, R.Z. Li, X.Y. Dong, Y. Xiao, Z.Q. Li, Temperature dependence of the excitonic spectra of monolayer transition metal dichalcogenides, *Frontiers of Physics*. 13 (2018). DOI:10.1007/s11467-018-0786-y.
- [50] E. Margapoti, M.M. Asmar, S.E. Ulloa, The Effects of Substrates on 2D Crystals, in: *Advanced 2D Materials*, wiley, 2016: pp. 67–113. DOI:10.1002/9781119242635.ch3.
- [51] U. Wurstbauer, B. Miller, S. Lippert, L.M. Schneider, D. Renaud, K.N. Kang, O. Ajayi, Influence of the substrate material on the optical properties of tungsten diselenide monolayers Influence of the substrate material on the optical properties of tungsten diselenide monolayers, (2017).
- [52] Y. Yu, Y. Yu, C. Xu, Y.Q. Cai, L. Su, Y. Zhang, Y.W. Zhang, K. Gundogdu, L. Cao, Engineering Substrate Interactions for High Luminescence Efficiency of Transition-Metal Dichalcogenide Monolayers, *Advanced Functional Materials*. 26 (2016) 4733–4739. DOI:10.1002/adfm.201600418.
- [53] S. Lippert, L.M. Schneider, D. Renaud, K.N. Kang, O. Ajayi, J. Kuhnert, M.U. Halbich, O.M. Abdulmunem, X. Lin, K. Hassoon, S. Edalati-Boostan, Y.D. Kim, W. Heimbrod, E.H. Yang, J.C. Hone, A. Rahimi-Iman, Influence

- of the substrate material on the optical properties of tungsten diselenide monolayers, *2D Materials*. 4 (2017).DOI:10.1088/2053-1583/aa5b21.
- [54] M. Buscema, G.A. Steele, H.S.J. van der Zant, A. Castellanos-Gomez, The effect of the substrate on the Raman and photoluminescence emission of single-layer MoS₂, *Nano Research*. 7 (2014) 561–571.DOI:10.1007/s12274-014-0424-0.
- [55] D. Rhodes, S.H. Chae, R. Ribeiro-Palau, J. Hone, Disorder in van der Waals heterostructures of 2D materials, *Nature Materials*. 18 (2019) 541–549.DOI:10.1038/s41563-019-0366-8.
- [56] D. Rhodes, S.H. Chae, R. Ribeiro-Palau, J. Hone, Disorder in van der Waals heterostructures of 2D materials, *Nature Materials*. 18 (2019) 541–549.DOI:10.1038/s41563-019-0366-8.
- [57] A.R. Cadore, E. Mania, A.B. Alencar, N.P. Rezende, S. de Oliveira, K. Watanabe, T. Taniguchi, H. Chacham, L.C. Campos, R.G. Lacerda, Enhancing the response of NH₃ graphene-sensors by using devices with different graphene-substrate distances, *Sensors and Actuators, B: Chemical*. 266 (2018) 438–446.DOI:10.1016/j.snb.2018.03.164.
- [58] E. Margapoti, M.M. Asmar, S.E. Ulloa, The Effects of Substrates on 2D Crystals, 2016.DOI:10.1002/9781119242635.ch3.
- [59] E. Courtade, B. Han, S. Nakhaie, C. Robert, X. Marie, P. Renucci, T. Taniguchi, K. Watanabe, L. Geelhaar, J.M.J. Lopes, B. Urbaszek, Spectrally narrow exciton luminescence from monolayer MoS₂ and MoSe₂ exfoliated onto epitaxially grown hexagonal BN, *Applied Physics Letters*. 113 (2018) 1–5.DOI:10.1063/1.5033554.
- [60] E. Mania, A.B. Alencar, A.R. Cadore, B.R. Carvalho, K. Watanabe, T. Taniguchi, B.R.A. Neves, H. Chacham, L.C. Campos, Spontaneous doping on high quality talc-graphene-hBN van der Waals heterostructures, *2D Materials*. 4 (2017).DOI:10.1088/2053-1583/aa76f4.

- [61] A.U. Federal, M. Gerais, M. Gerais, Experimental and theoretical investigations of monolayer and few-layer talc, (2015).DOI:10.1088/2053-1583/2/1/015004.
- [62] I.D. Barcelos, A.R. Cadore, A.B. Alencar, F.C.B. Maia, E. Mania, R.F. Oliveira, C.C.B. Bufon, Â. Malachias, R.O. Freitas, R.L. Moreira, H. Chacham, Infrared Fingerprints of Natural 2D Talc and Plasmon-Phonon Coupling in Graphene-Talc Heterostructures, *ACS Photonics*. 5 (2018) 1912–1918.DOI:10.1021/acsp Photonics.7b01017.
- [63] E. Mania, A.B. Alencar, A.R. Cadore, B.R. Carvalho, K. Watanabe, T. Taniguchi, B.R.A. Neves, H. Chacham, L.C. Campos, Spontaneous doping on high quality talc-graphene-hBN van der Waals heterostructures, *2D Materials*. 4 (2017).DOI:10.1088/2053-1583/aa76f4.
- [64] A. Castellanos-Gomez, M. Buscema, R. Molenaar, V. Singh, L. Janssen, H.S.J. Van Der Zant, G.A. Steele, Deterministic transfer of two-dimensional materials by all-dry viscoelastic stamping, *2D Materials*. 1 (2014).DOI:10.1088/2053-1583/1/1/011002.
- [65] P. Nagler, M. V. Ballottin, A.A. Mitioglu, M. V. Durnev, T. Taniguchi, K. Watanabe, A. Chernikov, C. Schüller, M.M. Glazov, P.C.M. Christianen, T. Korn, Zeeman Splitting and Inverted Polarization of Biexciton Emission in Monolayer WS₂, *Physical Review Letters*. 121 (2018) 57402.DOI:10.1103/PhysRevLett.121.057402.
- [66] M. Paur, A.J. Molina-Mendoza, R. Bratschitsch, K. Watanabe, T. Taniguchi, T. Mueller, Electroluminescence from multi-particle exciton complexes in transition metal dichalcogenide semiconductors, *Nature Communications*. 10 (2019) 1–7.DOI:10.1038/s41467-019-09781-y.
- [67] G. Plechinger, P. Nagler, A. Arora, R. Schmidt, A. Chernikov, A.G. del Águila, P.C.M. Christianen, R. Bratschitsch, C. Schüller, T. Korn, Trion fine

- structure and coupled spin-valley dynamics in monolayer tungsten disulfide, *Nature Communications*. 7 (2016).DOI:10.1038/ncomms12715.
- [68] Z. Li, T. Wang, S. Miao, Z. Lian, S.F. Shi, Fine structures of valley-polarized excitonic states in monolayer transitional metal dichalcogenides, *Nanophotonics*. 9 (2020) 1811–1829.DOI:10.1515/nanoph-2020-0054.
- [69] J. Shang, X. Shen, C. Cong, N. Peimyoo, B. Cao, M. Eginligil, T. Yu, Observation of excitonic fine structure in a 2D transition-metal dichalcogenide semiconductor, *ACS Nano*. 9 (2015) 647–655.DOI:10.1021/nn5059908.
- [70] M. Zinkiewicz, T. Woźniak, T. Kazimierczuk, P. Kapuscinski, K. Oreszczuk, M. Grzeszczyk, M. Bartoš, K. Nogajewski, K. Watanabe, T. Taniguchi, C. Faugeras, P. Kossacki, M. Potemski, A. Babiński, M.R. Molas, Excitonic Complexes in n-Doped WS₂ Monolayer, *Nano Letters*. 21 (2021) 2519–2525.DOI:10.1021/acs.nanolett.0c05021.

2. Published articles

This section presents the published articles that compose this doctoral thesis with the supplementary information.

2.1 - Revealing Excitonic Complexes in Monolayer WS₂ on Talc Dielectric

PHYSICAL REVIEW APPLIED **16**, 064055 (2021)

Revealing Excitonic Complexes in Monolayer WS₂ on Talc Dielectric

Gabriela Augusta Prando,¹ Marion E. Severijnen,^{2,3} Ingrid D. Barcelos⁴, Uli Zeitler^{2,3},
Peter C. M. Christianen,^{2,3} Freddie Withers⁵, and Yara Galvão Gobato^{1,2,*}


¹*Physics Department, Federal University of São Carlos, São Carlos, Brazil*

²*High Field Magnet Laboratory (HFML - EMFL), Radboud University, 6525 ED, Nijmegen, Netherlands*

³*Institute for Molecules and Materials, Radboud University, 6525 AJ, Nijmegen, Netherlands*

⁴*Brazilian Synchrotron Light Laboratory (LNLS), Brazilian Center for Research in Energy and Materials (CNPEM), 13083-970 Campinas, SP, Brazil*

⁵*College of Engineering, Mathematics and Physical Sciences, University of Exeter, Exeter EX4 4QF, United Kingdom*

 (Received 15 August 2021; revised 16 November 2021; accepted 17 November 2021; published 23 December 2021)

We report on a detailed study of low-temperature photoluminescence (PL) and magnetophotoluminescence under perpendicular magnetic fields (up to 30 T) and circularly polarized excitation on high-quality monolayer (ML) WS₂ on a thick layer (120 nm) of talc dielectric. Remarkably, we obtained high-quality samples without any evidence of localized exciton emission at low temperature and a PL linewidth comparable to that of WS₂/h-BN samples. As a consequence, we observe well-resolved emission peaks at low temperature due to the formation of excitonic complexes, including a dark-trion (DT) state and phonon replicas of the DT without the application of an in-plane magnetic field. The nature of the emission peaks, the magnetic field dependence of the degree of polarization, and *g* factors are discussed in detail and compared with the corresponding results obtained for h-BN encapsulated transition-metal dichalcogenide (TMD) samples. We observe that under σ^+ -polarized excitation the sign of the circular polarization of biexcitons is reversed under higher magnetic fields. In addition, the dark-trion polarization increases considerably with increasing perpendicular magnetic field, demonstrating different behavior compared with previous studies of dark trions on monolayer WSe₂. Our results suggest that talc is indeed a promising layered material for the surface protection of ML TMDs and to explore fundamental physics in view of applications in optoelectronic devices.

DOI: [10.1103/PhysRevApplied.16.064055](https://doi.org/10.1103/PhysRevApplied.16.064055)

Revealing Excitonic Complexes in Monolayer WS₂ on Talc dielectric

Gabriela Augusta Prando¹, Marion E. Severijnen^{2,3}, Ingrid D. Barcelos⁴, Uli Zeitler^{2,3}, Peter C. M. Christianen^{2,3}, Freddie Withers⁵, Yara Galvão Gobato^{1,2}

¹ Physics Department, Federal University of São Carlos, São Carlos, Brazil;

² High Field Magnet Laboratory (HFML - EMFL), Radboud University, 6525 ED Nijmegen, The Netherlands.

³ Radboud University, Institute for Molecules and Materials, 6525 AJ Nijmegen, The Netherlands.

⁴ Brazilian Synchrotron Light Laboratory (LNLS), Brazilian Center for Research in Energy and Materials (CNPEM), 13083-970 Campinas, SP, Brazil.

⁵ College of Engineering, Mathematics and Physical Sciences, University of Exeter, Exeter EX4 4QF, United Kingdom.

We report on a detailed study of low temperature photoluminescence (PL) and magneto-photoluminescence under perpendicular magnetic field (up to 30 T) and circularly polarized excitation on high quality monolayer (ML) WS₂ on a thick layer (120 nm) of talc dielectric. Remarkably, we have obtained high quality samples without any evidence of localized exciton emission at low temperature and a PL linewidth comparable to WS₂/h-BN samples. As a consequence, we have observed well resolved emission peaks at low temperature due to the formation of excitonic complexes, including dark trion (DT) state and phonon replicas of DT without the application of an in-plane magnetic field. The nature of the emission peaks, the magnetic field dependence of polarization degree and *g*-factors are discussed in detail and compared with corresponding results obtained in h-BN encapsulated transition metal dichalcogenide (TMD) samples. We have observed that under $\sigma+$ polarized excitation the sign of the circular polarization of biexcitons is reversed under higher magnetic fields. In addition, the dark trion polarization increases considerably with increasing perpendicular magnetic field, demonstrating a different behavior compared to previous studies of dark trions on monolayer WSe₂. Our results suggest that talc is indeed a promising layered material for surface protection of ML TMDs and to explore fundamental physics in view of applications in optoelectronic devices.

I. Introduction

Two-dimensional (2D) transition metal dichalcogenides (TMDs) are very attractive systems for studying the physics of strong spin-valley coupling and excitonic effects [1,2]. The strong Coulomb interaction in monolayer (ML) TMDs results in the formation of different excitonic complexes involving electrons and holes in the conduction (CB) and valence (VB) bands of the K and K' valleys [1–10]. Several dark and bright excitonic complexes were recently unveiled due to the improved optical quality of ML TMDs as a result of hexagonal Boron Nitride (h -BN) encapsulation, which reduces considerably the linewidth of the photoluminescence (PL) emission and increases its intensity [4,11]. Dark excitonic complexes are not allowed to undergo radiative recombination due to spin conservation and/or momentum selection rules [5,7,12–14]. Dark excitons are of particular interest because of their long lifetimes and possibly long valley coherence times [5,15]. Furthermore, despite intense recent investigations of the fine structure of bright and dark excitonic complexes in ML TMDs, the detailed nature of the lower energy emission peaks of monolayer TMDs, such as WS_2 , is still unresolved. Most of the magneto-PL studies have been performed on ML TMDs [16] on SiO_2 or on MLs encapsulated by h -BN, the latter of which shows high quality optical properties of significant relevance for future device applications and for fundamental physics investigations. However, it is also interesting to develop alternative, layered dielectric and atomically flat substrates, to circumvent the complex growth requirements for high quality h -BN. Moreover, from a fundamental point of view, studies on the impact of different dielectric materials on doping and the magneto-optical properties of monolayer TMDs are scarce.

Talc (chemical formula $Mg_3Si_4O_{10}(OH)_2$) is an abundant van der Waals layered magnesium silicate mineral [17], whose crystalline structure contains three octahedral Mg positions per four tetrahedral Si positions. It is an insulator with a high bandgap (~ 5.3 eV) [17] and a high dielectric constant up to 9 depending on its doping [18,19]. Talc has a high thermal stability [18] and is chemically inert [18,20]. In contrast to SiO_2 , talc is a genuine 2D natural silicate

dielectric material which possesses atomically flat surfaces [18,20]. Previous reports have demonstrated the use of talc within graphene transistors and the obtained results compare well to those obtained using *h*-BN substrates [18]. These properties are promising for possible applications as an insulating medium compatible with atomically thin *p-n* junctions and field-effect transistors for ultra-compact devices [18,20]. Therefore, talc has excellent properties making it a potential candidate as a low-cost dielectric material. More recently, it was observed that MoS₂/talc samples with a talc thickness of 30 nm present an enhancement in the PL intensity and a reduced PL linewidth (40 - 45 meV, depending on the laser position) at 300 K, as compared to MoS₂/SiO₂ (50 - 80 meV) [21]. It was also shown that talc is a promising dielectric for 2D devices [22]. However, there is no previous detailed study of PL and magneto-PL of ML TMD/talc at low temperatures. Since the PL linewidths at low temperature usually reflects homogeneous and/or inhomogeneous contributions to the PL spectrum, such experiments are essential to probe the ultimate optical quality of ML TMDs.

In this work, we have investigated the optical properties of ML WS₂ deposited on a thick talc layer. Our findings demonstrate that the use of a few layers of talc results in high-quality, doped WS₂ MLs with a reduced photoluminescence linewidth and interesting valley properties. We have probed the optical properties of ML WS₂ on talc at low temperature and magnetic fields up to 30 T. We observed several emission peaks due to the formation of different bright and dark exciton complexes with different *g*-factors. In general, our results show that talc is a promising layered material to explore fundamental physics and also for possible application in novel opto-electronic devices based on high quality doped TMDs.

II. Sample preparation and experimental methods

Our samples were prepared by conventional all-dry transfer techniques and consist of a ML of WS_2 (bulk crystals from HQ Graphene) on a layer of talc (natural crystal from a mine of Ouro Preto, Minas Gerais, Brazil). The talc layers were exfoliated by Scotch tape and placed onto SiO_2/Si substrates. The WS_2 MLs were first exfoliated by Scotch tape and later exfoliated again on a polydimethylsiloxane (PDMS) stamp and placed on a glass slide for inspection with an optical microscope.

For the experiments the ML WS_2 sample was mounted on Attocube piezoelectric x - y - z translation stages to control the sample position with submicron precision. The sample was cooled by helium exchange gas (temperatures around 4.2 K) within a liquid helium bath cryostat, placed in a Florida-Bitter magnet with a maximum magnetic field strength of $B = 30$ T. The PL measurements were performed using a continuous-wave green laser with a photon energy of 2.33 eV, which was focused by an Attocube objective (40x, numerical aperture $NA = 0.55$) to a spot size of about 3 μm . The resultant PL signal was collected by the same objective and measured by a Princeton spectrometer (Acton SpectraPro-300i) equipped with a liquid-nitrogen cooled Charge Coupled Device (PyLoN from Princeton Instruments). Circular polarization was controlled independently for the excitation and detection beams by using appropriate optics, consisting of quarter wave plates and linear polarizers. The light propagation was parallel to the direction of the magnetic field (Faraday configuration).

III. Results and discussion

Fig.1 shows schematically the configurations of the different excitonic states for a *n*-doped monolayer WS₂: the bright neutral exciton (X), dark neutral exciton (DX), bright intervalley negative trion (Tt), bright intravalley negative trion (Ts), negative dark trion (DT), biexciton (XX) and charged biexciton (XX⁻). Particularly, the dark exciton (DX) at the *K* valley has an electron in the lowest CB level and a hole in the highest VB level. A dark negative trion (DT) can be formed by an exciton in the *K* valley and an extra electron in the *K'* valley. Furthermore, strong Coulomb coupling gives rise to strong exciton–exciton interactions, resulting in the formation of biexcitons (XX), formed by bright and dark excitons in the *K* and *K'* valleys. Similarly, the charged biexciton (XX⁻) can be formed with an extra electron in the *K* valley [5]. Recently, it was reported that the negative dark trion (DT) configuration results in two different recombination channels [12,23], depending on the electron involved in the emission process itself. One emission pathway (TD) involves recombination of an electron-hole pair from the same *K* or *K'* point via an intravalley spin-forbidden transition [12]. The other transition (TI) involves recombination of an electron and a hole from different valleys through an intervalley momentum-forbidden transition [12]. The lower energy transition (TI) was recently observed at zero magnetic field and the higher energy transition (TD) was observed under an applied parallel magnetic field (Voigt configuration) [12]. The energy separation between these two dark trion transitions was reported to be on the order of 530 μeV for ML WS₂ and the reported *g*-factors values for the TD and TI transitions were found to be equal to -8.9 and -13.7, respectively [12].

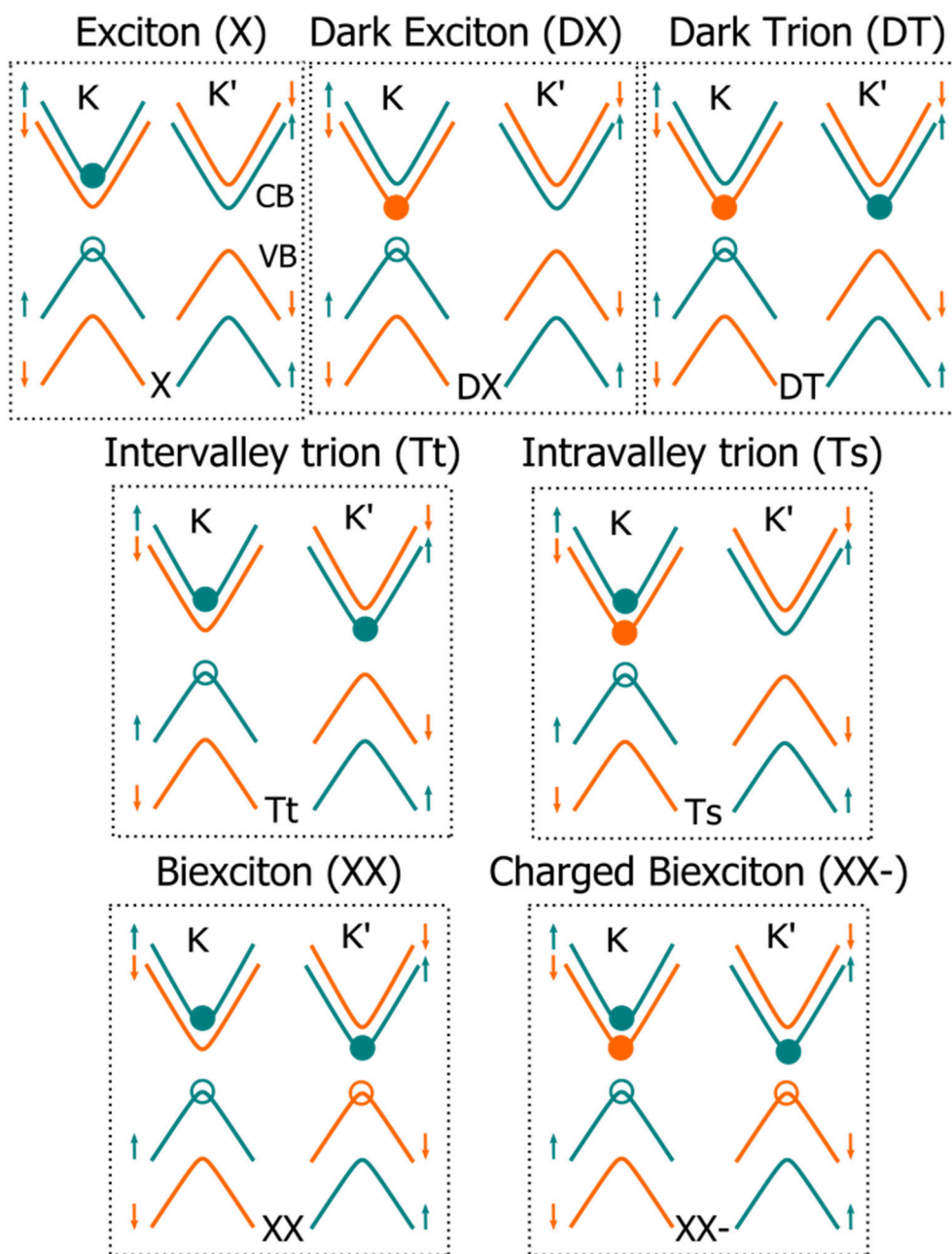


FIG. 1. Schematic configurations of the expected bright/dark excitons/trions, biexcitons (XX) and charged biexcitons (XX-) at the K and K' valleys for a n -doped monolayer WS_2 . The arrows and colors indicate the spin directions in the valence (VB) and conduction bands (CB). The bright excitons/trions (X/T) emit circularly polarized light in the out-of-plane direction; the dark excitons/trions (DX, DT) emit vertically polarized light in the in-plane direction.

Fig. 2(a) shows the optical microscopy image of a ML WS_2 /talc sample, together with the Atomic Force Microscopy (AFM) image of the talc layer. The AFM results demonstrate that the talc layer has a thickness of ≈ 120 nm and

provides an atomically flat surface (root mean square (rms) roughness $R_{rms} \approx 0.35\text{nm}$), which is an important property to obtain high quality samples. Fig. 2(b) shows typical low temperature (4.2 K) PL spectra for two different selected laser powers (5 and 120 μW) for the position labeled P1. The PL spectra were normalized to the intensity of the X peak. The PL spectra of the WS_2/talc sample were stable [22] and no photodoping effect [24] was observed. Fig. S1 in the supplemental material [25] shows in more details the spectra for different laser powers. Similar results were obtained for different laser positions on the sample (Fig. S2 in supplemental material [26]). The PL spectrum is composed of several emission peaks, associated to the emission of the different excitonic complexes. Specifically, we can identify the neutral exciton (X) emission at 2.086 eV and the negative trion recombination around an energy of 2.056 eV. The full-width-at-half maximum (FWHM) of the exciton peak is of the order of 10 meV at 4.5 K ($\approx 26 - 30$ meV at 300 K depending on the laser position) showing that talc is a promising dielectric to separate a monolayer TMD from the SiO_2 substrate. Indeed, this value is much lower than the reported value of ML WS_2 on SiO_2 , which is around 20 meV ($\approx 35 - 50$ meV at 300 K) [9,24,27] and comparable to ML WS_2 on $h\text{-BN}$ which are around 10 meV [28,29].

Our results also show an improved sample quality using a thicker talc layer (120 nm) as compared to previous work on MoS_2 . However, it isn't easy to compare results of FWHM for different TMD materials. In addition, it should be mentioned that the different values of the FWHM at 300 K for samples with a different talc thickness could be due to a different sample inhomogeneity introduced in the exfoliation/transfer method or due to a different doping level. Actually, typical impurities in our talc crystals are Fe and Al, of which it is known to result in p-doping of graphene [18]. It was shown that Fe/Al impurities occupy Si sites in talc and acts as acceptors [18]. Therefore, these impurities remove electrons from the graphene layer, resulting in a p-type doping effect [18]. A similar result is expected for ML TMD/talc heterostructures. Actually, we have observed recently that TMD/talc FET devices with a layer thickness below 40nm are slightly more p-type than MoS_2 and MoSe_2 transistors on $h\text{-BN}$ or SiO_2 dielectrics [22]. We anticipate that the FWHM of the X emission of WS_2/talc can

be further reduced by using an appropriate thermal treatment such as the standard procedures used for *h*BN-encapsulated TMD monolayers [30].

The trion peak exhibits a clear asymmetry, the appearance of which depends on the laser position on the sample. This observation strongly suggests that the WS₂/talc ML is *n*-doped, such that the trion emission is composed of two different bright negatively charged species, i.e., intralayer and interlayer trions, as illustrated in Fig. 1. In our case, the bright trion PL peak consists of a singlet (Ts) peak, around 2.053eV and a triplet (Tt) peak around 2.060 eV, split by the Coulomb exchange interaction [5,27,31] (Fig.1). The energy separation between the Tt and Ts peaks is on the order of 7 meV, similar to the trion splitting observed for WS₂ on *h*-BN [32,33]. The intensity of the total trion band for the two laser powers (5 and 120 μW) is approximately equal to the exciton intensity (Fig. 2(b)). The laser power dependencies of both the X and trion PL intensities, obtained by fitting the spectra by using Voigt functions (Fig. 2(c)), shows a linear relationship dependence with laser power (Fig. 2(d)). Using $I \propto P^\alpha$, where *I* is the integrated PL intensity and *P* the laser power, we have obtained $\alpha = 1.0$ for the exciton peak and $\alpha = 1.1$ for the trion peak. In contrast, the peak around 2.031 eV shows a super-linear behavior as a function of the laser power [5,34] ($\alpha = 1.2$). We attribute this peak to the emission of charged biexcitons (XX-) giving a binding energy of about 55 meV, consistent to previous reports in the literature [5,24,34–36]. It was shown that the emission of neutral biexcitons in MoSe₂, WSe₂ and WS₂ MLs is located at an energy in between the exciton and trions PL peaks, with a typical binding energy of around 20 meV, in agreement with theoretical predictions [5]. The unambiguous identification of both neutral and charged XX transitions was recently reported through experiments using electrostatic gating, ranging from hole- to electron-doping [5]. Therefore, the energy position and the laser power dependence of the 2.031 eV peak confirm its origin to be the emission of charged biexcitons (XX-) [5,24,34,36–38]. While a nearly quadratic power law is expected for full thermal equilibrium between neutral exciton and biexcitons, values smaller than 2, like we have observed, were reported recently in other TMD MLs [5,34–36,38].

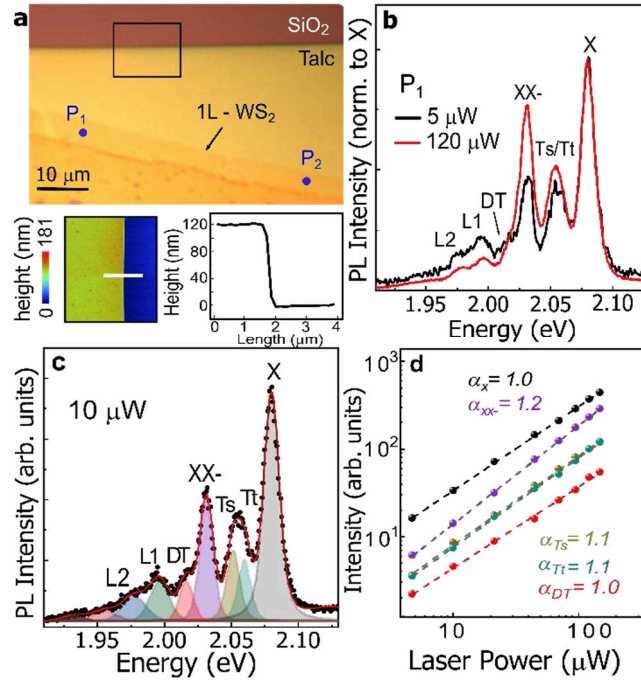


FIG. 2. (a) Optical microscope and AFM images of the WS₂/talc ML sample. (b) Typical PL spectra for position P1 for two selected laser powers (5 and 120 μW) at 4.5K (c) Typical fitting of the PL spectrum at zero magnetic field. (d) Double logarithmic plot of the integrated intensities of the different excitonic peaks as a function of laser power.

At lower laser powers (Fig. 2(b) and (c)) we observe clearly an additional emission peak around 2.016eV, which is attributed to dark trion (DT) emission [5]. Fig.S1 shows more details on the DT emission for different laser powers. As mentioned above, transitions of these dark states are optically forbidden for in-plane polarized light [5], i.e. in the backscattering geometry scheme we have used. However, it was shown that an objective with a large numerical aperture, as used in our experiments, permits the detection of dark exciton emission in ML TMDs [5]. In addition, emission of dark exciton states can also be caused by disorder/strain from the talc substrate, which can break the optical selection rules. Finally, we have observed additional lower intensity emission peaks at lower energies, labeled L1 and L2 in Fig. 2(b) and (c). We remark that for this position, P1, the energy separation of these peaks from the DT peak is ~ 20 meV for L1 and ~38 meV for L2, which are very close to phonon energies in ML WS₂ [12]. Therefore, a possible cause for the origin of these peaks could be the occurrence of phonon replicas [39] of dark trions.

Fig. 3 presents the polarization resolved magneto-PL spectra and corresponding false color PL intensity plots, as a function of magnetic field for position P2 using circularly polarized excitation. Fig. S3 in the supplemental material [40] shows similar magneto-PL results for position P1.

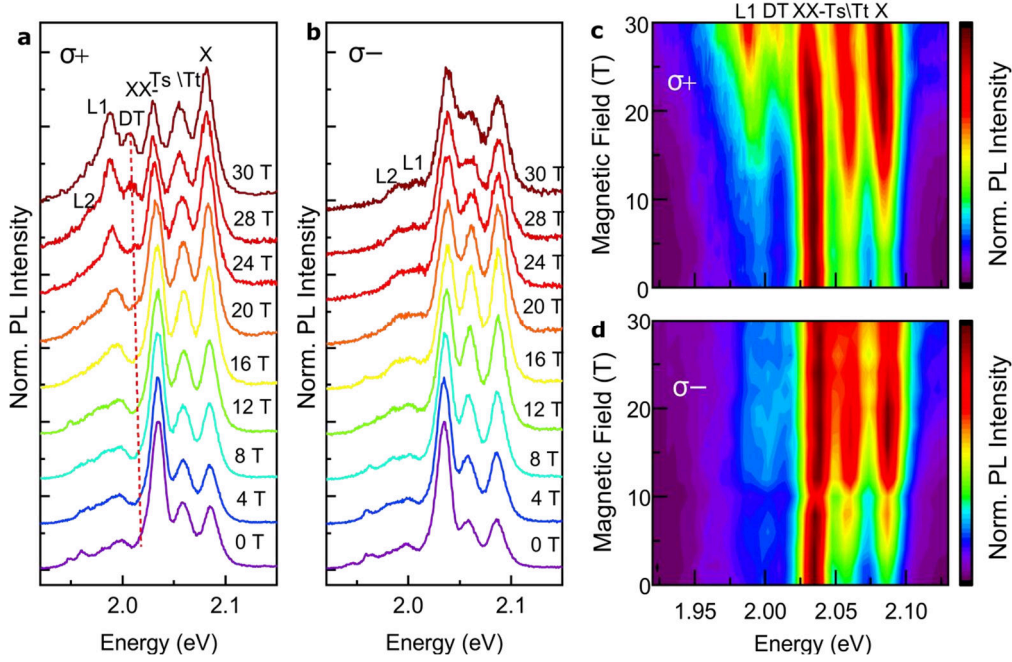


FIG. 3. PL spectra of the $WS_2/talc$ ML sample at 4.2 K for $\sigma+$ (a) and $\sigma-$ (b) detection, measured at position P2 and at different magnetic fields, using a laser power of 61 μW and circularly polarized excitation ($\sigma+$). For clarity the spectra are vertically shifted. (c) and (d) false color maps of the corresponding PL intensity as a function of magnetic field for respectively $\sigma+$ and $\sigma-$ detection.

With increasing magnetic field we have observed blue and red shifts respectively for the $\sigma-$ and $\sigma+$ circularly polarized PL, as expected [38,41–47]. We have fitted the magneto-PL spectra with a set of 8 Voigt functions and Fig.4(a) shows the PL peak positions E for the $\sigma-$ and $\sigma+$ circularly polarized emission, given by: $E = E_0 \pm \frac{1}{2}g \mu_B B$, where E_0 is the energy of each species at zero magnetic field, g is the g -factor of each excitonic complex and $\mu_B \sim 58 \mu eV/T$ is the Bohr magneton. Fig. 4(b) displays the corresponding magnetic field induced valley splittings. In order to extract the g -factors we have performed linear fittings of the Zeeman splittings ΔE using:

$$\Delta E = E^{\sigma+} - E^{\sigma-} = g \mu_B B \quad (1)$$

The fitting results are indicated by the solid lines in Fig.4(b). We obtained $g_x \approx -3.6$ for the exciton, $g_{Ts} = g_{Tt} = -3.9$ for the singlet and triplet trion states, $g_{xx} = -4.3$ for the charged biexciton and $g_{DT} \approx -9.3$ for the dark trions. The obtained values of the g factors for the bright excitons, trions and charged biexciton are consistent to previous values reported in the literature [5,12,32,34,47–49]. Furthermore, the g -factor of the spin forbidden dark trion peak is very similar to the values obtained for ML WSe₂ [5,6] and for the TD peak under tilted magnetic field in ML WS₂ [2,6].

Fig. 4(c) shows the magnetic field dependence of the degree of circular polarization of each species, defined by $P = (I_{\sigma^+} - I_{\sigma^-}) / (I_{\sigma^+} + I_{\sigma^-})$. It is important to note that in our experiments we have used circularly polarized excitation. Therefore, we observed that the polarization of the X emission is constant (around 15%) with varying magnetic field. This constant exciton polarization can be understood as a result of the valley selection effect under circularly polarized excitation, which is field independent for the W-based ML[45]. The trion polarization degrees are also consistent with those reported in previous studies in the literature [16,32]. For the singlet trions we observed a rather low value of polarization degree with small changes with increasing magnetic field with indications of a sign reversal at finite fields, in agreement with previous results [32]. For the triplet trions we observed a field depend, yet always positive, polarization degree. However, it is difficult to provide a detailed discussion of the field dependence of the trion polarizations as it is usually affected by different non-equilibrium phenomena, such as intervalley relaxation of carriers and spin-flip processes [16,32]. Therefore, further studies, including time resolved PL and magneto-PL, would be necessary to understand in more detail the magnetic field dependence of the trion polarization degrees.

The polarization of the charged biexciton peak shows a non-monotonous behaviour, increasing up to 10 T and a subsequent decreasing until it reverses sign at the highest magnetic field. To further illustrate this behavior, Fig. S4 in the supplemental material [50] shows the σ^- and σ^+ -polarized PL spectra for both the P1 and P2 positions for selected magnetic fields. At high fields (30 T) the σ^- -polarized high energy XX- peak is brighter than its low energy σ^+ polarized

counterpart, even for the σ^+ laser excitation used here, which leads to an overall higher σ^+ PL intensity due to the induced valley polarization. This peculiar behavior was previously observed [5,34] and is related to the fact that the energy difference between the two Zeeman states of the biexciton is determined by the total g -factor (gt), including the contributions from all four constituent particles of the biexciton [35]. In contrast, the spectral difference between the σ^- and σ^+ PL peaks in an applied magnetic field is determined by the Zeeman states of the emitting bright exciton, given by the spectral g -factor (gs). The different values, and signs, of the total g factor ($gt \approx +4$) and the spectral g -factor ($gs \approx -4.3$), therefore, this explains why the spectrally lower energy emission peak corresponds to a higher energy biexciton state and has lower intensity than its higher energy counterpart [5,35]. This effect is particularly evident when comparing the 30 T PL spectra obtained using parallel circular polarizations for excitation/detection (Fig. S5 in supplemental material [51]), removing the effect of the induced valley polarization present when comparing the intensities of the σ^- and σ^+ PL under σ^+ - excitation (Fig. S4). The biexciton peak at 2.038 eV for σ^-/σ^- polarization has higher intensity than the biexciton peak at 2.030 eV for σ^+/σ^+ polarization, in contrast to the regular behavior observed for the neutral exciton emission.

Finally, we have observed a clear increase with magnetic field of the PL intensity of the dark trions in σ^+ detection, resulting in a positive polarization degree. These results have been obtained using systematic fitting of the spectra for both detected polarizations (result in Fig. S6 in supplemental material [52]) on position P2. We remark that on position P1 (Fig. S2) the DT emission is more visible than for position P2, but for this position the DT emission peak can hardly be seen in σ^- - detection due to the superposition of this peak with the XX- emission peak. Previously, dark excitons/trions in monolayer WS_2 have been observed in parallel or tilted magnetic fields [6,53], where the in-plane magnetic field brighten the dark exciton/trion emission due to the mixing of the spin components of the conduction bands [53]. We attribute the observation of the dark trion emission in our experiment to the use of the high numerical aperture objective. The positive degree of circular polarization of the DT emission is related to the occurrence of

intervalley scattering mechanisms, where the possibility to emit a photon is determined by the optically excited minority carrier (holes for n -doping and electrons for hole-doping) under weak optical excitation conditions [5]. Therefore, the PL of the negatively charged dark exciton is expected to exhibit the same valley polarization as that from X , whereas the positively charged dark exciton is expected to have opposite valley polarization relative to X [5]. For our sample, we have observed the same polarization signs for the X and DT emissions, which indicates that monolayer WS_2 on talc is naturally n -doped and its doping is not affected by the talc layer, consistent with our interpretation of the PL spectrum at zero magnetic field described above.

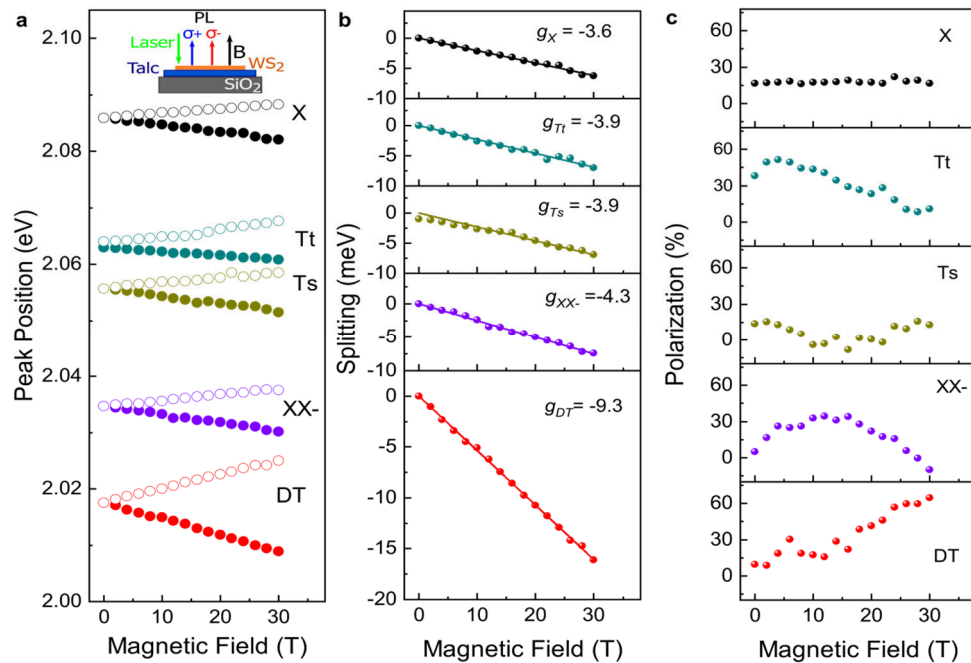


FIG. 4. (a) PL peak position versus magnetic field for $\sigma+$ (filled circles) and $\sigma-$ detection (open circles) of all observed excitonic species. (b) Corresponding splittings of the peaks versus magnetic field. (c) Corresponding polarization degrees as a function of magnetic field. All results have been obtained at position P2 using circularly polarization excitation ($\sigma+$).

This result is different from a previous work on graphene/talc [18] which have demonstrated a substrate-induced p -doping of graphene/talc. The PL decay time of the DT emission is much longer than that of the bright excitons and trions. Therefore, thermalization of the DT states occurs within their lifetime, resulting in

an increasing DT polarization with increasing magnetic field, in contrast to the constant circular polarization of X and to previous studies of DTs in ML WSe₂ [49].

In addition, we have also extracted the g -factors of the lower energy emission peaks at 2.000 eV (labelled L1) and 1.982 eV (labelled L2). Fig.S8 in supplemental material [54] shows the magnetic field dependence of the PL peak positions for σ^+ and σ^- detection and the valley Zeeman splitting of these peaks. These lower emission peaks follows selection rules similar to the bright exciton emission, i.e, they show conservation of excitation helicity in emission (circularly polarized emission). We obtained g -factors of ~ -12.3 and ~ -12.6 for the L1 and L2 emission peaks, respectively (Fig. S9 in supplemental material [55]). We remark that the energy separation of these peaks from the DT peak is ~ 17.8 meV for L1 and ~ 35.8 meV for L2. The nature of these peaks is not well established. Similar lower emission peaks having similar g -factors were recently reported for high quality ML WS₂ and associated to momentum forbidden dark trion with the emission of optical (E'') or acoustic (ZA , LA) phonons, i.e, phonon replicas of dark trions [5]. The positions of the phonon replicas of the dark trion emission are expected to be red shifted from the DT peak by the phonon energies of ML WS₂. Comparing the measured redshift (~ 35.8 meV) and the theoretical phonon energy (36.4 meV) [12], the peak at about 1.982 eV (L2 peak) could be identified as a phonon replica TD $E''(\Gamma)$. The shift of the L1 peak around 2.000 eV (~ 17.8 meV) is close to the theoretical energy values of the $TA(K)$ and $ZA(K)$ phonons (18.2 and 17.7 meV) [12]. Furthermore, other phonon replicas, which could involve a momentum flip, could be induced by phonons from the K point. It would be possible to transfer an electron (hole) between K valleys with emission of $E''(K)$ ($LA(K)$) phonons [12]. Their theoretical energies (43.0 meV and 22.6 meV) [12] are also close to the measured PL energy redshifts (35.8 meV and 17.8 meV) from the dark trion peaks in our samples. Therefore, the observed L1 and L2 peaks could be associated to dark trion replicas due to momentum forbidden dark transitions. Particularly, the obtained g -factors of L1 and L2 are consistent to previous reported values [2,6] for phonon replicas of dark trions TD $ZA(K)$ and TD $E''(K)$ respectively.

IV. Conclusion

We have investigated the low temperature photoluminescence and magneto photoluminescence of monolayer WS₂ on talc. We have obtained high quality samples showing the emission of different excitonic complexes in the PL spectra at low temperatures. At low temperature, we observed that the FWHM of the exciton peak is comparable with WS₂/h-BN, showing that talc is a promising dielectric to separate a monolayer TMD from the SiO₂ substrate. We have investigated the properties of all excitonic complexes under perpendicular magnetic fields up to 30 T and extracted the *g*-factor of all emission peaks. The obtained *g*-factors are in agreement with theoretical values in the literature [12]. In contrast to previous studies of graphene/talc [18], which have demonstrated a spontaneous *p*-doping, our magneto-PL results indicate that ML WS₂/talc is naturally *n*-doped, as revealed by the observation of the same valley polarization for the X and charged DT emission.

One possible explanation for this result is that the *p*-doping from talc could result in a reduction of the *n*-doping of ML WS₂, but it is not enough to affect the type of doping. In addition, we have observed that under $\sigma+$ polarized excitation the sign of circularly polarization biexcitons is reversed under higher magnetic fields, which shows that under very high fields the effect of thermalization is the dominant mechanism, as compared to valley selectivity. We have also observed that the polarization of the dark trion emission increases considerably with increasing magnetic field, in contrast to previous studies on ML WSe₂. In general, the improvement of the optical quality of TMD on talc dielectric also contributes to uncover further information on the valley physics of ML WS₂ particularly for the properties of biexcitons and dark trions under high perpendicular magnetic fields. Finally, our results suggest that talc is a promising low-cost layered material to explore fundamental physics and also for possible application in novel optoelectronic devices based on high quality doped TMD heterostructures.

Acknowledgements

The work has been supported by “Fundação de Amparo a Pesquisa do Estado de São Paulo (Fapesp) (grants no. 18/01808-5 and 19/23488-5), Conselho Nacional de Desenvolvimento Científico e Tecnológico (CNPQ) (grants 426634/2018-7 and 311678/2020-3) and the High Field Magnet Laboratory (HFMLRU/NWO-I), a member of the European Magnetic Field Laboratory (EMFL). G.P. acknowledges the —Coordenação de Aperfeiçoamento de Pessoal de Nível Superior (Capes) for financial support of her PhD fellowship. I. D. B. acknowledges the financial support from the Brazilian Nanocarbon Institute of Science and Technology (INCT/Nanocarbono), Brazilian Synchrotron Light Laboratory (LNLS), Fapesp (grant 2018/00823-0), CNPq (grant 311327/2020-6), and the award of L’ORÉAL-UNESCOABC for Women in Science - Brazil/2021. We would like to acknowledge F. Iikawa and O.D.D. Couto Jr for preliminary optical characterization of our samples and J. Buhot and M. Ballottin for optical alignment of the magneto-PL setup. The authors also would like to acknowledge to the IMBUA beamline at Brazilian Synchrotron Light Laboratory (LNLS) for the AFM facility.

References

- [1] G. Wang, A. Chernikov, M. M. Glazov, T. F. Heinz, X. Marie, T. Amand, B. Urbaszek, Colloquium: Excitons in Atomically Thin Transition Metal Dichalcogenides, *Rev. Mod. Phys.* **90**, 21001(2018). DOI: 10.1103/RevModPhys.90.021001
- [2] T. Mueller, E. Malic, Exciton Physics and Device Application of Twodimensional Transition Metal Dichalcogenide Semiconductors, *npj 2D Mater. Appl.* **2**, 29 (2018). DOI: 10.1038/s41699-018-0074-2
- [3] K. F. Mak, J. Shan, Photonics and Optoelectronics of 2D Semiconductor Transition Metal Dichalcogenides, *Nat. Photonics* **10**, 216 (2016). DOI: 10.1038/nphoton.2015.282
- [4] F. Cadiz, E. Courtade, C. Robert, G. Wang, Y. Shen, H. Cai, T. Taniguchi, K. Watanabe, H. Carrere, D. Lagarde, M. Manca, T. Amand, P. Renucci, S. Tongay, X. Marie, B. Urbaszek, Excitonic Linewidth Approaching the Homogeneous Limit in MoS₂-Based van der Waals Heterostructures, *Phys. Rev. X* **7**, 021026 (2017). DOI: 10.1103/PhysRevX.7.021026
- [5] Z. Li, T. Wang, S. Miao, Z. Lian, S. F. Shi, Fine Structures of Valley-polarized Excitonic States in Monolayer Transitional Metal Dichalcogenides, *Nanophotonics* **9**, 1811(2020). DOI: 10.1515/nanoph-2020-0054
- [6] M. Zinkiewicz, A. O. Slobodeniuk, T. Kazimierczuk, P. Kapuściński, K. Oreszczuk, M. Grzeszczyk, M. Bartos, K. Nogajewski, K. Watanabe, T. Taniguchi, C. Faugeras, P. Kossacki, M. Potemski, A. Babiński, M. R. Molas, Neutral and Charged Dark Excitons in Monolayer WS₂, *Nanoscale* **12**, 18153(2020). DOI: 10.1039/D0NR04243A
- [7] G. Wang, C. Robert, M. M. Glazov, F. Cadiz, E. Courtade, T. Amand, D. Lagarde, T. Taniguchi, K. Watanabe, B. Urbaszek, X. Marie, In-Plane Propagation of Light in Transition Metal Dichalcogenide Monolayers:

- Optical Selection Rules, *Phys. Rev. Lett.* **119**, 47401(2017).
DOI:10.1103/PhysRevLett.119.047401
- [8] H. Zeng, J. Dai, W. Yao, D. Xiao, X. Cui, Valley Polarization in MoS₂ Monolayers by Optical Pumping, *Nat. Nanotechnol.* **7**, 490 (2012). DOI: 10.1038/nnano.2012.95
- [9] G. Plechinger, P. Nagler, J. Kraus, N. Paradiso, C. Strunk, C. Schüller, T. Korn, Identification of Excitons, Trions and Biexcitons in Single-layer WS₂, *Phys. Status Solidi - Rapid Res. Lett.* **9**, 457 (2015). DOI: 10.1002/pssr.201510224
- [10] A. Steinhoff, M. Florian, A. Singh, K. Tran, M. Kolarczik, S. Helmrich, A. W. Achtstein, U. Woggon, N. Owschimikow, F. Jahnke, X. Li, Biexciton Fine Structure in Monolayer Transition Metal Dichalcogenides, *Nat. Phys.* **14**, 1199 (2018). DOI: 10.1038/s41567-018-0282-x
- [11] E. Mostaani, M. Szyniszewski, C. H. Price, R. Maezono, M. Danovich, R. J. Hunt, N. D. Drummond, V. I. Fal'Ko, Diffusion Quantum Monte Carlo Study of Excitonic Complexes in Two-dimensional Transition-metal Dichalcogenides, *Phys. Rev. B* **96**, 075431(2017). DOI: 10.1103/PhysRevB.96.075431
- [12] M. Zinkiewicz, T. Woźniak, T. Kazimierzuk, P. Kapuscinski, K. Oreszczuk, M. Grzeszczyk, M. Bartoš, K. Nogajewski, K. Watanabe, T. Taniguchi, C. Faugeras, P. Kossacki, M. Potemski, A. Babiński, M. R. Molas, Excitonic Complexes in n-Doped WS₂ Monolayer, *Nano Lett.* **6**, 2519 (2021). DOI: 10.1021/acs.nanolett.0c05021.
- [13] M. Danovich, V. Zólyomi, V. I. Fal'Ko, Dark Trions and Biexcitons in WS₂ and WSe₂ Made Bright by e-e Scattering, *Sci. Rep.* **7**, 45998 (2017). DOI: doi.org/10.1038/srep45998
- [14] Z. Li, T. Wang, C. Jin, Z. Lu, Z. Lian, Y. Meng, M. Blei, S. Gao, T. Taniguchi, K. Watanabe, T. Ren, S. Tongay, L. Yang, D. Smirnov, T. Cao, S. F. Shi,

Emerging Photoluminescence from the Dark-exciton Phonon Replica in Monolayer WSe₂, *Nat. Commun.* **10**, 2469 (2019). DOI: 10.1038/s41467-01910477-6

- [15] A. Arora, N. K. Wessling, T. Deilmann, T. Reichenauer, P. Steeger, P. Kossacki, M. Potemski, S. Michaelis De Vasconcellos, M. Rohlfing, R. Bratschitsch, Dark Trions Govern the Temperature-dependent Optical Absorption and Emission of Doped Atomically Thin Semiconductors, *Phys. Rev. B* **101**, 241413(R) (2020). DOI: 10.1103/PhysRevB.101.241413
- [16] A. Arora, Magneto-optics of Layered Two-dimensional Semiconductors and Heterostructures: Progress and Prospects, *J. Appl. Phys.* **129**, 120902 (2021). DOI: 10.1063/5.0042683
- [17] A. B. Alencar, A. P. M. Barboza, B. S. Archanjo, H. Chacham, B. R. A. Neves, Experimental and Theoretical Investigations of Monolayer and Few-layer Talc, *2D Mater.* **2**, 015004 (2015). DOI: 10.1088/2053-1583/2/1/015004
- [18] E. Mania, A. B. Alencar, A. R. Cadore, B. R. Carvalho, K. Watanabe, T. Taniguchi, B. R. A. Neves, H. Chacham, L. C. Campos, Spontaneous Doping on High Quality Talc-Graphene-hBN van der Waals Heterostructures, *2D Mater.* **4**, 031008 (2017). DOI: 10.1088/2053-1583/aa76f4
- [19] J. L. Rosenholtz, D. T. Smith, The Dielectric Constant of Mineral Powders, *Am. Mineral. J. Earth Planet. Mater.* **21**, 115 (1936). http://www.minsocam.org/msa/collectors_corner/amtoc/toc1936.htm
- [20] I. D. Barcelos, A. R. Cadore, A. B. Alencar, F. C. B. Maia, E. Mania, R. F. Oliveira, C. C. B. Bufon, Â. Malachias, R. O. Freitas, R. L. Moreira, H. Chacham, Infrared Fingerprints of Natural 2D Talc and Plasmon–Phonon Coupling in Graphene–Talc Heterostructures, *ACS Photonics* **5**, 1912 (2018). DOI: 10.1021/acsp Photonics.7b01017

- [21] A. C. Gadelha, T. L. Vasconcelos, L. G. Cançado, A. Jorio, Nano-optical Imaging of In-Plane Homojunctions in Graphene and MoS₂ van der Waals Heterostructures on Talc and SiO₂, *J. Phys. Chem. Lett.* **12**, 7625(2021). DOI: 10.1021/acs.jpcclett.1c01804
- [22] D. Nutting, G. A. Prando, M. Severijnen, I. Barcelos, S. Guo, P. C. M. Christianen, U. Zeitler, Y. Galvão Gobato, F. Withers, Electrical and Optical Properties of Transition Metal Dichalcogenides on Talc Dielectrics, *Nanoscale* **13**, 15853 (2021). DOI: 10.1039/d1nr04723j
- [23] E. Liu, J. Van Baren, C. T. Liang, T. Taniguchi, K. Watanabe, N. M. Gabor, Y. C. Chang, C. H. Lui, Multipath Optical Recombination of Intervalley Dark Excitons and Trions in Monolayer WSe₂, *Phys. Rev. Lett.* **124**, 196802(2020). DOI: 10.1103/PhysRevLett.124.196802
- [24] V. Orsi Gordo, M. A. G. Balanta, Y. Galvão Gobato, F. S. Covre, H. V. A. Galeti, F. Iikawa, O. D. D. Couto, F. Qu, M. Henini, D. W. Hewak, C. C. Huang, Revealing the Nature of Low-temperature Photoluminescence Peaks by Laser Treatment in van der Waals Epitaxially Grown WS₂ Monolayers, *Nanoscale* **10**, 4807 (2018). DOI: 10.1039/C8NR00719E
- [25] G. A. Prando, M. E. Severijnen, I. D. Barcelos, U. Zeitler, P. C. M. Christianen, F. Withers, Y. G. Gobato, *Fig. S1-Supplementary Inf.*
- [26] G. A. Prando, M. E. Severijnen, I. D. Barcelos, U. Zeitler, P. C. M. Christianen, F. Withers, Y. G. Gobato, *Fig. S2-Supplementary Inf.*
- [27] G. Plechinger, P. Nagler, A. Arora, R. Schmidt, A. Chernikov, A. G. Del Águila, P. C. M. Christianen, R. Bratschitsch, C. Schüller, T. Korn, Trion Fine Structure and Coupled Spin–valley Dynamics in Monolayer Tungsten Disulfide, *Nat. Commun.* **7**, 12715 (2016). DOI: 10.1038/ncomms12715
- [28] I. Paradisanos, K. M. McCreary, D. Adinehloo, L. Mouchliadis, J. T. Robinson, H. J. Chuang, A. T. Hanbicki, V. Perebeinos, B. T. Jonker, E. Stratakis, G. Kioseoglou, Prominent Room Temperature Valley Polarization

- in WS₂/Graphene Heterostructures Grown by Chemical Vapor Deposition, *Appl. Phys. Lett.* **116**, 203102 (2020). DOI: 10.1063/5.0002396
- [29] J. Jadczyk, L. Bryja, J. Kutrowska-Girzycka, P. Kapuściński, M. Bieniek, Y. S. Huang, P. Hawrylak, Room Temperature Multi-Phonon Upconversion Photoluminescence in Monolayer Semiconductor WS₂, *Nat. Commun.* **10**, 107 (2019). DOI: 10.1038/s41467-018-07994-1
- [30] Y. Liu, C. Liu, Z. Ma, G. Zheng, Y. Ma, Z. Sheng, Annealing Effect on Photoluminescence of Two Dimensional WSe₂/BN Heterostructure, *Appl. Phys. Lett.* **117**, 233103(2020). DOI:10.1063/5.0026971
- [31] T. P. Lyons, S. Dufferwiel, M. Brooks, F. Withers, T. Taniguchi, K. Watanabe, K. S. Novoselov, G. Burkard, A. I. Tartakovskii, The Calley Zeeman Effect in Inter- and Intra-Valley Trions in Monolayer WSe₂, *Nat. Commun.* **10**, 2330,(2019). DOI : 10.1038/s41467-019-10228-7 [32]
- [33] P. Kapuściński, D. Vaclavkova, M. Grzeszczyk, A. O. Slobodeniuk, K. Nogajewski, M. Bartos, K. Watanabe, T. Taniguchi, C. Faugeras, A. Babiński, M. Potemski, M. R. Molas, Valley Polarization of Singlet and Triplet Trions in a WS₂ Monolayer in Magnetic Fields, *Phys. Chem. Chem. Phys.* **22**,19155(2020). DOI : 10.1039/D0CP02737E
- [34] D. Vaclavkova, J. Wyzula, K. Nogajewski, M. Bartos, A. O. Slobodeniuk, Faugeras, M. Potemski, M. R. Molas, Singlet and Triplet Trions in WS₂ Monolayer Encapsulated in Hexagonal Boron Nitride ,*Nanotechnology* **29**, 325705 (2019). DOI :10.1088/1361-6528/aac65c
- [35] P. Nagler, M. V Ballottin, A. A. Mitioglu, M. V Durnev, T. Taniguchi, K. Watanabe, A. Chernikov, C. Schüller, M. M. Glazov, P. C. M. Christianen, T. Korn, Zeeman Splitting and Inverted Polarization of Biexciton Emission in Monolayer WS₂, *Phys. Rev. Lett.* **121**, 57402 (2018). DOI : 10.1103/PhysRevLett.121.057402

- [36] Z. Li, T. Wang, Z. Lu, C. Jin, Y. Chen, Y. Meng, Z. Lian, T. Taniguchi, K. Watanabe, S. Zhang, D. Smirnov, S.-F. Shi, Revealing the Biexciton and Trion-Exciton Complexes in BN Encapsulated WSe₂, *Nat. Commun.* **9**, 3719 (2018). DOI : 10.1038/s41467-018-05863-5
- [37] M. Barbone, A. R. P. Montblanch, D. M. Kara, C. Palacios-Berraquero, A. R. Cadore, D. De Fazio, B. Pingault, E. Mostaani, H. Li, B. Chen, K. Watanabe, T. Taniguchi, S. Tongay, G. Wang, A. C. Ferrari, M. Atatüre, Charge-tuneable Biexciton Complexes in Monolayer WSe₂, *Nat. Commun.* **9**, 3721 (2018). DOI: 10.1038/s41467-018-05632-4
- [38] C. Robert, When Bright and Dark Bind Together, *Nat. Nanotechnol.* **13**, 982 (2018). DOI: 10.1038/s41565-018-0281-1
- [39] Y. You, X. X. Zhang, T. C. Berkelbach, M. S. Hybertsen, D. R. Reichman, T. F. Heinz, Observation of Biexcitons in Monolayer WSe₂, *Nat. Phys.* **11**, 477 (2015). DOI: 10.1038/nphys3324
- [40] M. He, P. Rivera, D. Van Tuan, N. P. Wilson, M. Yang, T. Taniguchi, K. Watanabe, J. Yan, D. G. Mandrus, H. Yu, H. Dery, W. Yao, X. Xu, Valley Phonons and Exciton Complexes in a Monolayer Semiconductor, *Nat. Commun.* **11**, 618 (2020). DOI: 10.1038/s41467-020-14472-0
- [41] G. A. Prando, M. E. Severijnen, I. D. Barcelos, U. Zeitler, P. C. M. Christianen, F. Withers, Y. G. Gobato, *Fig. S3-Supplementary Inf.*
- [42] G. Aivazian, Z. Gong, A. M. Jones, R. L. Chu, J. Yan, D. G. Mandrus, C. Zhang, D. Cobden, W. Yao, X. Xu, Magnetic Control of Valley Pseudospin in Monolayer WSe₂, *Nat. Phys.* **11**, 148 (2015). DOI: 10.1038/nphys3201
- [43] Y. Li, J. Ludwig, T. Low, A. Chernikov, X. Cui, G. Arefe, Y. D. Kim, A. M. Van Der Zande, A. Rigosi, H. M. Hill, S. H. Kim, J. Hone, Z. Li, D. Smirnov, T. F. Heinz, Valley Splitting and Polarization by the Zeeman Effect in Monolayer MoSe₂, *Phys. Rev. Lett.* **113**, 266804 (2014). DOI: 10.1103/PhysRevLett.113.266804

- [44] A. Srivastava, M. Sidler, A. V. Allain, D. S. Lembke, A. Kis, A. Imamoglu, Valley Zeeman Effect in Elementary Optical Excitations of Monolayer WSe₂, *Nat. Phys.* **11**, 141(2015). DOI: 10.1038/nphys3203
- [45] D. Macneill, C. Heikes, K. F. Mak, Z. Anderson, A. Kormányos, V. Zólyomi, J. Park, D. C. Ralph, Breaking of Valley Degeneracy by Magnetic Field in Monolayer MoSe₂, *Phys. Rev. Lett.* **114**, 037401(2015). DOI: 10.1103/PhysRevLett.114.037401
- [46] G. Wang, L. Bouet, M. M. Glazov, T. Amand, E. L. Ivchenko, E. Palleau, X. Marie, B. Urbaszek, Magneto-Optics in Transition Metal Diselenide Monolayers, *2D Mater.* **2**, 34002 (2015). DOI: 10.1088/2053-1583/2/3/034002
- [47] A. V. Stier, K. M. McCreary, B. T. Jonker, J. Kono, S. A. Crooker, Exciton diamagnetic shifts and valley Zeeman effects in monolayer WS₂ and MoS₂ to 65 Tesla, *Nat. Commun.* **7**, 10643(2016). DOI: 10.1038/ncomms10643
- [48] G. Plechinger, P. Nagler, A. Arora, A. Granados Del Águila, M. V. Ballottin, T. Frank, P. Steinleitner, M. Gmitra, J. Fabian, P. C. M. Christianen, R. Bratschitsch, C. Schüller, T. Korn, Excitonic Valley Effects in Monolayer WS₂ under High Magnetic Fields, *Nano Lett.* **16**, 7899 (2016). DOI: 10.1021/acs.nanolett.6b04171
- [49] M. Goryca, J. Li, A. V. Stier, T. Taniguchi, K. Watanabe, E. Courtade, S. Shree, . Robert, B. Urbaszek, X. Marie, S. A. Crooker, Revealing Exciton Masses and Dielectric Properties of Monolayer Semiconductors with High Magnetic Fields ,*Nat. Commun.* **10**, 4172 (2019). DOI: 10.1038/s41467-019-12180-y
- [50] Z. Li, T. Wang, Z. Lu, M. Khatoniar, Z. Lian, Y. Meng, M. Blei, T. Taniguchi, K. Watanabe, S. A. McGill, S. Tongay, V. M. Menon, D. Smirnov, S. F. Shi, Direct Observation of Gate-Tunable Dark Trions in Monolayer WSe₂, *Nano Lett.* **19**, 6886 (2019). DOI: 10.1021/acs.nanolett.9b02132

- [51] G. A. Prando, M. E. Severijnen, I. D. Barcelos, U. Zeitler, P. C. M. Christianen, F. Withers, Y. G. Gobato, *Fig. S4-Supplementary Inf.*
- [52] G. A. Prando, M. E. Severijnen, I. D. Barcelos, U. Zeitler, P. C. M. Christianen, F. Withers, Y. G. Gobato, *Fig. S5-Supplementary Inf.*
- [53] G. A. Prando, M. E. Severijnen, I. D. Barcelos, U. Zeitler, P. C. M. Christianen, F. Withers, Y. G. Gobato, *Fig. S6-Supplementary Inf.* C. Robert, B. Han, P. Kapuscinski, A. Delhomme, C. Faugeras, T. Amand, M. R. Molas, M. Bartos, K. Watanabe, T. Taniguchi, B. Urbaszek, M. Potemski, X. Marie, Measurement of the Spin-forbidden Dark Excitons in MoS₂ and MoSe₂ Monolayers. *Nat. Commun.* **11**, 4037 (2020). DOI: 10.1038/s41467-02017608-4 G. A. Prando, M. E. Severijnen, I. D. Barcelos, U. Zeitler, P. C. M. Christianen, F. Withers, Y. G. Gobato, *Fig. S8-Supplementary Inf.*
- [54] G. A. Prando, M. E. Severijnen, I. D. Barcelos, U. Zeitler, P. C. M. Christianen, F. Withers, Y. G. Gobato, *Fig. S9-Supplementary Inf.*

Supplementary Information

Revealing excitonic complexes in monolayer WS₂ on talc dielectric

Figure S0 shows typical AFM results for talc flakes with different thickness.

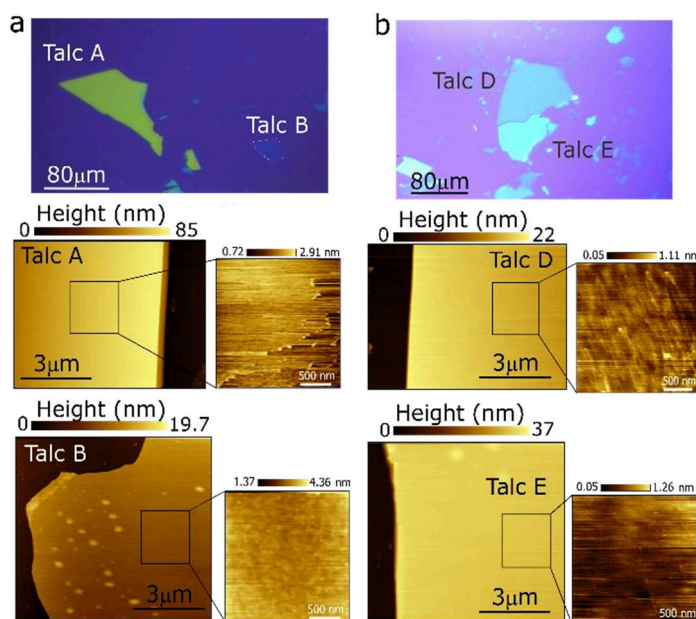


Figure S0 - Optical image and AFM topography image of Talc flakes with different thicknesses: (a) Talc A (~85 nm) and Talc B (~19.7 nm) and (b) Talc D (~22 nm) and Talc E (~37 nm).

We have found that talc show atomically flat (root mean square (rms) roughness, $R_{rms} = 0.35\text{nm}$) surfaces. The R_{rms} measured in our samples are: Talc A (~85 nm) - $R_{rms} = 0.35\text{nm}$, Talc B (~19.7 nm) – $R_{rms} = 0.17\text{nm}$, Talc D (~22 nm) – $R_{rms} = 0.14\text{nm}$, Talc E (~37 nm) – $R_{rms} = 0.19\text{nm}$. Our results indicate that talc has a good surface topography, and the roughness does not vary significantly with the thickness.

Figure S1(a) shows the normalized PL spectra at 300K for the ML WS₂/talc (talc thickness $\approx 120\text{nm}$) and ML WS₂/SiO₂. We usually observe an improvement of PL intensity in ML WS₂/talc (not shown here) and an improvement of FWHM as compared to samples on SiO₂ (Figure S1). Figure S1(b) shows the PL spectra at 4.2K of the ML WS₂/talc for different laser powers for the position P1. Figure S2(a) illustrates typical PL spectra for position P2 for 6 and 128 μW laser powers,

showing a super-linear dependence for the XX- peak. Figure S2(b) shows typical fitted curves of the PL spectra. Figure S2(c) shows the laser power dependence of the PL peaks in a double logarithmic representation. The slopes for each of the PL peaks are similar to the results obtained for position P1 on the sample (compare to Figure 2)

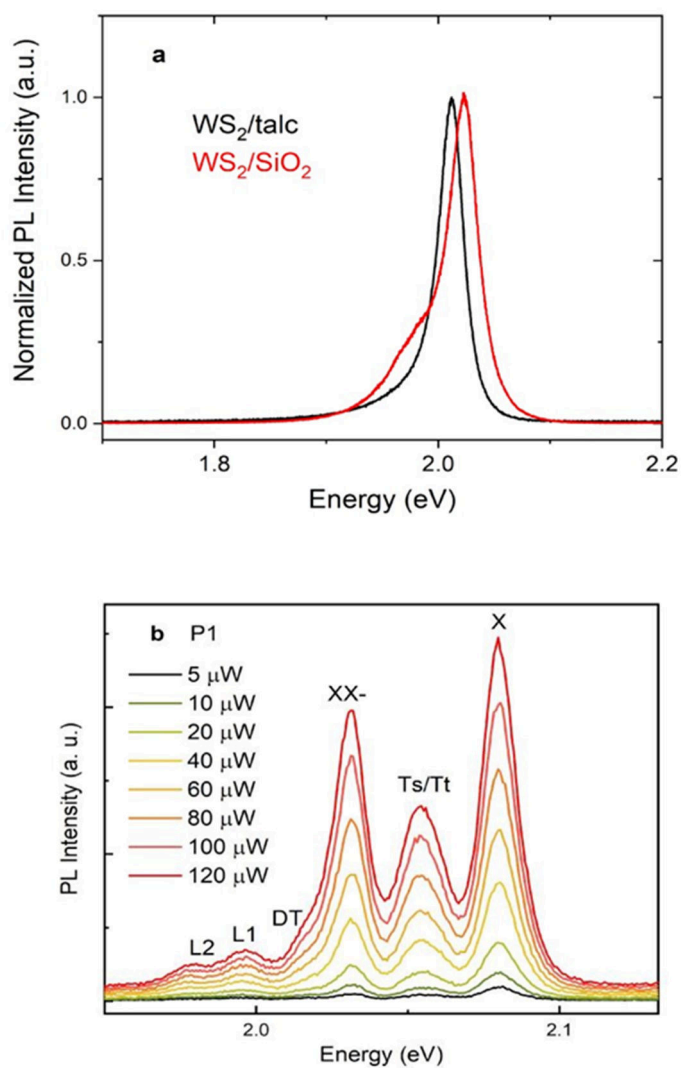


Figure S1- (a) Typical PL spectra of ML WS_2 on talc and on SiO_2 at 300K (b) PL spectra of $MLWS_2/\text{talc}$ for different laser powers for position P1 at 4.2K.

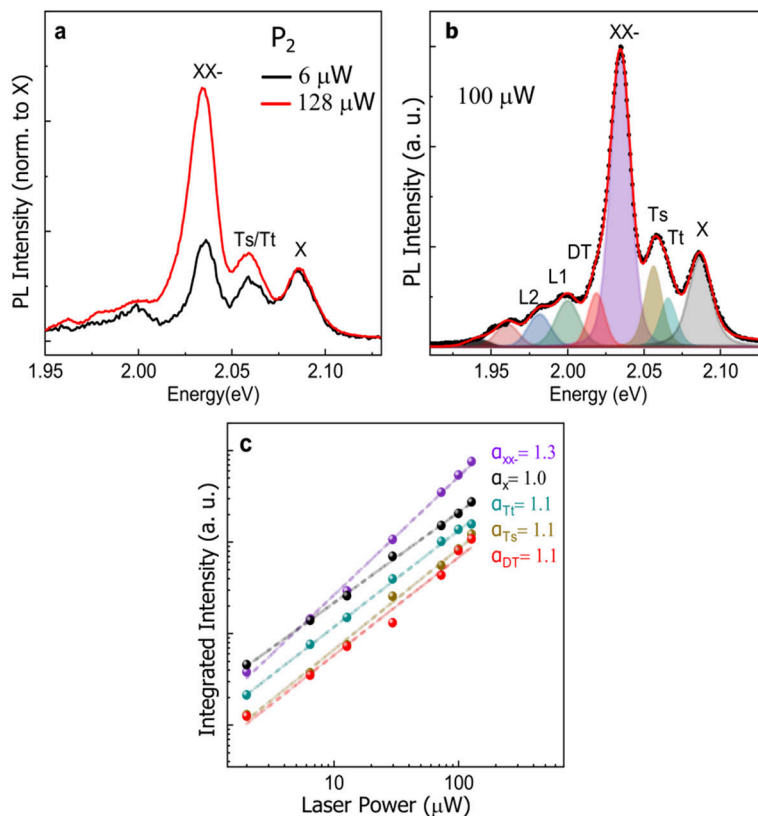


Figure S2. (a) Typical PL spectra of WS₂ monolayer on talc for position P2 and different laser powers (6 and 128 μW) at 4.2K (b) Typical fitted curves of the PL spectrum at 100 μW. (c) Double logarithmic representation of the integrated PL intensity as a function of laser power.

Figure S3 shows the magneto-PL results for position P1. The obtained results are also similar to the results shown in Figure 3. Figure S4 shows the polarized resolved PL under $\sigma+$ laser excitation for both positions P1 and P2. The inverted polarization of the XX- peaks is clearly observed at high magnetic fields.

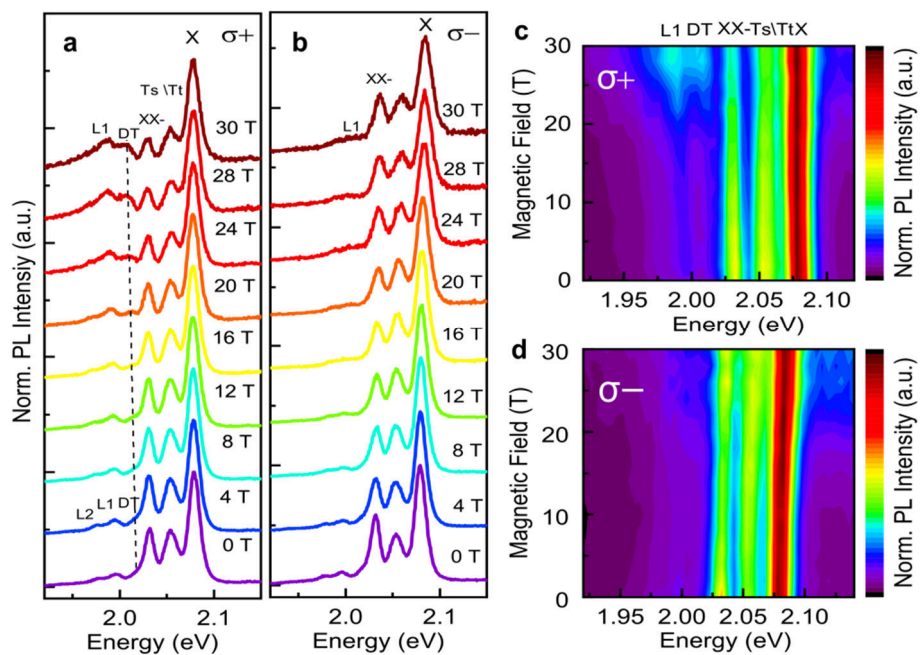


Figure S3 - PL spectra of the WS₂/talc ML sample at 4.2 K for σ^+ (a) and σ^- (b) detection, measured at position P1 and at different magnetic fields, using a laser power of 86 μ W and circularly polarized excitation (σ^+). For clarity the spectra are vertically shifted. (c) and (d) false color maps of the corresponding PL intensity as a function of magnetic field for for respectively σ^+ and σ^- detection.

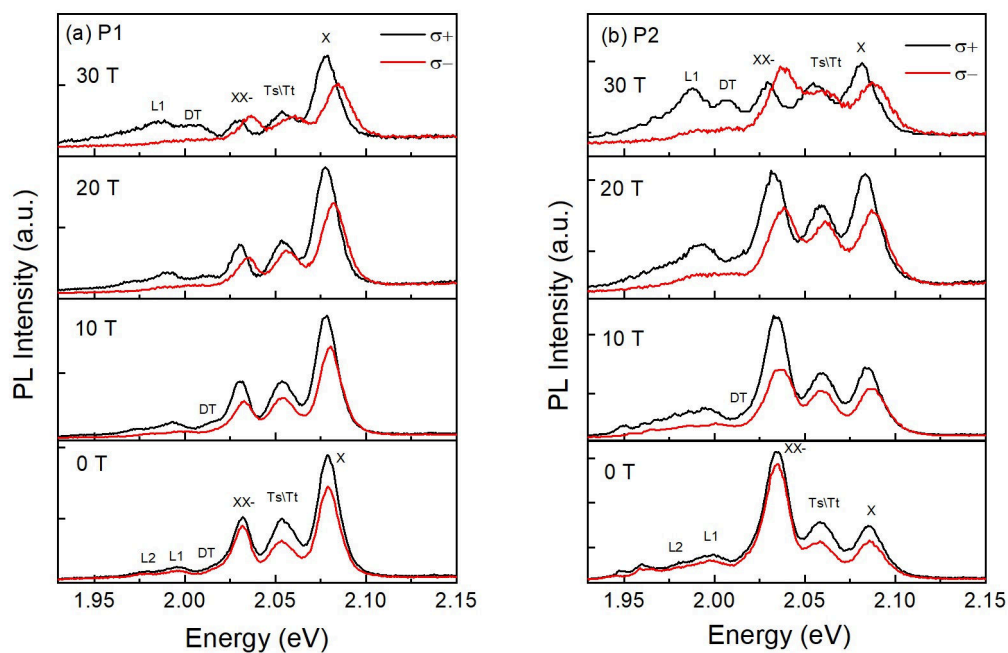


Figure S4 - (a) Typical polarization-resolved PL spectra under $\sigma+$ laser excitation for positions P1 and P2 and at selected magnetic fields at 4.2K.

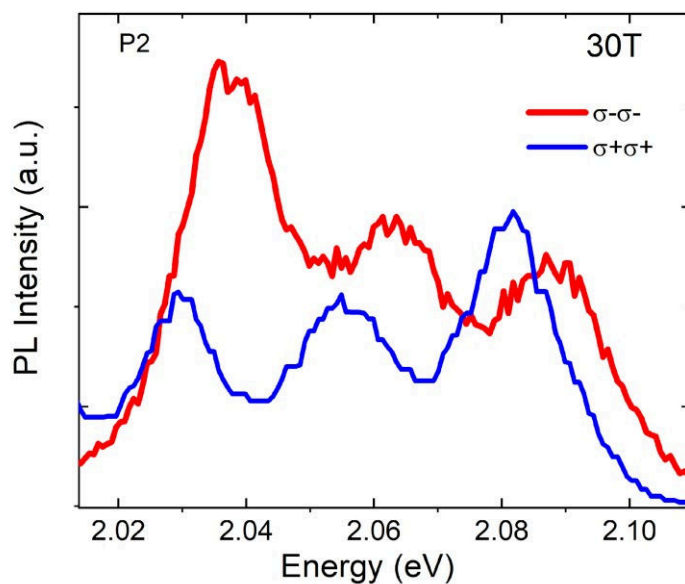


Figure S5 - Polarized PL spectra for position P2 at 30 T for the $\sigma-\sigma-$ and $\sigma+\sigma+$ configurations at 4.2K. We observed that the $XX-$ emission exhibits an inverted PL intensity (high PL intensity for the high energy component), in contrast to the regular behaviour of the X peak.

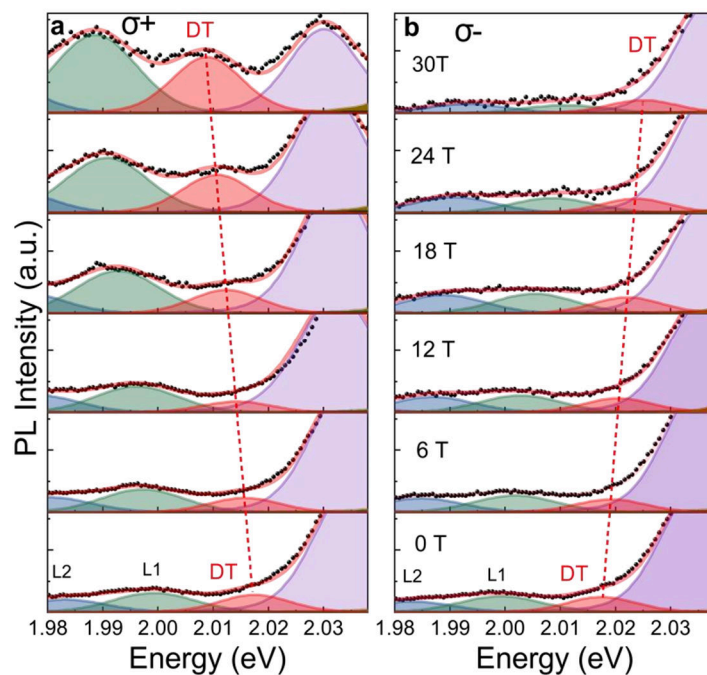


Figure S6. Typical fitted curves of the circularly polarized PL spectra for σ^+ excitation for the P2 position at 4.2K. We observed a red and blue shift of the DT emission peak for σ^+ and σ^- detection respectively with increasing magnetic field.

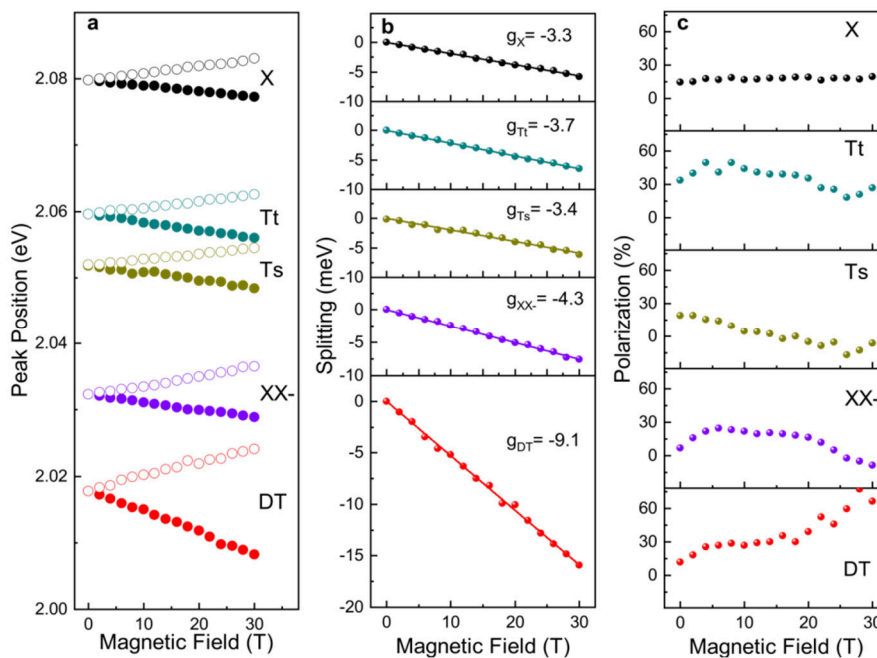


Figure S7. (a) PL peak positions for σ^+ and σ^- emission for position P1 versus magnetic field at 4.2K (b) Corresponding Zeeman splitting versus magnetic field and (c) Corresponding polarization degree as a function of magnetic field.

Figure S6 shows the magnetic field dependence of the PL peak positions (a), energy splittings (b) and polarization degrees (c) for all excitonic complexes for position P1. The obtained results are similar to the results in Figure 4. Figure S7 shows the circularly polarized PL spectra for the position P2 at 30 T for the σ^- - σ^- (σ^- -excitation and σ^- collection) and $\sigma^+\sigma^+$ configurations (σ^+ excitation and σ^+ collection). We observed that the σ^- emission shows an inverse PL intensity, relative to the σ^+ emission. Figure S8 shows the typical polarization-resolved PL spectra under σ^+ excitation in the energy range of the L1 and L2 emission peaks for different values of the magnetic field. Figure S9 shows the PL peak positions and Zeeman splittings of the L1 and L2 peaks as a function of magnetic field at 4 K. The extracted g-factors are also shown in this figure.

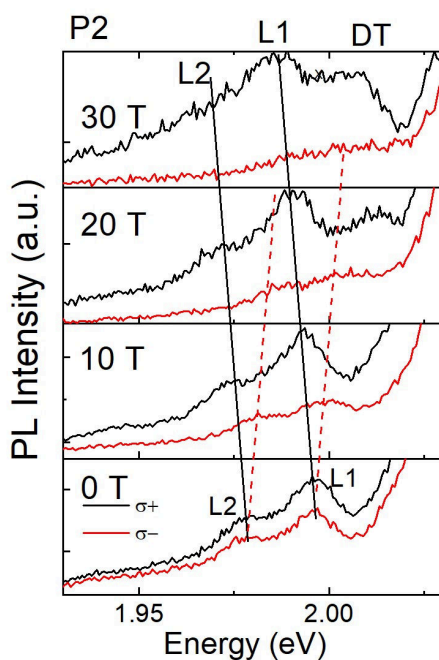


Figure S8. Details of the L1 and L2 emission peaks at position P2 under σ^+ excitation for different magnetic fields at 4.2K.

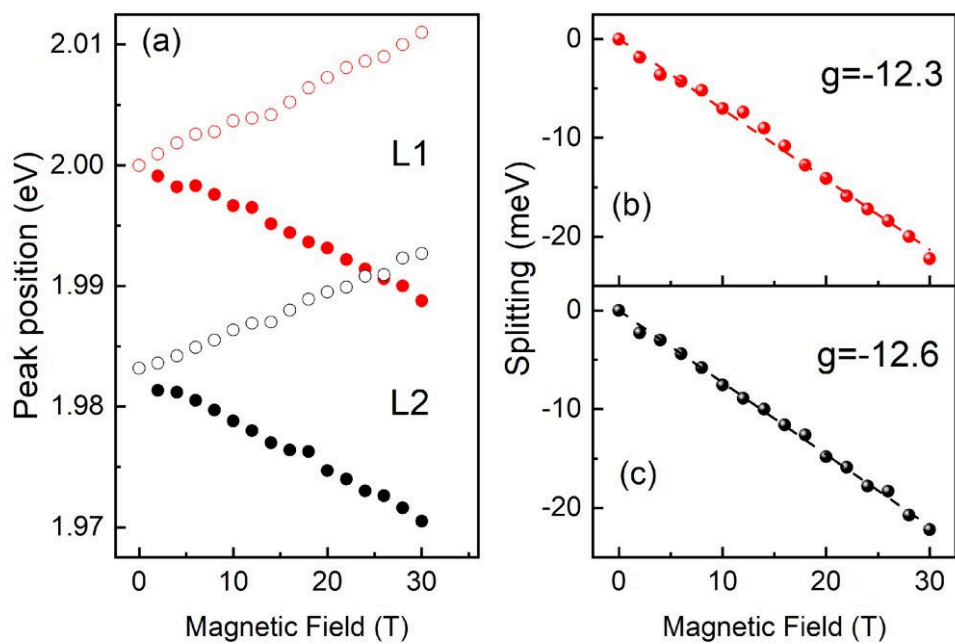


Figure S9. (a) PL peak positions and Zeeman splitting of peaks L1 (b) and L2 (c) as a function of magnetic field at 4.2 K for position P2.

2.2 Electrical and optical properties of transition metal dichalcogenides on talc dielectrics

Nanoscale



PAPER

[View Article Online](#)
[View Journal](#) | [View Issue](#)



Cite this: *Nanoscale*, 2021, **13**, 15853

Electrical and optical properties of transition metal dichalcogenides on talc dielectrics†

Darren Nutting,^a Gabriela A. Prando,^{a,b} Marion Severijnen,^c Ingrid D. Barcelos,^{id d} Shi Guo,^a Peter C. M. Christianen,^c Uli Zeitler,^c Yara Galvão Gobato ^{id *b,c} and Freddie Withers ^{id *a}

Advanced van der Waals (vdW) heterostructure devices rely on the incorporation of high quality dielectric materials which need to possess a low defect density as well as being atomically smooth and uniform. In this work we explore the use of talc dielectrics as a potentially clean alternative substrate to hexagonal boron nitride (hBN) for few-layer transition metal dichalcogenide (TMDC) transistors and excitonic TMDC monolayers. We find that talc dielectric transistors show small hysteresis which does not depend strongly on sweep rate and show negligible leakage current for our studied dielectric thicknesses. We also show narrow photoluminescence linewidths down to 10 meV for different TMDC monolayers on talc which highlights that talc is a promising material for future van der Waals devices.

Received 20th July 2021.
Accepted 29th August 2021
DOI: 10.1039/d1nr04723j

rsc.li/nanoscale

Electrical and optical properties of transition metal dichalcogenides on Talc dielectrics

Darren Nutting,^a Gabriela A. Prando,^{a,b} Marion Severijnen,^c Ingrid D. Barcelos^d Shi Guo^a, Peter C. M. Christianen^c Uli Zeitler^c Yara Galvão Gobato^{b,c} and Freddie Withers^a.

^aCollege of Engineering, Mathematics and Physical Sciences, University of Exeter, Exeter EX4 4QF, UK.

^bPhysics Department, Federal University of São Carlos, São Carlos, Brazil.

^cHigh Field Magnet Laboratory (HFML – EMFL), Radboud University, 6525 ED Nijmegen, The Netherlands.

^dBrazilian Synchrotron Light Laboratory, Brazilian Center for Research in Energy and Materials, Campinas, Brazil.

Advanced van der Waals (vdW) heterostructure devices rely on the incorporation of high quality dielectric materials which need to possess a low defect density as well as being atomically smooth and uniform. In this work we explore the use of talc dielectrics as a potentially clean alternative substrate to hexagonal boron nitride (hBN) for few-layer transition metal dichalcogenide (TMDC) transistors and excitonic TMDC monolayers. We find that talc dielectric transistors show small hysteresis which does not depend strongly on sweep rate and show negligible leakage current for our studied dielectric thicknesses. We also show narrow photoluminescence linewidths down to 10 meV for different TMDC monolayers on talc which highlights that talc is a promising material for future van der Waals devices.

I. Introduction

The field effect transistor (FET) is the fundamental building block of modern integrated circuits, which are used for information processing and data storage [1]. FETs typically have at least three contact terminals designated as source, drain and gate, and in principle rely on controlling the current flow through a channel material by applying an electric field across dielectric barrier in order to modulate the density of free charge carriers and hence the channel conductivity. Downscaling of transistor devices are required for miniaturized devices. State of the art transistor devices have been scaled down to the nanometre scale and are now approaching their fundamental size limitations [2]. Moore's law has shown an exponential increase in FET number density with time and, in turn, requires the length scales associated with the device to decrease, eventually reaching fundamental physical length scales. In addition to this, future FETs need to show continual improvement in their electrical performance such as having increased switching speeds, reduced energy cost per switch and improved sub-threshold swing [3]. In order to satisfy Moore's law, significant research efforts have been made to replace ultra-thin channel materials with high carrier mobility materials and significant down scaling. One possible avenue for improvement is the use of two-dimensional (2D) transition metal dichalcogenides (TMDCs) as alternative channel material instead of Si [4–7] or ultrathin van der Waals dielectrics such as hexagonal boron nitride (hBN) [8]. TMDCs have the chemical formula MX_2 , where M is a transition metal (for instance Mo or W) and X is a chalcogen (S, Se or Te). TMDC materials form layered hexagonally bonded structures of the form X–M–X with adjacent layers being held together by weak van der Waals forces, allowing for the exfoliation of monolayer flakes in a manner similar to graphene [10,11] and show promise for future optoelectronic device applications. Important for FETs, TMDCs also possess a band gap,[12–15] have high carrier mobility [5,16–18] and offer the choice of monolayer channel thicknesses, which facilitates improved FET switching behaviour whilst at the same time mitigating scaling issues such as source–drain tunnelling. Furthermore, these materials are also semi-transparent and flexible, allowing for the creation of a new generation of transparent and flexible electronics [19,20].

Therefore, significant steps have been made regarding the incorporation of TMDC monolayers into FET prototypes with the goal of producing devices which can compete with commercially available FETs based on Si. Although still in an embryonic stage of development, TMDC-based FETs have demonstrated competitive switching behavior [11,21,22] and subthreshold swing [23,24] compared to the theoretical limit of Si-based transistors [25,26]. Despite this, TMDC channels consistently underperform when compared to their maximum theoretical potential [11,27], a direct result of both extrinsic (adsorbents, lattice vacancies, etc.) and intrinsic (channel and channel dielectric interface phonon) scattering, both of which drastically lower the carrier mobility and hence electrical performance of the FET [28]. Consequently, it is important to keep in mind the FET performance not only depends on the channel material but also on the choice of dielectric substrate and metallic contact material as well. Ideally, the barrier material will have a large band gap and high permittivity, an atomically flat surface free of dangling bonds and a large band offset with the channel material to prevent leakage current, and as a result dielectrics such as hBN [29,30,31], HfO₂ [32,33] and Al₂O₃ [34] have been shown to drastically improve the electrical performance when incorporated into TMDC-based FETs. Therefore, investigation of the entire dielectric parameter space is required in order to identify materials which could potentially alleviate these issues and thus optimize device performance. One such overlooked material group are the layered oxides. Specifically in this work we focus on the material Talc, which is insulating crystalline magnesium silicate which has the complex chemical composition Mg₃Si₄O₁₀(OH)₂ [35] a large band gap (5 eV at the Γ -point) [35], dielectric constant of 2–4 [36] and a layered structure allowing for mechanical exfoliation into atomically flat monolayers [35–41], thus making it a potential candidate dielectric material for future TMDC-based FETs. Moreover, recent work incorporating this dielectric within graphene transistors has shown comparable performance to commercially available hBN dielectric crystals [36]. As of yet a detailed study into the optical and electrical performance of TMDC materials placed on these substrates has not been done. In this work we study, through a combination of electrical transport and photoluminescence measurements, the performance of this emerging dielectric material.

II. Results

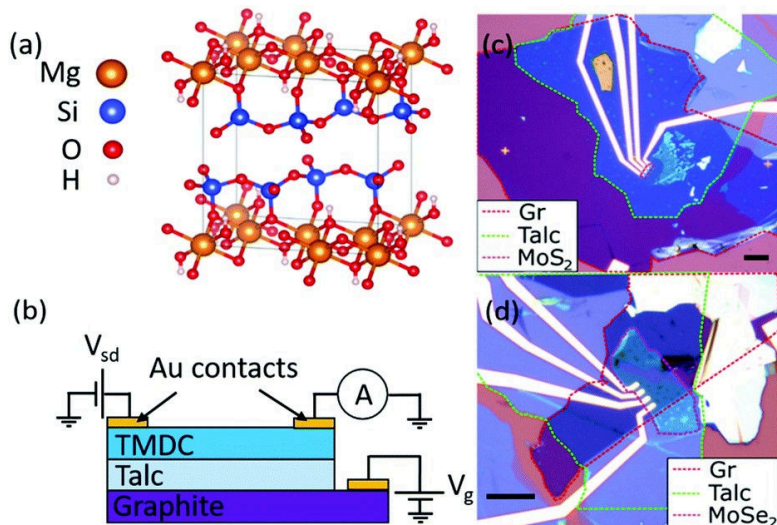


Fig. 1(a) illustrates the crystal structure of the talc used as a dielectric within our devices.

Each individual talc layer consists of a layer of Mg atoms situated between two quartzlike Si–O layers, with additional hydroxyl units present. Weak vdW forces hold the adjacent layers together [42] allowing for the exfoliation of few layer flakes via the usual scotch-tape method [43]. Fig.1(b) illustrates the device architecture of the MoS₂ and MoSe₂ FETs, shown in (c,d), respectively, used within this study. In both devices, talc flakes are used as a dielectric layer and graphite flakes serve as electrical contacts for application of a back-gate voltage, V_g . All structures were created using standard mechanical transfer techniques [44]. The source and drain channel contacts, along with the back-gate contact on the underlying graphite, were patterned using standard electron beam lithography. Finally, Cr/Au (5 nm/50 nm) contacts were then deposited through thermal evaporation.

FET characterization

An important property for any dielectric material is the breakdown electric field. To determine this, we produced a simple graphite-talc-Au device on a quartz substrate, see ESI (Fig.S2). From the I – V curves measured in ambient conditions we found that the average breakdown field to be, $E_{BD} = 0.5 \pm 0.2 \text{ V nm}^{-1}$. This value is found to be similar to our thermally grown SiO₂ oxides measured under

the same conditions (Our 300 nm thick thermally grown SiO₂ wafers typically break down at 0.4–0.5 V nm⁻¹) and consistent with earlier reports [36]. However, under inert conditions (He atmosphere) our talc dielectric was found not to break-down even at fields as high as 1.2 V nm⁻¹, Fig. S4. Such large values of breakdown field are comparable to highest quality hBN crystals [45]. In order to understand the electrical transport measurements, it is necessary to measure the physical dimensions of the individual layers, particularly that of the talc dielectric as this is needed to estimate the field-effect mobility, μ , for each device. Atomic force microscopy (AFM) was used to determine the talc thickness, see ESI (Fig. S1), which were measured for two devices, $d_{\text{talc}} = 18.4 \pm 1.9$ nm and 29.4 ± 3.3 nm in the MoS₂ and MoSe₂ FETs, respectively. In addition to this, AFM was also used in conjunction with Raman microscopy, see ESI (Fig. S1), to determine the thickness [46,47] of the MoS₂ and MoSe₂ channels, which were measured as 4.5 ± 0.3 nm and 40.1 ± 6.9 nm, respectively.

Fig. 2(a, b, d and e) shows, for both channel materials, the typical source–drain ($I_{\text{sd}}-V_{\text{sd}}$) sweeps taken at different values of V_{g} in each device, whilst Fig. 2(c and f) shows I_{sd} versus V_{g} at $V_{\text{sd}} = 0.03$ V. Additional measurements at higher bias voltages are available within the ESI, Fig. S4. Measurements were performed using a two-terminal configuration in a He atmosphere at $T = 270$ K. Additional measurements at cryogenic temperatures are available within the ESI, Fig. S3. Hysteresis can be seen within Fig. 2(c and f), likely the result of defects at the channel-dielectric interface charging as V_{g} is swept [48] which scatter charge carriers within the channel material. This is a consequence of surface adsorbates and natural impurities within the composition of our talc crystals (expected to be Fe and Al) [49]. The magnitude of the hysteresis width (the difference between forward and backward-sweep threshold voltages) can be controlled by the back-gate sweep rate and shows a small increase above ~ 0.5 Vs⁻¹ in both MoS₂ and MoSe₂ FETs (see ESI, Fig. S4).

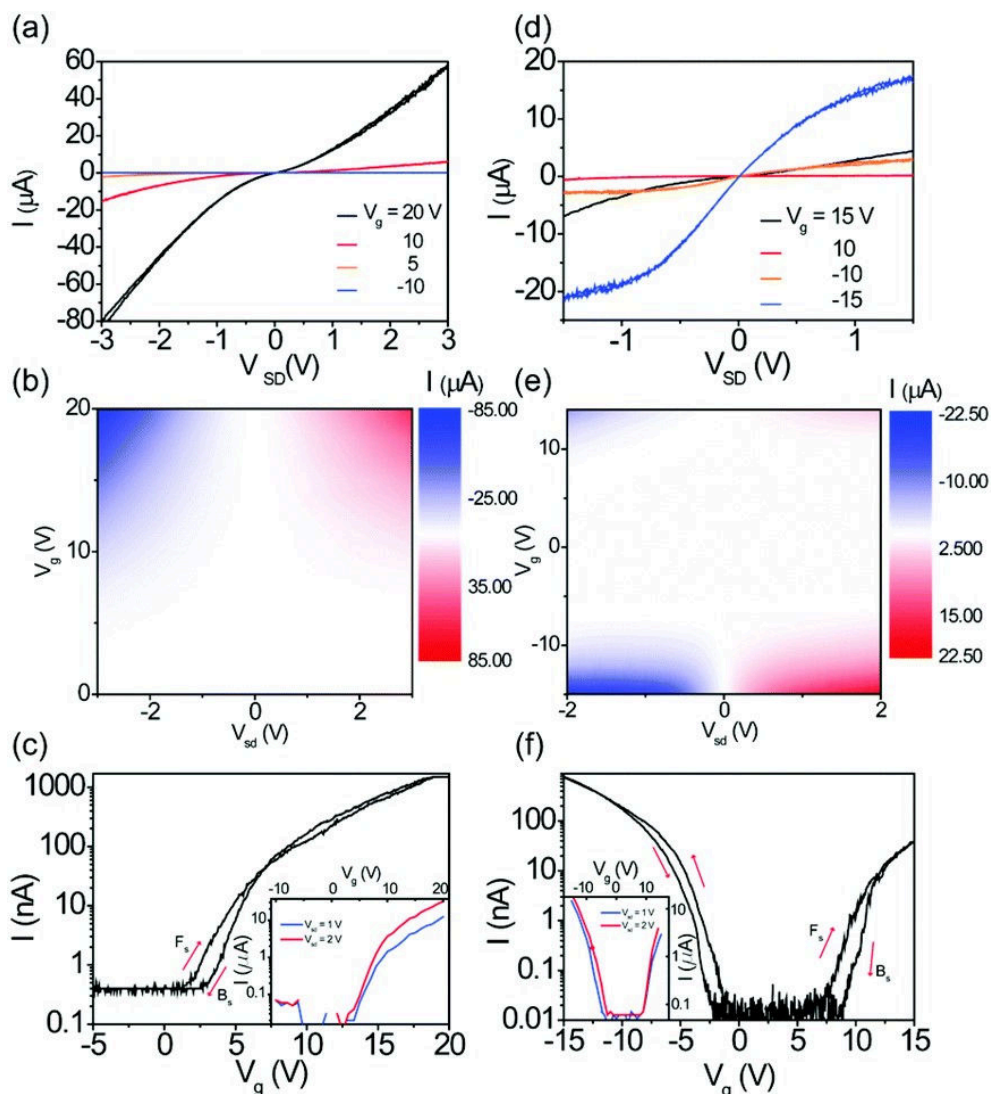


Fig. 2 Electrical transport measurements ($T = 270\text{K}$, Helium atmosphere). (a–c) Electronic transport measurements on the MoS_2 FET device. (d–f) Electronic transport measurements on the MoSe_2 device. (a and d) I_{SD} versus V_{SD} for select values of V_g , with complete contour plots shown in (b, e), highlighting ambipolar behaviour in the MoSe_2 FET. (c, f) Representative I_{SD} versus V_g with $V_{\text{SD}} = 0.03\text{ V}$, where F_s and B_s represent the forwards and backwards sweeps, respectively. Insets: I – V_g for larger values of V_{SD} .

The change in threshold voltage between forwards and backwards sweeps, ΔV_{th} , is approximately constant in our devices for sweep rates up to at least 0.6 V s^{-1} , with $\Delta V_{\text{th,e}} \sim 2\text{ V}$ for electron conduction in both FETs and $\Delta V_{\text{th,h}} \sim 0.75\text{ V}$ for hole conduction within the MoSe_2 -based FET. There is a wide range of hysteresis widths reported in the literature for both MoS_2 and MoSe_2 FETs utilizing either SiO_2 or hBN as a dielectric (see ESI, Table S1), a result of several factors such as the measurement conditions, dielectric material used and

whether or not the devices were encapsulated [50–52]. All these factors determine the concentration of adsorbates both on the surface of the channel material and at the channel-dielectric interface [1,51] which can become charged and introduce hysteretic effects into the measurements. Despite the lack of encapsulation in our FETs, the hysteresis widths generally compare favorably with similar devices in the literature, indicating the optimization of future FET prototypes using talc as a gate dielectric material. The

MoS₂-based FET is unipolar across $-5 \text{ V} \leq V_g \leq 20 \text{ V}$ with a forward sweep threshold voltage, $V_{th, f}$, of $\sim 1 \text{ V}$ and backwards-sweep threshold voltage of $V_{th, b} \sim 3 \text{ V}$ at room temperature. The MoSe₂-based FET shows typical ambipolar behavior [53,54] across $-15 \text{ V} \leq V_g \leq 15 \text{ V}$ with $V_{th, f} \sim -2.5 \text{ V}$ (7 V) and $V_{th, b} \sim -0.5 \text{ V}$ (8 V) for hole (electron) conduction at room temperature. At a bias voltage of $V_{sd} = 0.03 \text{ V}$, the MoS₂-based FET was found to display an on/off ratio of 4×10^3 for electron conduction at $V_g = 20 \text{ V}$, an off-state current, $I_{off} \sim 350 \text{ pA}$, a sub-threshold swing $SS = 1.60 \pm 0.07 \text{ V dec}^{-1}$ and, using $\epsilon = 3$ as the permittivity of talc [36], an electron mobility of $\sim 0.81 \text{ cm}^2 \text{ V}^{-1} \text{ s}^{-1}$. This electron mobility is less than reported in MoS₂/hBN and MoS₂/HfO₂-based FETs [4,55], although it is comparable to MoS₂/SiO₂[10] and MoS₂/Al₂O₃[34] FETs. The low mobility is well known to be due to the large Schottky barriers at the TMDC Cr/Au contacts [56]. The large value of sub-threshold swing is a result of the thickness of the talc dielectric used. At a bias voltage $V_{sd} = 0.03 \text{ V}$, the MoSe₂-based FET had an on/off current ratio of 1×10^5 (5×10^3) for hole (electron) conduction at $V_g = -15 \text{ V}$ (15 V), an off-state current $I_{off} \sim 10 \text{ pA}$, a sub-threshold swing $SS = 1.39 \pm 0.12 \text{ V dec}^{-1}$ ($1.17 \pm 0.15 \text{ V dec}^{-1}$) and, with $\epsilon = 3$, a carrier mobility of $\sim 5.1 \text{ cm}^2 \text{ V}^{-1} \text{ s}^{-1}$ ($\sim 3.3 \text{ cm}^2 \text{ V}^{-1} \text{ s}^{-1}$). Similar to our MoS₂-based FETs, the carrier mobilities in this device are lower than those reported in MoSe₂/hBN and also MoSe₂/SiO₂-based MoSe₂/SiO₂ [57]. One point to note is the doping of our material which we find to be n-type for MoS₂ however p-type for MoSe₂. Overall, we find that our TMDC channel materials are slightly more p-type than MoS₂ and MoSe₂ transistors on hBN or SiO₂ dielectrics.

Photoluminescence characterization of TMDC's on talc substrates

We now turn our attention to the optical performance of monolayer TMDCs placed on a talc dielectric. In general, an enhancement of photoluminescence (PL) signal and reduced linewidth was observed compared to emission from TMDCs placed directly on SiO₂.

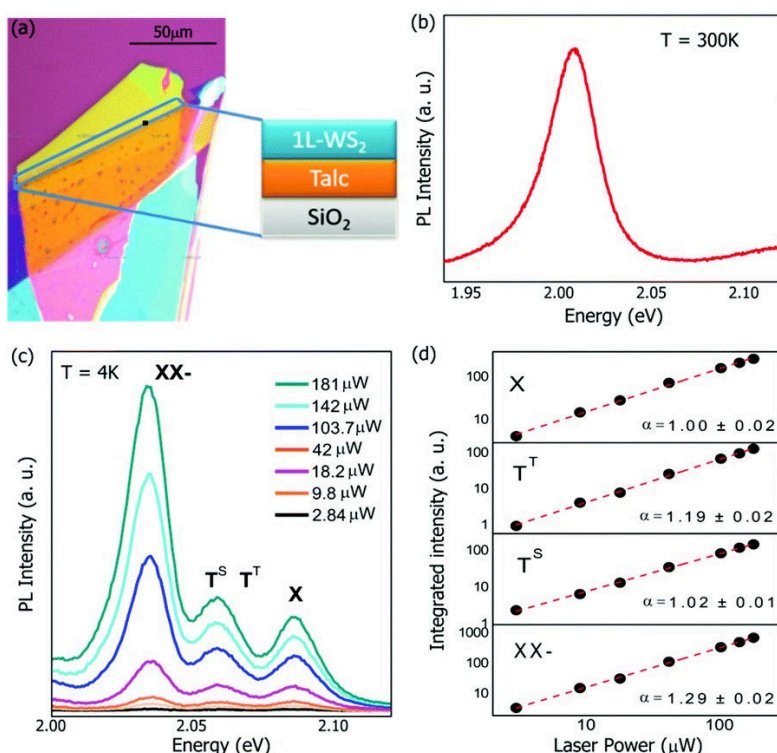


Fig. 3 - (a) Optical micrograph of a WS₂/talc sample. (b) Typical PL spectrum of a WS₂ monolayer on talc at 300 K. (c) PL spectra at 4 K for different incident laser powers, (d) Double logarithmic representation of Integrated PL intensity as a function of laser power.

Fig. 3(a) shows a typical WS₂/talc heterostructure device with the monolayer region highlighted by a blue perimeter. Fig. 3(b) shows a typical PL spectrum at room temperature for a WS₂ monolayer on talc. A peak is observed at 2.008 eV with a full-width half-maximum (FWHM) of ~30 meV, a reduction compared to WS₂/SiO₂ samples which are ~50 meV [58]. We also measured the photoluminescence properties of the structure at cryogenic temperatures; Fig. 3(c) shows the PL spectrum at low temperature (4 K) for a variety of different laser power excitations. The typical FWHM of the Exciton peak at 4 K is ~10 meV which is once again a reduction compared to monolayers of WS₂ placed on SiO₂,

which are typically ~ 20 meV [59,60] and comparable to WS_2/hBN which typically show linewidths $\sim 10\text{--}15$ meV [61,62].

Furthermore, these values of FWHM for monolayer TMDCs on talc substrates can be further reduced by using appropriate thermal treatment such as the standard procedures used for hBN-encapsulated TMDC monolayers. The observed small FWHM and strong PL intensity suggests that talc can serve as an effective material for isolating TMDC monolayers from SiO_2 and consequently preserve the intrinsic optical properties of the TMDC. For example, both the neutral exciton and trion emission peaks can be observed at 2.086 eV and 2.056 eV, respectively. The latter of these corresponds to a trion binding energy ~ 30 meV smaller than is typically observed for monolayer WS_2/hBN heterostructures. Moreover, the trion peak presents a clear asymmetry which is associated with unresolved PL emission from different trion species. Therefore, the trion peak was deconvolved into two separate peaks, one at 2.053 eV and the other at 2.060 eV which are associated to singlet (T^S) and triplet (T^T) trion states formed *via* the Coulomb exchange interaction [63]. In addition to these, another strong PL peak at 2.034 eV (along with several low intensity peaks at lower energies) were observed, which, at first glance, are usually attributed to the recombination of carriers localized at defects. However, measurements at varying incident laser power indicate that the additional strong PL peak at 2.034 eV seems to be due to charged biexciton emission (XX^-) instead [64,65]. In order to further analyse these peaks, we have fitted the PL spectra using Voigt functions. Fig. 3(d) shows the PL intensity of these additional peaks as a function of incident laser power. The power law dependence of PL intensity can be expressed as $I \propto P^\alpha$, where I is the integrated PL intensity and P is the laser power. By fitting the spectra with Voigt functions, we obtain $\alpha = 1$ for the neutral Exciton emission, $\alpha = 1.19$ and 1.02 for emission from the triplet and singlet trion states, and $\alpha = 1.30$ for the lower energy peak associated to the charged biexciton. Therefore, the observed laser power dependencies for all emission peaks are consistent to previous interpretations of the PL spectra measured from WS_2 monolayers reported in the literature [63–65].

III. Conclusion

In conclusion we have characterised the optical and electronic properties of various TMDCs on talc dielectrics. We find that our FETs show small hysteresis compared to SiO₂ and comparable electron transport characteristics compared to similar devices using hBN as a dielectric. We also show that the PL properties of monolayer WS₂ indicate an improvement compared to exfoliated WS₂ on SiO₂ substrates [58– 60] and comparable to WS₂/hBN [61, 62]. Overall, this work indicates that talc dielectrics can serve as a promising alternative to commonly used hBN to produce future vdW electronic devices as well as a suitable substrate within TMDC-based optoelectronic devices.

Methods

Materials

Talc is a soft magnesium silicate mineral with a crystalline structure that contains three octahedral Mg positions per four tetrahedral Si positions with the chemical formula $\text{Mg}_3\text{Si}_4\text{O}_{10}(\text{OH})_2$. The bulk crystals were purchased in Ouro Preto, Brazil from a talc and soapstone mine. Conventional mechanical exfoliation methods were used to produce few-layer talc atop a substrate, which consisted of p-doped Si covered by a 300 nm thick SiO_2 layer. TMDC monolayers were obtained from the same crystal purchased from HQ Graphene. Flakes of WS_2 , MoS_2 and MoSe_2 were exfoliated on commercial PDMS film (Gel-Film® PF-40-X4-A sold by Gel Pak) using adhesive tape. The PDMS stamp with TMDC attached was placed onto a transparent quartz plate and brought into contact with a thin Au film (formed through sputtering onto Si) at room temperature. The ensemble was heated to 65 °C for two minutes using a Peltier module beneath the Si/ SiO_2 substrate. After allowing the ensemble to cool down, the PDMS stamp was slowly detached, leaving behind the exfoliated flakes transferred on top. The transfer processes we performed in a cleanroom at 23 °C \pm 1 °C with a humidity of 55% \pm 5%.

Materials characterisation

Micro-Raman spectroscopy was carried out using a Renishaw RM1000 system which uses 532 nm excitation at 1 mW laser power, which was focused into a 1 μm diameter spot. AFM was performed using a Bruker Innova system operating in the tapping mode to ensure minimal damage to the sample surface. The tips used were Nanosensors PPP = NCHR, which have a radius of curvature <10 nm, spring constant of 42 N m^{-1} and operate at a nominal frequency of 330 kHz.

Photoluminescence measurements

Micro-PL measurements were carried out at 300 K and 4 K using 532 nm laser excitation with varying laser power. The samples were placed within an attocube positioner inside of a cryostat. The laser was focused using a 50 \times

Attocube objective lens within the cryostat resulting in a 4 μm diameter spot size. The PL signals were collected and focused onto a Spectra Pro 300i spectrometer coupled to a PyLon Princeton instruments Si CCD.

Electrical measurements

Electrical measurements were carried out in AC (37 Hz) using a 7265 DSP Lock-in amplifier in conjunction with a Femto DLPCA-200 current amplifier. DC measurements utilized two Keithley 2400 source-meters. One was used to provide source–drain bias and the second biased the graphite gate.

Conflicts of interest

There are no conflicts to declare.

Acknowledgements

I. D. B. acknowledges the financial support from the Brazilian Nanocarbon Institute of Science and Technology (INCT/Nanocarbono), Brazilian Synchrotron Light Laboratory (LNLS) and Fapesp (grant 18/00823-0). YGG and GP acknowledge financial support from CAPES and Fapesp (grants 18/01808-5 and 19/23488-5). D. N. acknowledges support from the Leverhulme trust.

References

1. F. Schwierz , J. Pezoldt and R. Granzner , *Nanoscale*, 2015, **7** , 8261 — 8283.
2. G. E. Moore *Isscc Dig. Tech. Pap. I*, 2003, **46** , 20 —23.
3. J. A. del Alamo *Nature*, 2011, **479** , 317 —323.
4. B. Radisavljevic , A. Radenovic , J. Brivio , V. Giacometti and A. Kis , *Nat. Nanotechnol.*, 2011, **6** , 147 —150.
5. S. Larentis , B. Fallahazad and E. Tutuc , *Appl. Phys. Lett.*, 2012, **101** , 223104.
6. W. S. Hwang , M. Remskar , R. S. Yan , V. Protasenko , K. Tahy , S. D. Chae , P. Zhao , A. Konar , H. L. Xing , A. Seabaugh and D. Jena , *Appl. Phys. Lett.*, 2012, **101** , 013107 .
7. M. Tosun , S. Chuang , H. Fang , A. B. Sachid , M. Hettick , Y. J. Lin , Y. P. Zeng and A. Javey , *ACS Nano*, 2014, **8** , 4948 —4953 .
8. C. R. Dean , A. F. Young , I. Meric , C. Lee , L. Wang , S. Sorgenfrei , K. Watanabe , T. Taniguchi , P. Kim , K. L. Shepard and J. Hone , *Nat. Nanotechnol.*, 2010, **5** , 722 —726 .
9. S. Ahmed and J. B. Yi , *Nano-Micro Lett.*, 2017, **9** , 50 .
10. K. S. Novoselov , D. Jiang , F. Schedin , T. J. Booth , V. V. Khotkevich , S. V. Morozov and A. K. Geim , *Proc. Natl. Acad. Sci. U. S. A.*, 2005, **102** , 10451 — 10453 .
11. L. T. Liu , S. B. Kumar , Y. Ouyang and J. Guo , *IEEE Trans. Electron Devices*, 2011, **58** , 3042 —3047 .
12. K. F. Mak , C. Lee , J. Hone , J. Shan and T. F. Heinz , *Phys. Rev. Lett.*, 2010, **105** , 136805 .

13. S. Tongay , J. Zhou , C. Ataca , K. Lo , T. S. Matthews , J. B. Li , J. C. Grossman and J. Q. Wu , *Nano Lett.*, 2012, **12** , 5576 —5580 .
14. A. L. Elias , N. Perea-Lopez , A. Castro-Beltran , A. Berkdemir , R. T. Lv , S. M. Feng , A. D. Long , T. Hayashi , Y. A. Kim , M. Endo , H. R. Gutierrez , N. R. Pradhan , L. Balicas , T. E. Mallouk , F. Lopez-Urias , H. Terrones and M. Terrones , *ACS Nano*, 2013, **7** , 5235 —5242 .
15. W. J. Zhao , Z. Ghorannevis , L. Q. Chu , M. L. Toh , C. Kloc , P. H. Tan and G. Eda , *ACS Nano*, 2013, **7** , 791 —797 .
16. W. Z. Bao , X. H. Cai , D. Kim , K. Sridhara and M. S. Fuhrer , *Appl. Phys. Lett.*, 2013, **102** , 042104 —042107 .
17. Y. Cui , R. Xin , Z. H. Yu , Y. M. Pan , Z. Y. Ong , X. X. Wei , J. Z. Wang , H. Y. Nan , Z. H. Ni , Y. Wu , T. S. Chen , Y. Shi , B. G. Wang , G. Zhang , Y. W. Zhang and X. R. Wang , *Adv. Mater.*, 2015, **27** , 5230 —5234 .
18. H. Fang , S. Chuang , T. C. Chang , K. Takei , T. Takahashi and A. Javey , *Nano Lett.*, 2012, **12** , 3788 —3792 .
19. Y. K. Hong , G. Yoo , J. Kwon , S. Hong , W. G. Song , N. Liu , I. Omkaram , B. Yoo , S. Ju , S. Kim and M. S. Oh , *AIP Adv.*, 2016, **6** , 222105 —22110 .
20. W. G. Song , H. J. Kwon , J. Park , J. Yeo , M. Kim , S. Park , S. Yun , K. U. Kyung , C. P. Grigoropoulos , S. Kim and Y. K. Hong , *Adv. Funct. Mater.*, 2016, **26** , 2426 —2434 .
21. Y. Y. Illarionov , K. K. H. Smithe , M. Wlatl , T. Knobloch , E. Pop and T. Grasser , *IEEE Electron. Device Lett.*, 2017, **38** , 1763 —1766 .
22. Y. Y. Illarionov, K. K. H. Smithe, M. Wlatl, R. W. Grady, S. Deshmukh, E. Pop and T. Grasser, 2018 76th Device Research Conference (Drc), 2018.
23. P. Kumar , M. Gupta and K. Singh , *Silicon*, 2020, **12** , 1857 —1864 .

24. P. Bolshakov , P. Zhao , A. Azcatl , P. K. Hurley , R. M. Wallace and C. D. Young , *Appl. Phys. Lett.*, 2017, **111** , 032110 —032114 .
25. Q. Chen , B. Agrawal and J. D. Meindl , *IEEE Trans. Electron Devices*, 2002, **49** , 1086 —1090 .
26. G. Pei , J. Kedzierski , P. Oldiges , M. leong and E. C. C. Kan , *IEEE Trans. Electron Devices*, 2002, **49** , 1411 —1419 .
27. Y. Yoon , K. Ganapathi and S. Salahuddin , *Nano Lett.*, 2011, **11** , 3768 —3773 .
28. Z. H. Yu , Z. Y. Ong , S. L. Li , J. B. Xu , G. Zhang , Y. W. Zhang , Y. Shi and X. R. Wang , *Adv. Funct. Mater.*, 2017, **27** , 1604093 —10604109 .
29. K. K. Kim , H. S. Lee and Y. H. Lee , *Chem. Soc. Rev.*, 2018, **47** , 6342 —6369 .
30. F. Withers , T. H. Bointon , D. C. Hudson , M. F. Craciun and S. Russo , *Sci Rep.*, 2014, **4** , 4967 .
31. H. C. P. Movva , A. Rai , S. Kang , K. Kim , B. Fallahazad , T. Taniguchi , K. Watanabe , E. Tutuc and S. K. Banerjee , *ACS Nano*, 2015, **9** , 10402 —10410 .
32. C. D. Young , P. Zhao , P. Bolshakov-Barrett , A. Azcatl , P. K. Hurley , Y. Gomeniuk , M. Schmidt , C. Hinkle and R. M. Wallace , *Sci. Adv.*, 2016, **75** , 153 —162 .
33. N. Peimyoo , M. D. Barnes , J. D. Mehew , A. De Sanctis , I. Amit , J. Escolar , K. Anastasiou , A. P. Rooney , S. J. Haigh , S. Russo , M. F. Craciun and F. Withers , *Sci. Adv.*, 2019, **5** , eaau0906 .
34. H. Bergeron , V. K. Sangwan , J. J. McMorow , G. P. Campbell , I. Balla , X. L. Liu , M. J. Bedzyk , T. J. Marks and M. C. Hersam , *Appl. Phys. Lett.*, 2017, **110** , 053101 .

35. A. B. Alencar , A. P. M. Barboza , B. S. Archanjo , H. Chacham and B. R. A. Neves , *2D Mater.*, 2015, **2** , 015004 .
36. E. Mania , A. B. Alencar , A. R. Cadore , B. R. Carvalho , K. Watanabe , T. Taniguchi , B. R. A. Neves , H. Chacham and L. C. Campos , *2D Mater.*, 2017, **4** , 031008 .
37. A. Harvey , J. B. Boland , I. Godwin , A. G. Kelly , B. M. Szydłowska , G. Murtaza , A. Thomas , D. J. Lewis , P. O'Brien and J. N. Coleman , *2d Mater.*, 2017, **4** , 025054 .
38. I. D. Barcelos , A. R. Cadore , A. B. Alencar , F. C. B. Maia , E. Mania , R. F. Oliveira , C. C. B. Bufon , A. Malachias , R. O. Freitas , R. L. Moreira and H. Chacham , *ACS Photonics*, 2018, **5** , 1912 —1918 .
39. R. Frisenda , Y. Niu , P. Gant , M. Munoz and A. Castellanos-Gomez , *npj 2D Mater. Appl.*, 2020, **4** , 38.
40. B. Vasic , C. Czibula , M. Kratzer , B. R. A. Neves , A. Matkovic and C. Teichert , *Nanotechnology*, 2021, **32** , 265701 .
41. A. R. Cadore , E. Mania , A. B. Alencar , N. P. Rezende , S. de Oliveira , K. Watanabe , T. Taniguchi , H. Chacham , L. C. Campos and R. G. Lacerda , *Sens. Actuators, B*, 2018, **266** , 438 —446.
42. W. Ward and J. M. Phillips , *Surf. Sci.*, 1971, **25** , 379 —384 .
43. K. S. Novoselov , A. K. Geim , S. V. Morozov , D. Jiang , Y. Zhang , S. V. Dubonos , I. V. Grigorieva and A. A. Firsov , *Science*, 2004, **306** , 666 —669 .
44. A. Castellanos-Gomez , M. Buscema , R. Molenaar , V. Singh , L. Janssen , H. S. J. van der Zant and G. A. Steele , *2D Mater.*, 2014, **1** , 011002 .
45. Y. Hattori , T. Taniguchi , K. Watanabe and K. Nagashio , *ACS Nano*, 2015, **9** , 916 —921 .

46. H. Li , Q. Zhang , C. C. R. Yap , B. K. Tay , T. H. T. Edwin , A. Olivier and D. Baillargeat , *Adv. Funct. Mater.*, 2012, **22** , 1385 —1390 .
47. P. Tonndorf , R. Schmidt , P. Bottger , X. Zhang , J. Borner , A. Liebig , M. Albrecht , C. Kloc , O. Gordan , D. R. T. Zahn , S. M. de Vasconcellos and R. Bratschitsch , *Opt. Express*, 2013, **21** , 4908 —4916 .
48. A. Di Bartolomeo , L. Genovese , F. Giubileo , L. Iemmo , G. Luongo , T. Foller and M. Schleberger , *2D Mater.*, 2018, **5** , 015014 .
49. M. L. M. Rodrigues and R. M. F. Lima , *J. Cleaner Prod.*, 2012, **32** , 149 — 156 .
50. D. J. Late , B. Liu , H. S. S. Ramakrishna Matte , V. P. Dravid and C. N. R. Rao , *ACS Nano*, 2012, **6** , 5635 —5641 .
51. Y. Y. Illarionov , G. Rzepa , M. Waihl , T. Knobloch , A. Grill , M. M. Furchi , T. Mueller and T. Grasser , *2D Mater.*, 2016, **3** , 035004 .
52. C. Lee , S. Rathi , M. A. Khan , D. Lim , Y. Kim , S. J. Yun , D. H. Youn , K. Watanabe , T. Taniguchi and G. H. Kim , *Nanotechnology*, 2018, **29** , 335202 .
53. N. R. Pradhan , D. Rhodes , Y. Xin , S. Memaran , L. Bhaskaran , M. Siddiq , S. Hill , P. M. Ajayan and L. Balicas , *ACS Nano*, 2014, **8** , 7923 —7929 .
54. D. N. Ortiz , I. Ramos , N. J. Pinto , M. Q. Zhao , V. Kumar and A. T. C. Johnson , *AIP Adv.*, 2018, **8** , 035014.
55. G. H. Lee , Y. J. Yu , X. Cui , N. Petrone , C. H. Lee , M. S. Choi , D. Y. Lee , C. Lee , W. J. Yoo , K. Watanabe , T. Taniguchi , C. Nuckolls , P. Kim and J. Hone , *ACS Nano*, 2013, **7** , 7931 —7936 .
56. D. S. Schulman , A. J. Arnold and S. Das , *Chem. Soc. Rev.*, 2018, **47** , 3037 — 3058 .

57. B. Chamlagain , Q. Li , N. J. Ghimire , H. J. Chuang , M. M. Perera , H. G. Tu , Y. Xu , M. H. Pan , D. Xiao , J. Q. Yan , D. Mandrus and Z. X. Zhou , *ACS Nano*, 2014, **8** , 8710 —8710 .
58. F. Cadiz , E. Courtade , C. Robert , G. Wang , Y. Shen , H. Cai , T. Taniguchi , K. Watanabe , H. Carrere , D. Lagarde , M. Manca , T. Amand , P. Renucci , S. Tongay , X. Marie and B. Urbaszek , *Phys. Rev. X*, 2017, **7** , 021026 .
59. G. Plechinger , P. Nagler , J. Kraus , N. Paradiso , C. Strunk , C. Schuller and T. Korn , *Phys. Status Solidi RRL*, 2015, **9** , 457 —461 .
60. G. Plechinger , P. Nagler , A. Arora , R. Schmidt , A. Chernikov , A. G. del Aguila , P. C. M. Christianen , R. Bratschitsch , C. Schuller and T. Korn , *Nat. Commun.*, 2016, **7** , 12715 .
61. J. Jadczyk , L. Bryja , J. Kutrowska-Girzycka , P. Kapuscinski , M. Bieniek , Y. S. Huang and P. Hawrylak , *Nat. Commun.*, 2019, **10** , 107 .
62. J. Jadczyk , J. Kutrowska-Girzycka , M. Bieniek , T. Kazimierczuk , P. Kossacki , J. J. Schindler , J. Debus , K. Watanabe , T. Taniguchi , C. H. Ho , A. Wojs , P. Hawrylak and L. Bryja , *Nanotechnology*, 2021, **32** , 145717 .
63. P. Nagler , M. V. Ballottin , A. A. Mitioglu , M. V. Durnev , T. Taniguchi , K. Watanabe , A. Chernikov , C. Schuller , M. M. Glazov , P. C. M. Christianen and T. Korn , *Phys. Rev. Lett.*, 2018, **121** , 057402 .
64. M. Barbone , A. R. P. Montblanch , D. M. Kara , C. Palacios-Berraquero , A. R. Cadore , D. De Fazio , B. Pingault , E. Mostaani , H. Li , B. Chen , K. Watanabe , T. Taniguchi , S. Tongay , G. Wang , A. C. Ferrari and M. Atature , *Nat. Commun.*, 2018, **9** , 3721 .
65. V. O. Gordo , M. A. G. Balanta , Y. G. Gobato , F. S. Covre , H. V. A. Galeti , F. Iikawa , O. D. D. Couto , F. Qu , M. Henini , D. W. Hewak and C. C. Huang , *Nanoscale*, 2018, **10** , 4807 —4815 .

Supplementary Information:

Electrical and optical properties of transition metal dichalcogenides on
Talc dielectrics.

1. Characterisation of FET devices

1.1. AFM characterisation

Figure S1 illustrates AFM images of the MoS₂, MoSe₂ and talc layers within our FETs. These images, and their corresponding line profiles, were computed using Gwyddion analysis software ¹. The large error on the thickness of the MoSe₂ channel given in the main text is a result of non-uniformity in channel thickness across its length, as shown by the blue profile in Figure S1 (h).

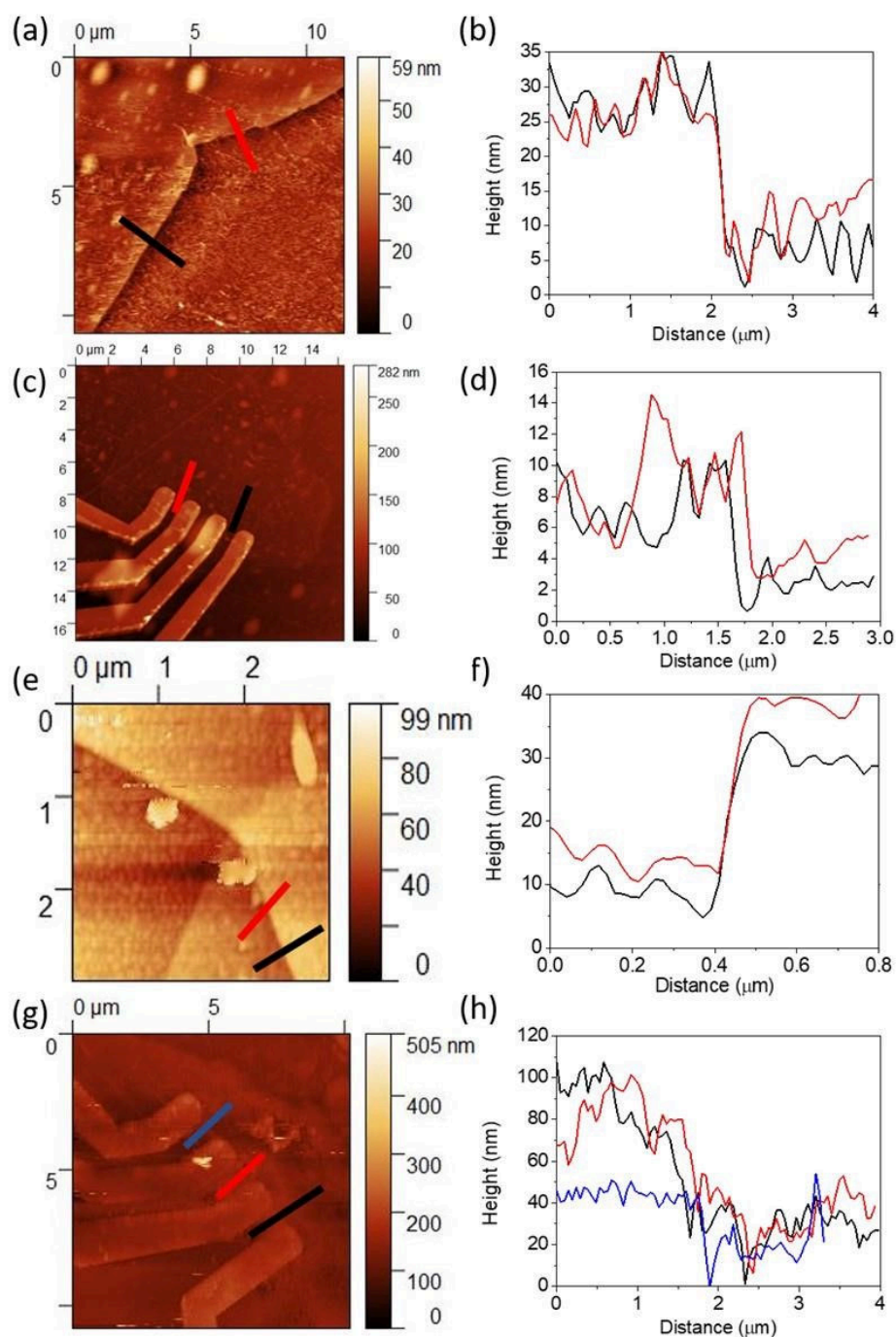


Figure S1. AFM characterisation of TMDC/talc heterostructures. (a, b) and (c, d) AFM image and line profile of the talc dielectric and MoS₂ channel within the MoS₂/talc FET, respectively. (e, f) and (g, h) AFM image and line profile of the talc dielectric and MoSe₂ channel within the MoSe₂/talc FET, respectively.

1.2. Breakdown electric field in ambient conditions

Figure S2 shows the breakdown voltage I-V traces for a 15 ± 3 nm thick talc dielectric barrier. We find the breakdown electric field of talc dielectrics to be $E_{BD} = 0.5 \pm 0.2 \text{ V}_{nm}^{-1}$

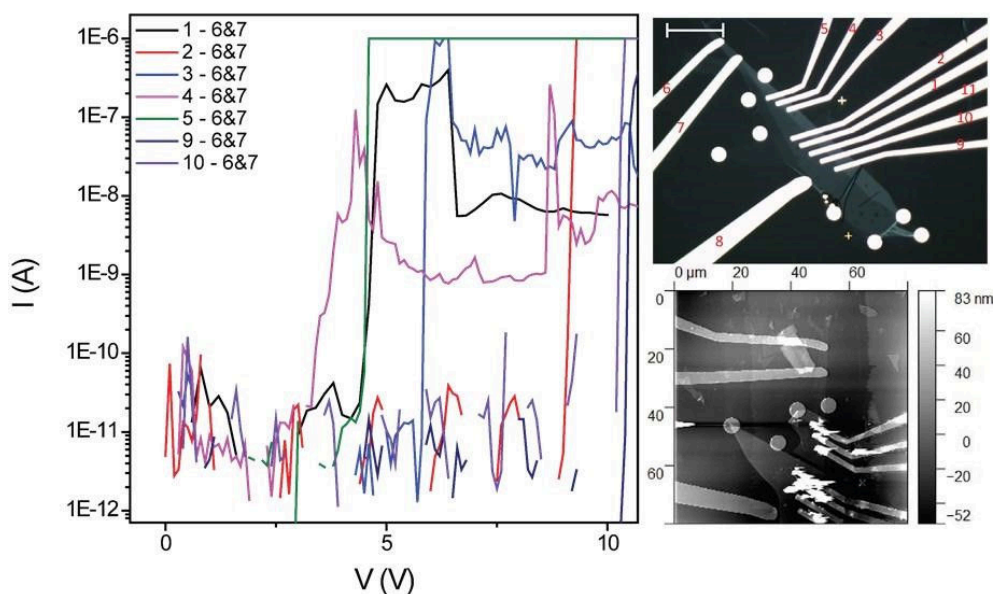


Figure S2. Breakdown characteristics of talc dielectrics. (left) I-V traces for the breakdown of the talc dielectric. (Top right) Optical micrograph of the device on a quartz substrate (Scale bar: 20 μm). (Bottom right) AFM topology of the device after breakdown measurements.

1.3 MoS₂ FET Leakage current & high V_{sd} behaviour

Figure S3 shows the field effect behaviour of our MoS₂ FET measured after 12 months stored in ambient conditions. A reduction in conductivity is seen likely due to degradation of the contacts. However, the gate leakage shows little change as can be seen in figure S3 B, with the onset of leakage occurring at $V_{gs} = 13$ V. Given the talc dielectric thickness was measured to be 18 nm, this corresponds to an electric field of $E_{th} \sim 0.7 \text{ V/nm}$ before leakage current becomes measurable.

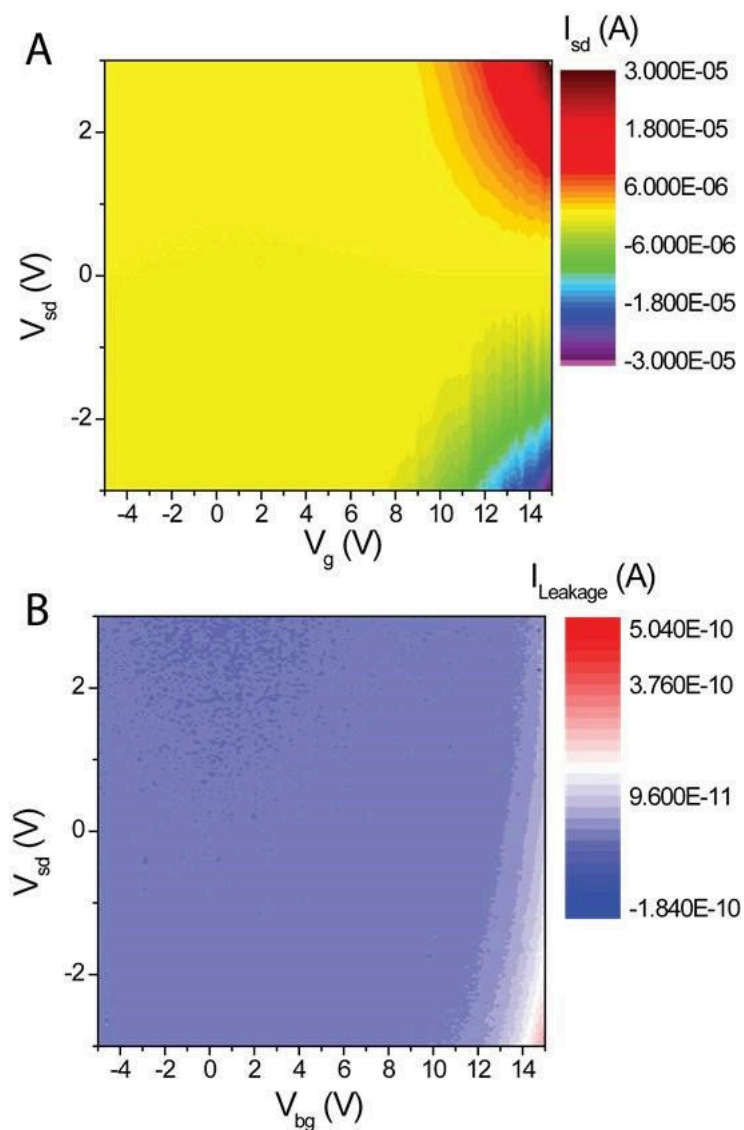


Figure S3. Repeat measurements of the MoS2 FET. (A) Field effect dependence of the MoS2 FET shown in figure 2 after being left for 12 months in ambient conditions. (B) Shows the corresponding gate leakage current, with onset of leakage occurring at $V_{gs} \sim 13$ V. $T = 270$ K, helium atmosphere.

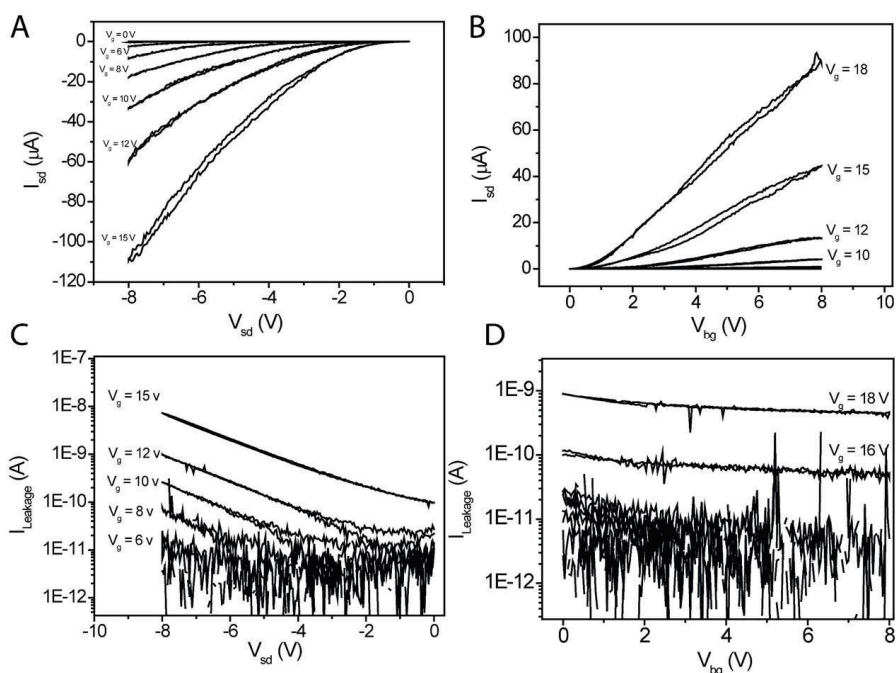


Figure S4. Leakage at higher bias. (A,B) I_{sd} - V_{sd} curves for increasing gate voltage for negative (A) and positive (B) source-drain voltage. (C, D) corresponding leakage current which shows an onset at $V_{gs} \sim 13V$ which agrees with the data shown in figure S3 B. $T=270$ K, helium atmosphere.

Figure S4(A,B) shows the I_{sd} - V_{sd} for increasing back gate voltage with the corresponding leakage current shown in S4(C,D). The onset of measurable leakage current occurs at $V_{gs}=13$ V. We found that when we increased V_{gs} to 20 V electric breakdown occurred which yields a breakdown field of ~ 1.3 V/nm, approximately twice the value obtained in ambient conditions and comparable with hBN dielectric.

1.2 Raman characterisation

Figure S5 shows the Raman spectra used to characterise our FETs, with (a, b) and (c, d) corresponding to the MoS₂ and MoSe₂ FETs, respectively. In (a, c), the peaks at ~ 520 cm⁻¹ and ~ 960 cm⁻¹ correspond to the underlying Si substrates, while those at ~ 1350 cm⁻¹, ~ 1580 cm⁻¹ and ~ 2710 cm⁻¹ come from the graphite contacts. Talc does not have a Raman response between 200 cm⁻¹ and 3000 cm⁻¹ as shown in Figure S5 (e).

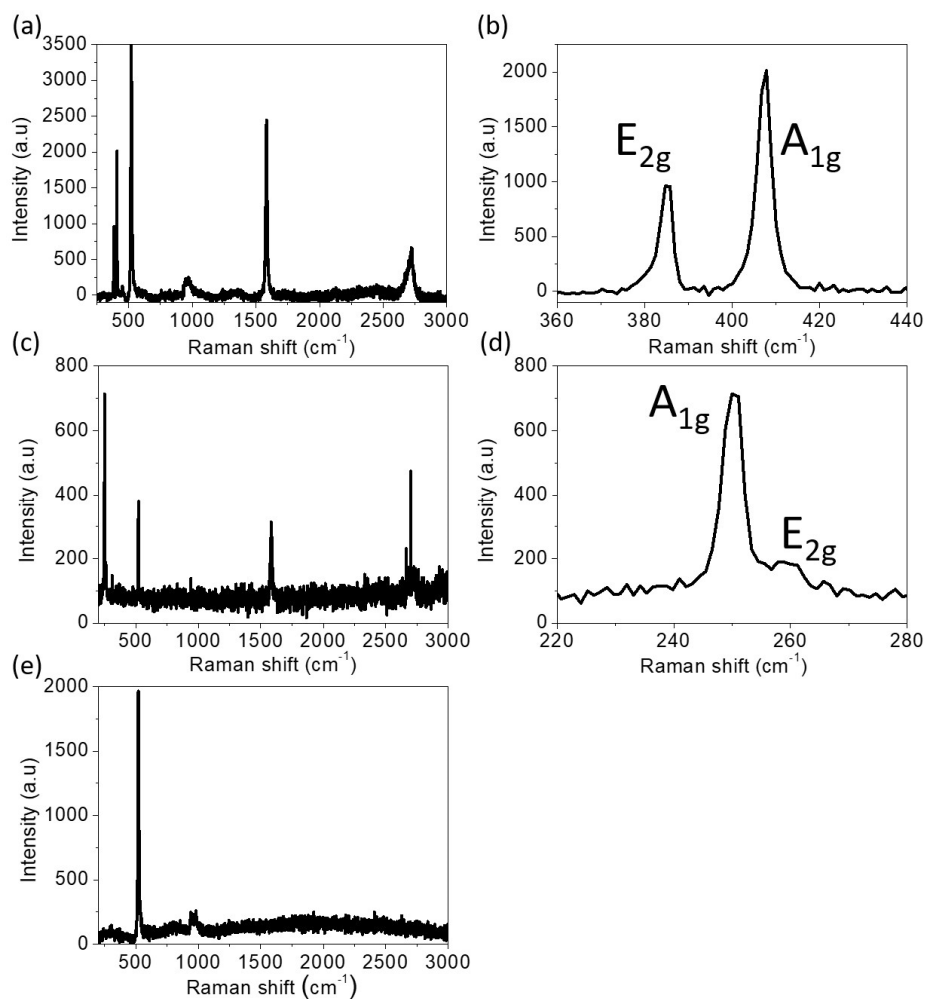


Figure S5. Raman characterisation of TMDC/talc heterostructures. (a) Full Raman spectrum of the MoS₂/talc/graphite FET. (b) The same Raman spectrum as (a) between 360 cm⁻¹ and 440 cm⁻¹, highlighting the characteristic peaks of MoS₂. (c) Full Raman spectrum of the MoSe₂/talc/graphite FET. (d) The same Raman spectrum (c) between 220 cm⁻¹ and 280 cm⁻¹, highlighting the characteristic peaks of MoSe₂.

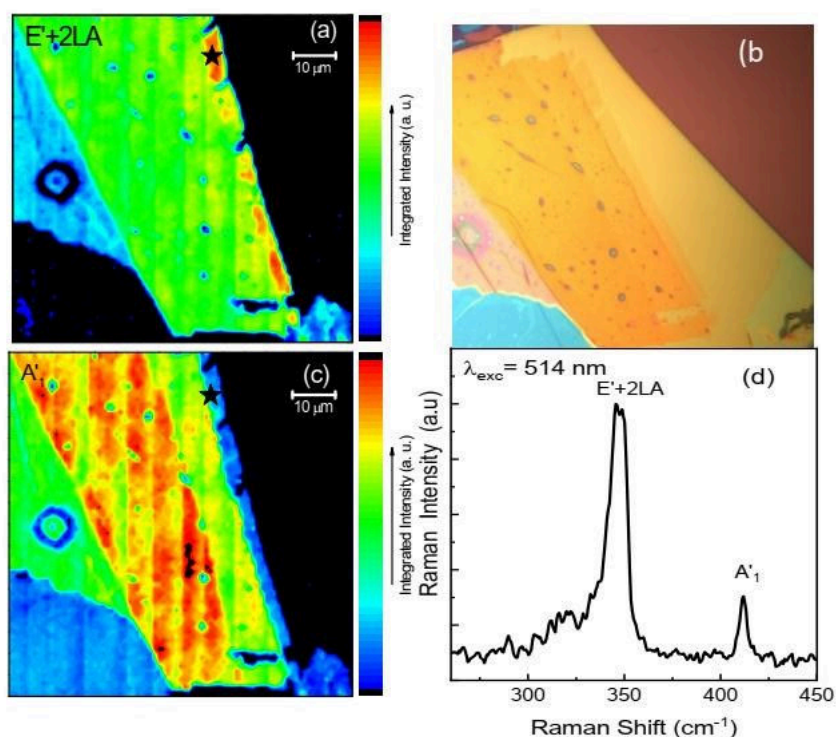


Figure S6. Raman characterisation of WS₂/talc heterostructure. (a) and (c) Raman mapping of the integrated intensity of peak E'+2LA modes (b) and A' mode for sample talc\WS₂ (b) Optical image and (d) Raman spectra of a single point (ML WS₂ region) indicated in the mapping.

Figure S6(a) and (c) show the Raman mapping of different Raman modes of the WS₂ –talc sample using 514nm laser excitation. Figure S6(b) shows the optical image and Figure S6(d) the Raman spectrum in the ML WS₂ region. The Raman positions and Raman mode relative intensity of Raman peaks are fully consistent to the ML WS₂.

1.3 Electrical characterisation

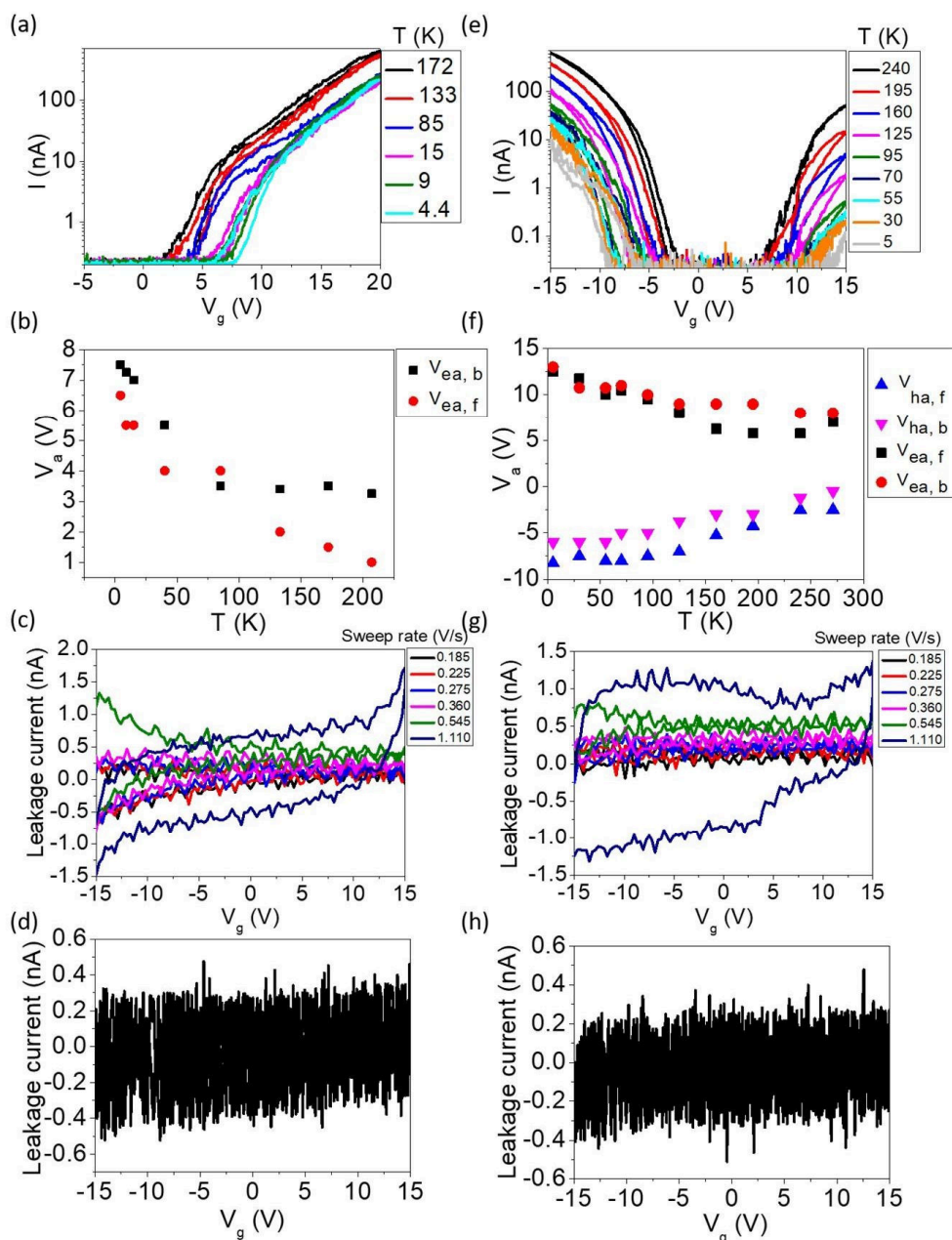


Figure S7. Electrical characterisation of TMDC/talc/graphite FETs. (a,e) I - V_g curves for our FET devices. (b, f) Temperature dependence of the activation energy, V_a . (c,g), where $V_{ea, f}$ ($V_{ea, b}$) and $V_{ha, f}$ ($V_{ha, b}$) are the activation energies corresponding to electron and hole conduction during forward (backwards) sweeps of the gate voltage, respectively. Gate leakage current vs V_g for a number of different voltage sweep rates. Representative leakage current vs V_g during electrical measurements. For the above, (a, b, c, d) are from the MoS₂/talc/graphite FET whilst (e, f, g, h) are from the MoSe₂/talc/graphite FET.

Figure S7 (a, e) shows the current vs applied back gate voltage, V_g , for a range of temperatures and for a gate voltage range of $-15 < V_g < 15$ V with $V_{sd} = 30$ mV. Freeze-out of the charge carriers can clearly be seen in both devices by the reduction of current magnitude and the drift of the activation voltages, as is illustrated in (b, f). Figure S7 (c, g) shows the at leakage

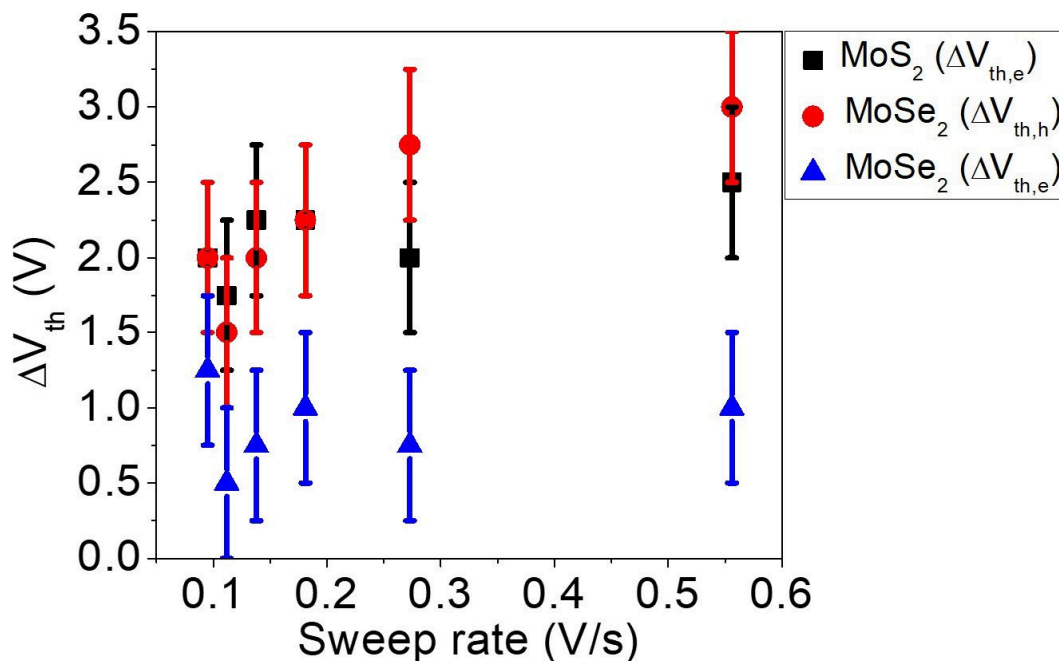


Figure S8. Change in threshold voltage vs sweep rate. The change in threshold voltage between forwards and backwards sweeps in V_g , ΔV_{th} , for the MoS₂-based FET and for both electron ($\Delta V_{th,e}$) and hole ($\Delta V_{th,h}$) conduction in the MoSe₂-based FET as a function of V_g sweep rate.

Figure S7 (a, e) shows the current vs applied back gate voltage, V_g , for a range of temperatures and for a gate voltage range of $-15 < V_g < 15$ V with $V_{sd} = 30$ mV. Freeze-out of the charge carriers can clearly be seen in both devices by the reduction of current magnitude and the drift of the activation voltages, as is illustrated in (b, f). Figure S7 (c, g) shows the gate leakage current for increasing sweep rates of the back-gate voltage, while (d, h) highlights the magnitude of leakage current during a typical device measurement. As can be seen in Figure S8, there is little change in the magnitude of hysteresis for V_g sweep rates < 0.6 V_s⁻¹. This value for the upper limit of sweep rate was decided based on Figure S3 (c,g), and was not exceeded for fear of damaging the devices.

FET architecture	Key parameters: Environment/ Production Encapsulation/ Annealing/ Sweep rate (Vs^{-1})	Hysteresis width (V)	Talc dielectric diminution factor ($\Delta V_{\text{th},x}/\Delta V_{\text{th,talc}}$)	Comments
$\text{MoS}_2/\text{SiO}_2/\text{Si}^2$	Ambient/Exfoliated/ No/No/0.5	15	6.67	
$\text{MoS}_2/\text{SiO}_2/\text{Si}^3$	Vacuum/Exfoliated/ No/Yes/0.1	~ 0.5	~ 0.29	Annealed at 85 °C for 12 hr.
$\text{MoS}_2/\text{hBN}/\text{Si}^3$	Vacuum/Exfoliated/ No/Yes/0.1	~ 0.5	~ 0.29	Annealed at 85 °C for 12 hr.
$\text{hBN}/\text{MoS}_2/\text{hBN}/\text{SiO}_2/\text{Si}^4$	Ambient/Exfoliated/ Yes/No/2	~ 7.5	~ 4.3	Hysteresis width increases for decreasing sweep rate ²⁻⁶ , and so the talc diminution factor at comparable sweep rates to those in Figure S4 would be even higher.
$\text{hBN}/\text{MoS}_2/\text{SiO}_2/\text{Si}^4$	Ambient/Exfoliated/ Yes/No/2	~ 22.5	~ 12.9	Hysteresis width increases for decreasing sweep rate ²⁻⁶ , and so the talc diminution factor at comparable sweep rates to those in Figure S4 would be even higher.
$\text{MoSe}_2/\text{SiO}_2/\text{Si}^6$	Vacuum/Exfoliated/ No/No/0.1	~ 1.5	~ 2	

Table S1: Comparison of hysteresis widths for a number of MoS2 and MoSe2-based FETs using different dielectrics within the literature. As can be seen within Table S1, the hysteresis widths present in comparable devices within the literature is widely varied, depending on a number of factors such as measurement conditions, dielectric material and if the devices were encapsulated or not. The lack of available data within the literature prevents a like-for-like comparison of the hysteresis widths of our devices, and thus Table S1 only serves as an approximate guide here.

2. Optical characterisation

Figure S9 shows the PL mapping and a typical PL spectrum of the sample WS₂-talc at 300K.

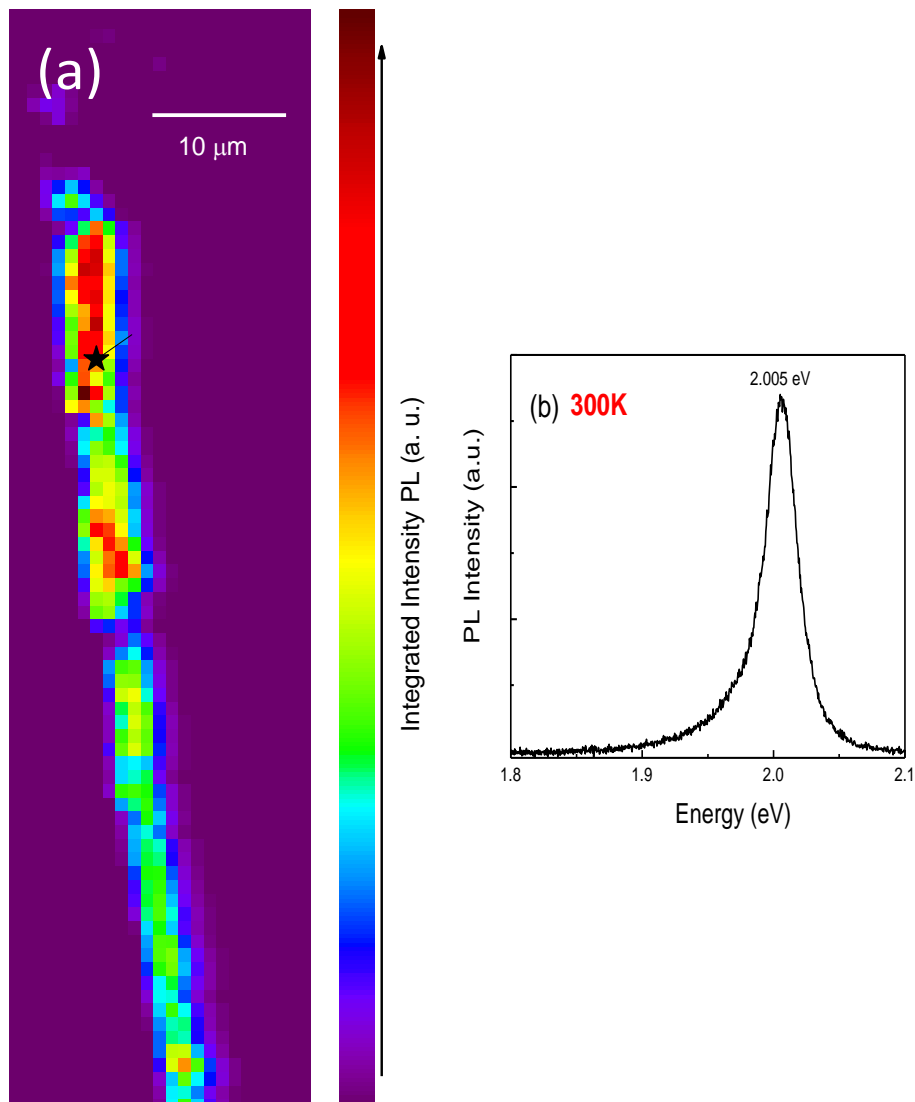


Figure S9. (a) PL mapping of the ML WS₂-talc at 300K (b) Typical PL spectrum. Figure S10 shows the PL color-plot versus time for a ML WS₂ on talc. We have observed that the PL signal is very stable on increasing time. Therefore, no photo-doping effect was observed for ML WS₂ on talc substrate which shows that talc is a promising substrate for ML TMD.

Figure S10 shows the PL color-plot versus time for ML WS₂ on talc. We have observed that the PL signal is very stable on increasing time. Therefore, no photodoping effect was observed for ML WS₂ on talc substrate which shows that talc is a promising substrate for ML TMD .

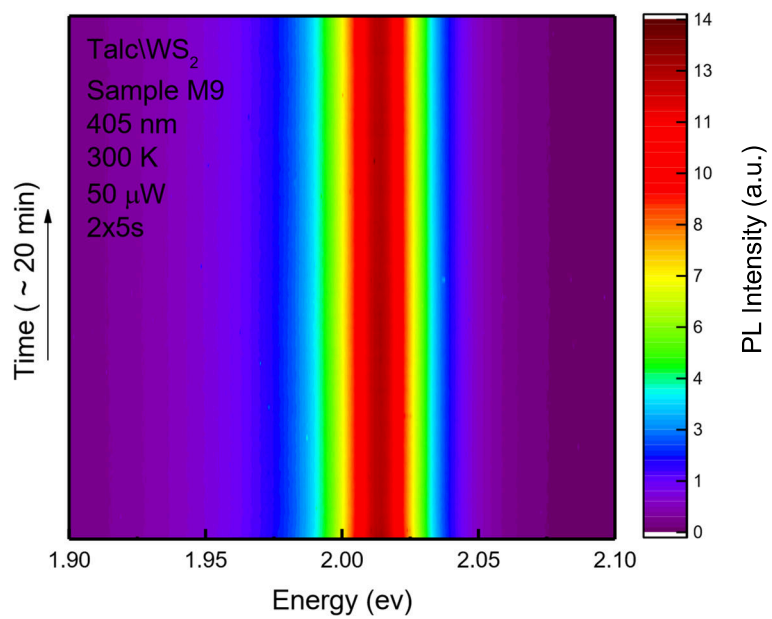


Figure S10. Color plot of PL versus time at 300K

References

1. D. Necas and P. Klapetek, *Cent Eur J Phys*, 2012, **10**, 181-188.
2. D. J. Late, B. Liu, H. S. S. R. Matte, V. P. Dravid and C. N. R. Rao, *Acs Nano*, 2012, **6**, 5635-5641.
3. Y. Y. Illarionov, G. Rzepa, M. Wlatl, T. Knobloch, A. Grill, M. M. Furchi, T. Mueller and T. Grasser, *2d Mater*, 2016, **3**.
4. C. Lee, S. Rathi, M. A. Khan, D. Lim, Y. Kim, S. J. Yun, D. H. Youn, K. Watanabe, T. Taniguchi and G. H. Kim, *Nanotechnology*, 2018, **29**.
5. T. Knobloch, G. Rzepa, Y. Y. Illarionov, M. Wlatl, F. Schanovsky, B. Stampfer, M. Furchi, T. Mueller and T. Grasser, *Ieee J Electron Devi*, 2018, **6**, 972-978.
6. Y. Y. Illarionov, A. J. Molina-Mendoza, M. Wlatl, T. Knobloch, M. M. Furchi, T. Mueller and T. Grasser, *Int Reliab Phy Sym*, 2018.

3. Conclusions

We have prepared different samples of 2D TMDs on talc dielectrics. We have studied the low-temperature photoluminescence of TMD/talc samples, which evidenced the optical quality of our samples. We have also studied the magneto-photoluminescence spectra of WS_2/hBN samples under perpendicular magnetic fields (up to 30T). These samples have shown various emission peaks associated with different excitonic complexes such as excitons, trions, biexcitons, dark trions, and phonon replicas of dark trions. We have investigated the magneto-optical properties of all excitonic complexes up to 30 T with circularly polarized laser excitation. The nature of the observed emission peaks was discussed in detail and compared with previous studies in the literature. Interestingly, we observed a significant increase in the PL intensity of dark trions and phonon replicas of dark trions, which is a different result compared to previous works in the literature [1–5]. This result may suggest that the emission of dark trions in $WS_2/Talc$ samples is probably favored by a possible effect of dielectric disorder caused by the talc dielectric, which could break the selection rules[6]. However, further studies would be needed to understand this effect in detail. We also observed that the polarization degree of the exciton and dark trion emissions have the same signal, which is evidence that the sample is n-doped. This result is very different from previous results obtained with graphene/talc, which showed a significant p-doping effect related to the natural impurities of the talc crystal [7]. A possible explanation for our result could be that the p-doping effect due to the impurities of the talc crystal is lower than the natural n-doping of the WS_2 samples. In addition, we observed that with σ_{\pm} polarized excitation, the sign of the circular polarization of the biexciton emission reverses at higher magnetic fields, suggesting that at very high fields, the effect of thermalization is the dominant mechanism compared to the valley selectivity due to the use of σ_{\pm} polarized excitation.

In addition, we have prepared several field-effect devices (FET) based on $MoSe_2/talc$ and $MoS_2/talc$ heterostructures. The electrical properties of these devices have been studied in detail and compared with those of devices based

on SiO₂ and hBN. Our devices have shown good quality, with a small hysteresis observed, comparable to devices using hBN as the dielectric. The characteristics of our devices do not depend strongly on the sweep rate and have negligible leakage current. In general, our results suggest that talc is a promising low-cost layered material for the protection of van der Waals (vdW) heterostructures/devices.

Our work shows a distinct behavior of the dark complexes for the parallel magnetic field. We expect that this will stimulate further theoretical investigations and experimental studies on talc-encapsulated samples, in turn leading to a better understanding of the dielectric disorder caused by the talc.

References

- [1] C. Robert, T. Amand, F. Cadiz, D. Lagarde, E. Courtade, M. Manca, T. Taniguchi, K. Watanabe, B. Urbaszek, X. Marie, Fine structure and lifetime of dark excitons in transition metal dichalcogenide monolayers, *Physical Review B*. 96 (2017) 155423. DOI:10.1103/PhysRevB.96.155423.
- [2] J. Shang, X. Shen, C. Cong, N. Peimyoo, B. Cao, M. Eginligil, T. Yu, Observation of excitonic fine structure in a 2D transition-metal dichalcogenide semiconductor, *ACS Nano*. 9 (2015) 647–655. DOI:10.1021/nn5059908.
- [3] E. Liu, J. van Baren, Z. Lu, M.M. Altairy, T. Taniguchi, K. Watanabe, D. Smirnov, C.H. Lui, Gate Tunable Dark Trions in Monolayer WSe₂, *Physical Review Letters*. 123 (2019). DOI:10.1103/PhysRevLett.123.027401.
- [4] G.A. Prando, M.E. Severijnen, I.D. Barcelos, U. Zeitler, P.C.M. Christianen, F. Withers, Y. Galvão Gobato, Revealing Excitonic Complexes in Monolayer WS₂ on Talc Dielectric, *Physical Review Applied*. 16 (2021). DOI:10.1103/PhysRevApplied.16.064055.

- [5] M. Zinkiewicz, T. Woźniak, T. Kazimierczuk, P. Kapuscinski, K. Oreszczuk, M. Grzeszczyk, M. Bartoš, K. Nogajewski, K. Watanabe, T. Taniguchi, C. Faugeras, P. Kossacki, M. Potemski, A. Babiński, M.R. Molas, Excitonic Complexes in n-Doped WS₂ Monolayer, *Nano Letters*. 21 (2021) 2519–2525. DOI:10.1021/acs.nanolett.0c05021.
- [6] D. Rhodes, S.H. Chae, R. Ribeiro-Palau, J. Hone, Disorder in van der Waals heterostructures of 2D materials, *Nature Materials*. 18 (2019) 541–549. DOI:10.1038/s41563-019-0366-8.
- [7] E. Mania, A.B. Alencar, A.R. Cadore, B.R. Carvalho, K. Watanabe, T. Taniguchi, B.R.A. Neves, H. Chacham, L.C. Campos, Spontaneous doping on high quality talc-graphene-hBN van der Waals heterostructures Spontaneous doping on high quality talc-graphene-hBN van der Waals heterostructures, (2017).

Annex A

Peak	Excitonic complexes					Dark Trion Phonon Replicas	
	Exciton (X)	Dark Trion (DT)	Inter valley Trion (Tt)	Intra valley Trion (Ts)	Charged Biexciton (XX-)	ZA(K) (L1)	E'(K) (L2)
Experimental Values P1	-3.3	-9.1	-3.7	-3.4	-4.3	-14.4	-13.3
Experimental Values P2	-3.6	-9.3	-3.9	-3.9	-4.3	-12.3	-12.6
Literature Values	-3.5 ^E [1] -3.7 ^E [2]**	-8.9 ^E [1] -8.73 ^T [1]	-3.9 ^E [1] -3.56 ^T [1] -4.0 ^E [2]	-4.0 ^E [1] -3.56 ^T [1] -4.5 ^E [2]	-4.1 ^E [1] -5.3 ^E [2]	-13.7 ^E [1] -12.2 ^T [1]	-13.3 ^E [1] -12.2 ^T [1]

Table A.1.g factors extracts from magneto -PL measurements. Font: elaborated by the author

Notes:

* Coefficient of PL Intensity (I) dependence with Laser Power (P), using $I \propto P^\alpha$;

^E Experimental;

^T Theoretical.

References:

- [1] M. Zinkiewicz, T. Woźniak, T. Kazimierczuk, P. Kapuscinski, K. Oreszczuk, M. Grzeszczyk, M. Bartoš, K. Nogajewski, K. Watanabe, T. Taniguchi, C. Faugeras, P. Kossacki, M. Potemski, A. Babiński, M. R. Molas, Excitonic Complexes in n-Doped WS₂ Monolayer, *Nano Lett.* **6**, 2519 (2021). DOI: 10.1021/acs.nanolett.0c05021.
- [2] Z. Li, T. Wang, S. Miao, Z. Lian, S. F. Shi, Fine Structures of Valley-polarized Excitonic States in Monolayer Transitional Metal Dichalcogenides, *Nanophotonics* **9**, 1811(2020). DOI: 10.1515/nanoph-2020-0054

